FORMATION MECHANISM OF CASTING DEFECTS AND MACROSEGREGATION GENERATED BY BRIDGING DURING SOLIDIFICATION

馬, 聚懐

FORMATION MECHANISM OF CASTING DEFECTS AND MACROSEGREGATION GENERATED BY BRIDGING DURING SOLIDIFICATION

MA JUHUAI

九州大学
KYUSHU UNIVERSITY

Formation mechanism of casting defects and macrosegregation generated by bridging during solidification

By

MA JUHUAI

A thesis submitted to Kyushu University

for the degree of Doctor of Engineering

Department of Materials Process Engineering

Graduate School of Engineering

Kyushu University

Fukuoka, Japan

CONTENTS

Chapter 1. Introduction

1.1 Fundamental of solidification

Solidification is a process in which a substance undergoes a phase transition from a liquid state to a solid state. This phenomenon is ordinary but essential and widely used in life and production. Especially in metal parts manufacturing, since liquid metal is weak to resist shear stress, it can be shaped with less energy than solid, and this method is called casting in the industry.[1)] For the castings that are directly put into use, there may be problems of inhomogeneity in composition and solidification microstructure in different casting parts, and these could also directly affect the overall performance of the casting. Since the microstructure and solidification defects formed during the solidification process of castings are difficult to be eliminated entirely even after subsequent processing, it is essential to understand the factors that affect the solidification structure for the regulation of the entire solidification process.[2)]

Considering the solidified structure obtained by casting, several typical characteristic structures exist, as shown in Fig. 1.1.1.[1)] The region near the surface of the mold with small equiaxed grain with random orientation is formed by a high cooling rate. Then these grains grow into dendrites along their preferred crystallographic directions. And the dendrite with a preferred orientation antiparallel to the direction of heat flow could grow rapidly into a columnar dendrite in the competitive growth period. As the solidification proceeds, the liquid phase in the central region of the casting locally changes from superheating into supercooling to nucleate, and also, some free dendrites from the columnar dendrite region will grow in this region. Thus another equiaxed dendrite region is formed in the center of the casting.

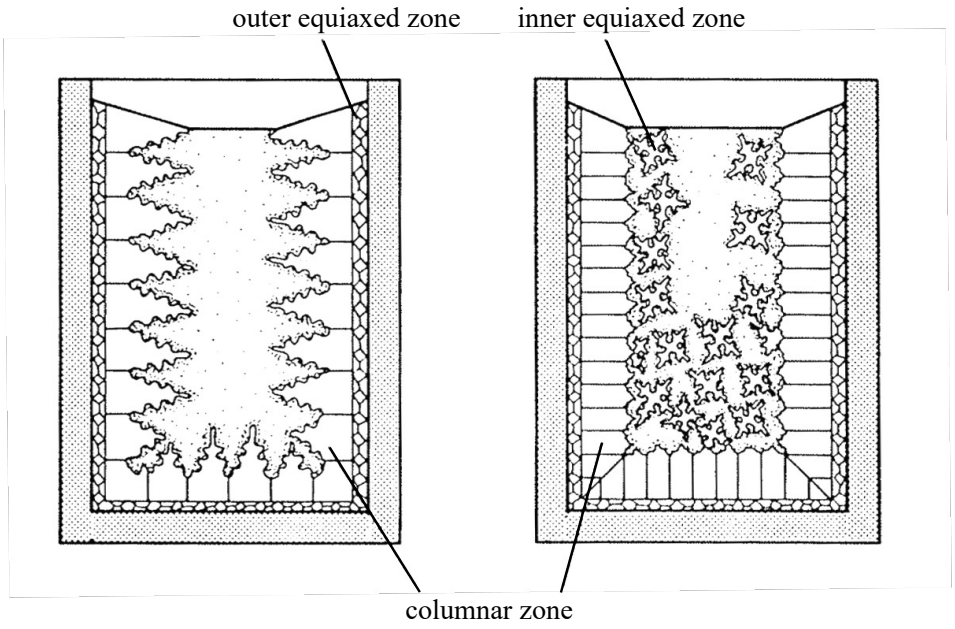

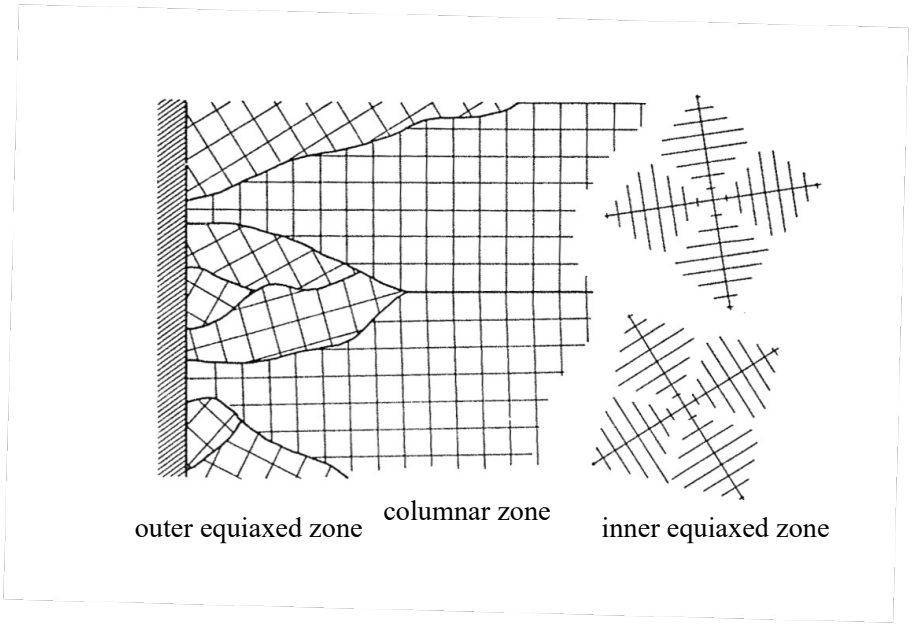

Fig. 1.1.1. Schematic drawing of solidification structures in the casting.[1)]

1.2 Segregation in solidification

As far as metals growing under normal solidification conditions are concerned, local equilibrium is assumed to hold at the solid/liquid interface. Then, at the interface, the solid concentration is related to the liquid concentration by the equilibrium distribution coefficient. This composition difference will always lead to concentration variations, which are known as segregation, in the solidified alloy. And segregation always occurs in the castings. During solidification, as shown in Fig. 1.2.1, the redistribution of alloying elements will cause microsegregation inside the dendrite and interdendritic region. In the case of casting with a large size, convection can lead to the transport of mass[3)] over a very large distance and may cause the concentration or dilution of alloying elements, which is defined as macrosegregation. The part where the concentration is higher than the average value is called positive segregation, and the part where the concentration is lower than the average value is called negative segregation. Because the solute can be transported by diffusion or by convection (or both), the segregation pattern will be quite different. The main macrosegregation classifications and characteristics are shown in Fig. 1.2.2.

(1) Normal segregation: The solute concentration in the center of the alloy ingot with an equilibrium distribution coefficient of less than 1 is higher than that in the periphery.

(2) Reverse segregation: Contrary to positive segregation, the solute concentration on the surface of the ingot is higher than the average solute concentration and gradually decreases inside the ingot.

(3) Positive or negative segregation: The solute concentration in the local area of the alloy ingot is higher or lower than the mean value of the ingot.

(4) Banded segregation: Discontinuous segregation bands of solute concentration parallel to the surface of the ingot with a small width and often appear periodically.

(5) Gravity segregation: The segregation that is observed in the vertical direction of the steel ingot due to the precipitated crystals or the migration of solute-rich melts based on density differences from the bulk liquid.

(6) V segregation: a V-shaped segregation layer that appears in the axial center of the longitudinal section of the ingot. It is also formed in the axial core part of the slab.

(7) Inverted V-shaped segregation: A-type segregation is distributed in an inverted V-shape in linear or granular. It is produced by the settlement of concentrated melt in the solidification transition zone due to the movement of density difference.

(8) Corner ghosting: small segregation lines generated at the corner or surface of the ingot in the early stage of solidification.

(9) Center segregation: In the continuous casting, it refers to the solute concentration that occurs in the central area where the tips of the columnar crystals developed from both sides face or contact each other, which is attributed to the suction effect due to the solidification contraction.

(10) White band: In the continuous casting of steel, the area where solidification is progressed by electromagnetic stirring may appear as a white band due to differences in corrosion. This is because the low solid fraction region of the solidification transition layer was washed away by the flow and the solute concentration in the dendrite interstices decreased rapidly, resulting in low-concentration crystal crystallization.

(11) Semi-macro segregation and point segregation: Electromagnetic stirring can improve central segregation to a certain extent with a different point of view. It means segregation is dispersed throughout the slab, resulting in equiaxed crystal regions inside the slab.

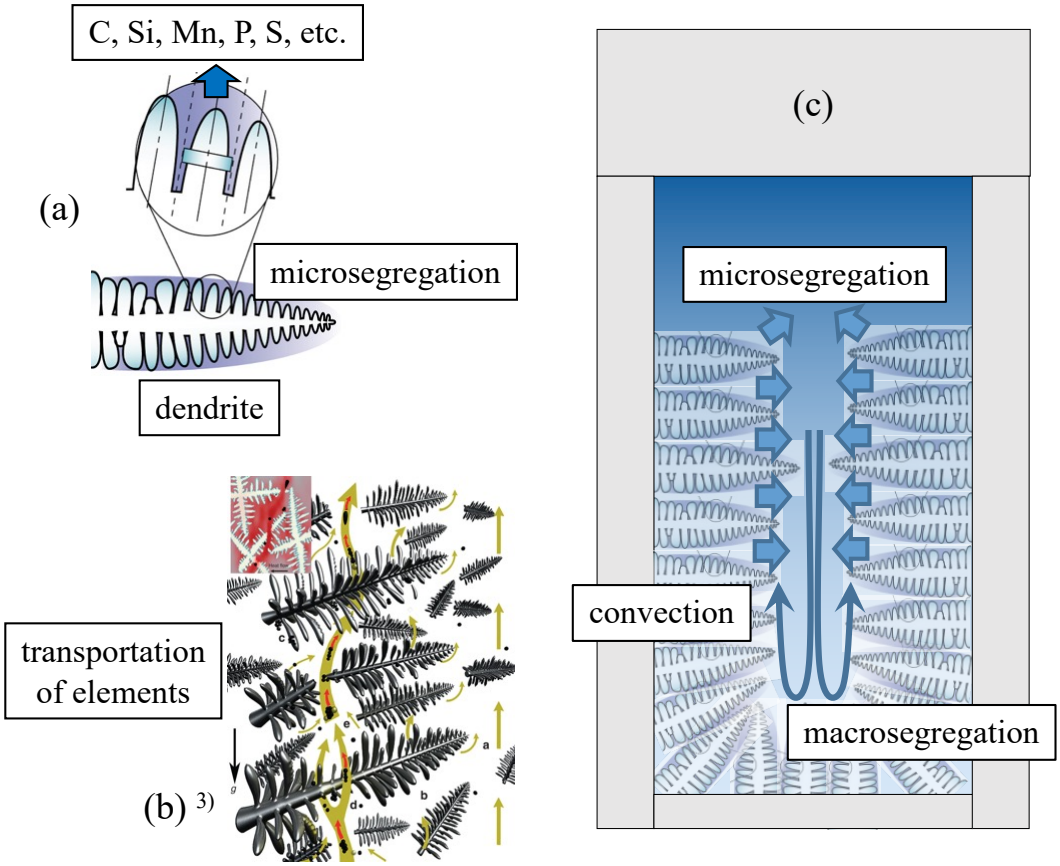

Fig. 1.2.1. Schematic drawing of the segregation in the solidification of the casting.

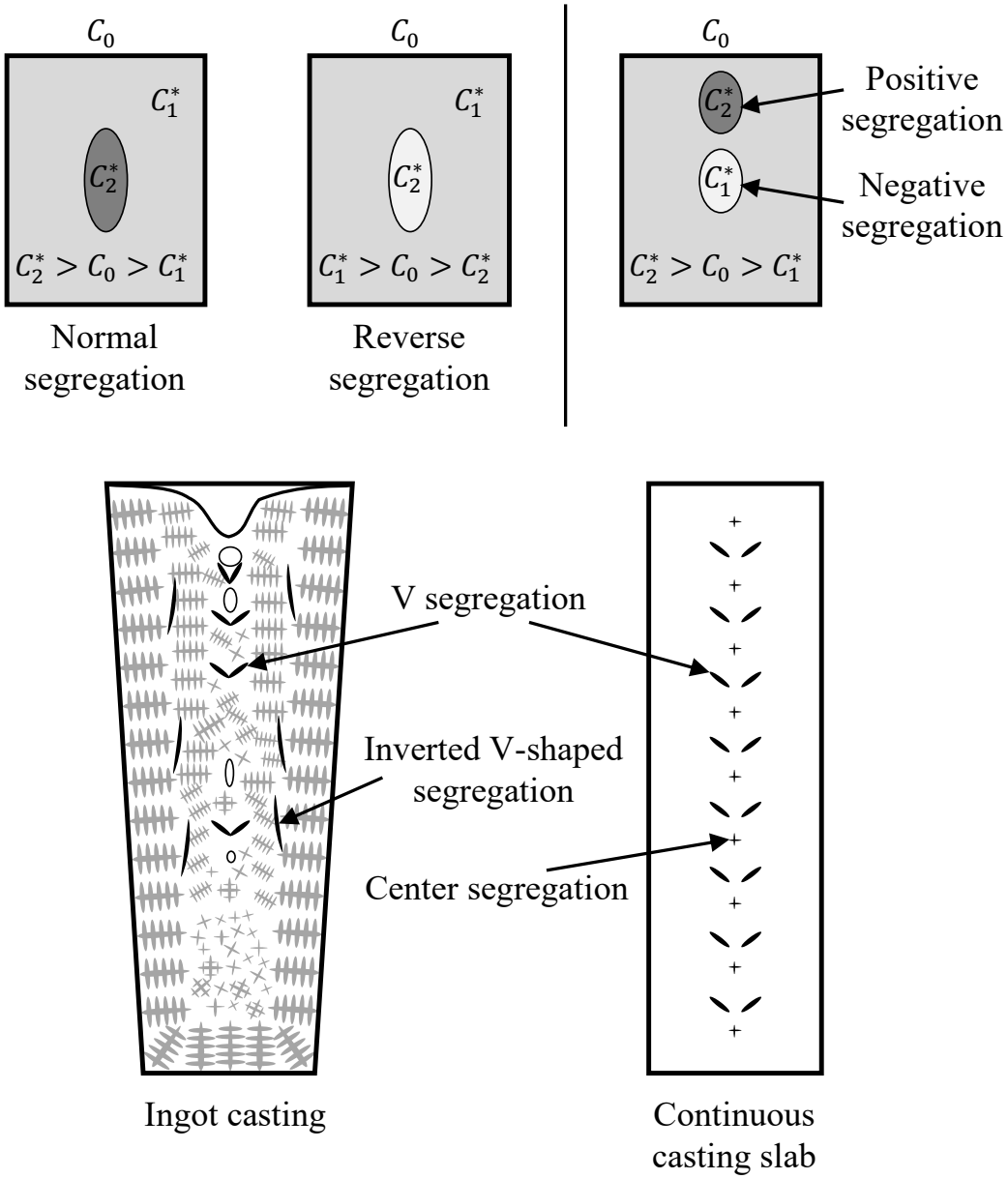

Fig. 1.2.2. Schematic drawing of the main macrosegregation classifications and characteristics in the large castings.

1.3 Problem and research objectives

In the continuous casting process and ingot casting, macrosegregation and casting defects are known to occur when the thickness of the solidified layer becomes non-uniform due to bridging during solidification. As shown in Fig. 1.3.1, sometimes there are cases where the cooling rate is too fast due to the rolls, and it leads to the bridging of columnar dendrites in a local area, but, the upper and lower parts of this area are still liquid phase. In addition, under the influence of suction by solidified area and forced flow by extrusion of rolling, this situation may lead to shrinkage porosity and severe macrosegregation. Since macrosegregation directly affects the cracking of slabs and the deterioration of mechanical properties, it is desirable to reduce it as much as possible. However, macrosegregation enhanced by convection is greatly influenced by the mold and casting conditions, and it is difficult to perform quantitative and highly reproducible analysis. Since the contraction flow occurs three-dimensionally and the macrosegregation also exists with a three-dimensional spread, therefore, it is necessary to be able to reproduce this macrosegregation phenomenon at the experimental level and perform the analysis from a three-dimensional perspective. Ultimately, it would be necessary to develop a comprehensive macrosegregation model that considers the motion of the solid and liquid phases, so as to establish and standardize a three-dimensional evaluation method for its solidified structures. Moreover, only by accurately predicting the location of segregation can effectively control the quality of the casting.

Recently, a method has been proposed in which a local part of the mold is forcibly cooled to form a non-uniform solidified layer and analyze the macrosegregation[5]. Therefore, in this study, the effectiveness of the local chilled mold for cast steel samples

was investigated, and the effect of bridging on macrosegregation and solidification defects was investigated using the improved mold and simulation.

In addition, as a verification of a method of reducing central segregation and V-segregation of cast steel, the direct current (DC) was applied to Al-15mass%Cu alloy during solidification, as shown in Fig. 1.3.2, and the effectiveness for equiaxed crystallization of dendrite dominated by Joule heat was investigated.

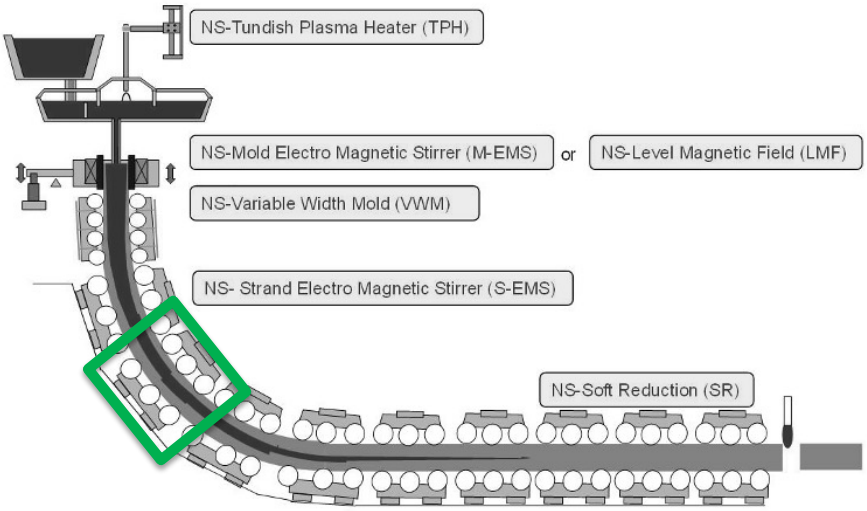

Slab Continuous Caster (SL-CC)[4)]

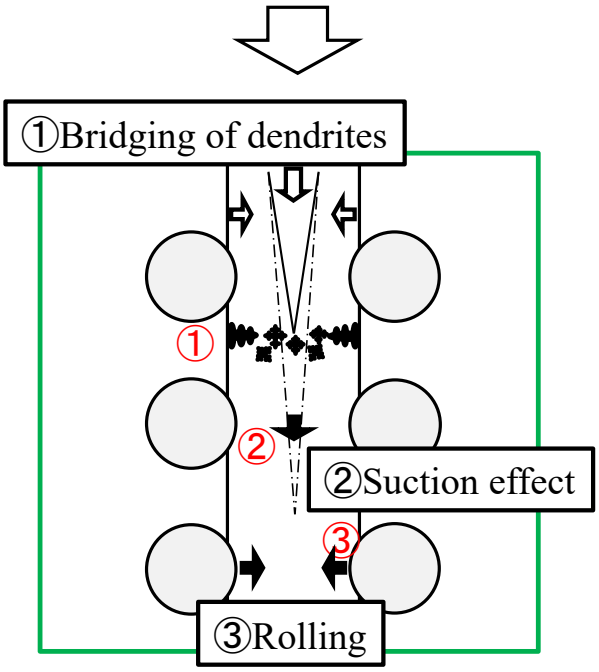

Schematic drawing of the solidified region

Fig. 1.3.1. Schematic drawing of the solidified area of the simplified model of continuous casting.

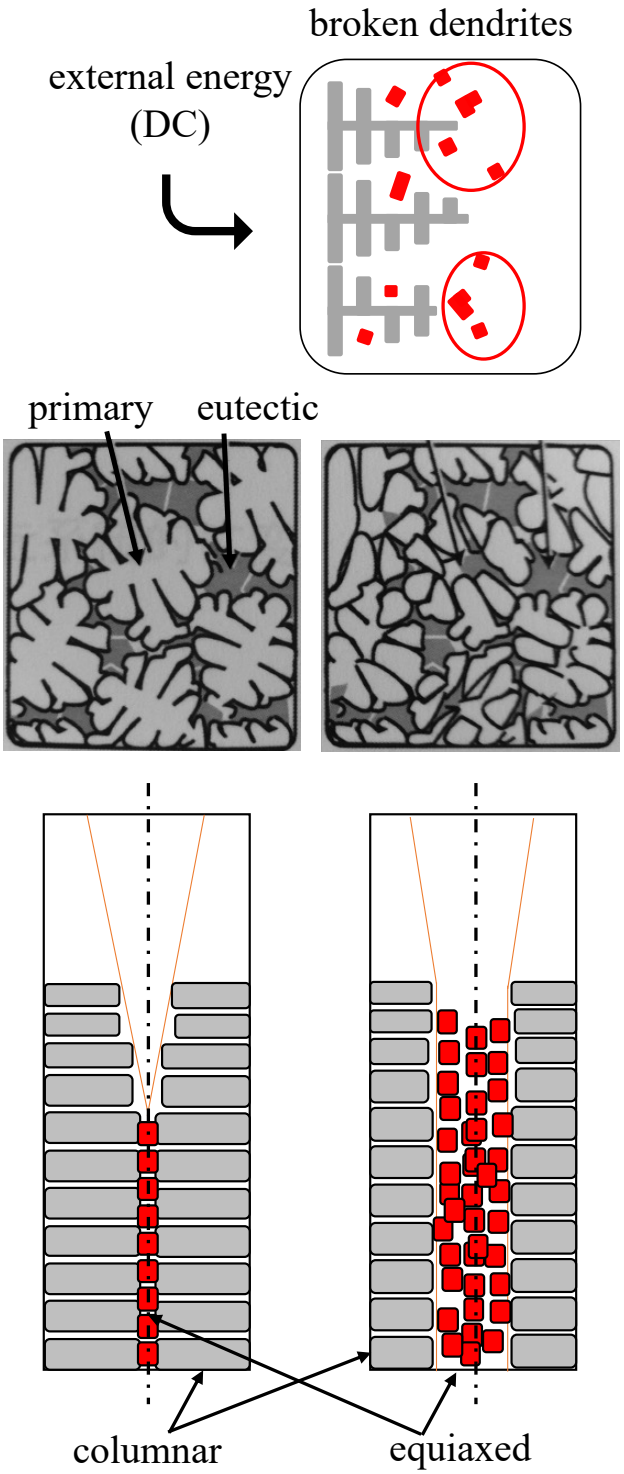

Fig. 1.3.2. Schematic drawing of the solidified area of the equiaxed crystallization of dendrite with the effect of direct current.

1.4 Outline of the thesis

This thesis consists of five chapters, including the introduction in Chapter 1 and the summary in Chapter 5.

In Chapter 2, the effectiveness of the local chilled mold to reproduce segregation in cast steel samples was investigated, and a model casting experiment was adopted to understand the formation mechanism of macrosegregation of steel casting that occurred by local bridging during solidification with a laboratory-scale local-chilled mold. In addition, an improved model casting experiment was adopted, and the effect of bridging on macrosegregation was investigated.

In Chapter 3, the simulation of the solidification process by local cooling was evaluated. Various changes in the solidification process were calculated. And the in-situ observations of the solidification by a water model were carried out to evaluate the progress of solidification and the convection flow in the mold with and without local cooling to better understand the effects of columnar bridging on central segregation.

In Chapter 4, the DC was applied to the Al-15mass%Cu alloy in the branching and coarsening regions during solidification, as a model experiment for reducing macrosegregation in continuous casting of steel. The effect of DC on dendrite melting and equiaxed crystallization was evaluated.

Chapter 5 is the summary of this research.

References

1) W. Kurz, and D. J. Fisher: Fundamentals of Solidification, 3rd edition, Trans. Tech. Publ., (1989).
2) M. C. Flemings: Solidification Processing, McGraw-Hill, NY, (1974).
3) D. Li *et al.*, *Nat. Commun.*, **5** (2014), 5572.
4) NIPPON STEEL ENGINEERING CO., LTD. https://www.eng.nipponsteel.com/business/steelplants/casting/slab_continuous_caster/
5) F. Satou, H. Esaka, and K. Shinozuka: *Tetsu-to-Hagané*, **99** (2013), 101. (in Japanese). https://doi.org/10.2355/tetsutohagane.99.101

Chapter 2. Effect of local bridging during solidification

2.1 Solidification microstructure and segregation in the medium-carbon steel cast with a laboratory-scale local-chilled mold

2.1.1 Introduction

In the industrial steel manufacturing process, segregation[1,2] occurs in many castings.[3,4] It is considered that redistribution of alloying elements causes microsegregation between the dendrite and the interdendritic region, and convection flow causes concentration or dilution of alloying elements, defined as macrosegregation[4,5]. Since it is difficult to make it harmless in the rolling process after casting and heat treatment, there has been a demand for technological development that does not cause macrosegregation in the casting process, such as continuous casting and ingot casting. Solidification structure control is regarded as a macrosegregation reduction technology to improve macrosegregation. To improve the quality of products, it is necessary to understand the solidified structure to optimize production processes. In particular, the structure formation mechanism in the vicinity of the surface of the casting is different from that inside due to the effect of bridging[6] and contraction flow during solidification.[7] Some dendrites bridged together during the middle solidification period to block the free melt flow, causing casting defects, such as huge shrinkage and severe segregation.[8]

Satou *et al.*[9] developed a mold to produce macrosegregation, intentionally bringing about the bridging in the middle of a cast, to investigate the relationship between solidified structure and macrosegregation using Al-Cu alloy. In the experiments of Al-Cu alloys, where the size and morphology of the equiaxed crystals varied independently, Aritaka *et al.*[10] demonstrated the possibility of controlling macrosegregation by the size and shape of equiaxed grains.

In this study, to clarify the principle of casting defects, such as porosity and segregation due to the formation of bridging[6] during the solidification of steel, the samples were cast by a laboratory-scale local-chilled mold developed by Satou[9], in which the central part was forcedly cooled to cause bridging. The dendrite morphology was observed, and segregation in the ingot was investigated.

2.1.2 Experimental

A kind of medium-carbon steel was used in this study. The chemical composition (in mass%) of the sample was 0.45% Carbon, 0.5% Silicon, 0.8% Manganese, 0.06% Phosphorus, and 0.03% Sulfur.

The schematic drawing of the observation part in the ingot without sprue is shown in Fig. 2.1.1. The inner dimension of the Satou[9] mold used in this study was 30 mm (T) × 50 mm (W) × 130 mm (H). The narrow side of the mold used was thermally insulated with porous alumina ceramic plates. The bottom and the broad side were made of SUS304 to give strength, and a BN-based mold release agent was used. Using a vacuum induction melting furnace, 1.1 kg of electrolytic iron, *etc.*, were melted under an Ar atmosphere. And the steel was cast in the Satou mold through a tundish. The liquidus temperature was calculated by the Kawawa equation[11,12] (Eqs. (2.1.1)).

$$T_L = 1538 - 55(\%C) - 80(\%C)^2 - 13.0(\%Si) - 4.8(\%Mn) \\ -34.4(\%P) - 38(\%S) \qquad (2.1.1)$$

Where T_L is the liquidus temperature, the unit of T_L is °C, and ($\%X$) indicates the mass% of the alloying element in the steel. Sample No.1 was cast by the superheating[13-15] (Casting temperature, ΔT, Eqs. (2.1.2)) of 100 ± 2 °C, and the ΔT of sample No.2 was 30 ± 2 °C.

$$\Delta T = T - T_L \qquad (2.1.2)$$

After grinding with SiC papers and mirror polishing by diamond paste, shrinkage porosity was observed. The concentrations of the alloying elements were analyzed by an electron probe micro-analyzer (EPMA, Shimadzu EPMA 1600) on polished surfaces. Line analysis was performed with an accelerating voltage of 20 kV, a beam current of 10 nA, a beam size of 100 μm, and a step size of 20 μm. The observed surfaces were etched with the saturated picric acid aqueous solution, the dendrite structure was observed by an optical microscope, and the secondary dendrite arm spacing[16,17] (SDAS) was measured. The heat flow and solidification progress were numerically analyzed using JSCAST Ver.13 software[18].

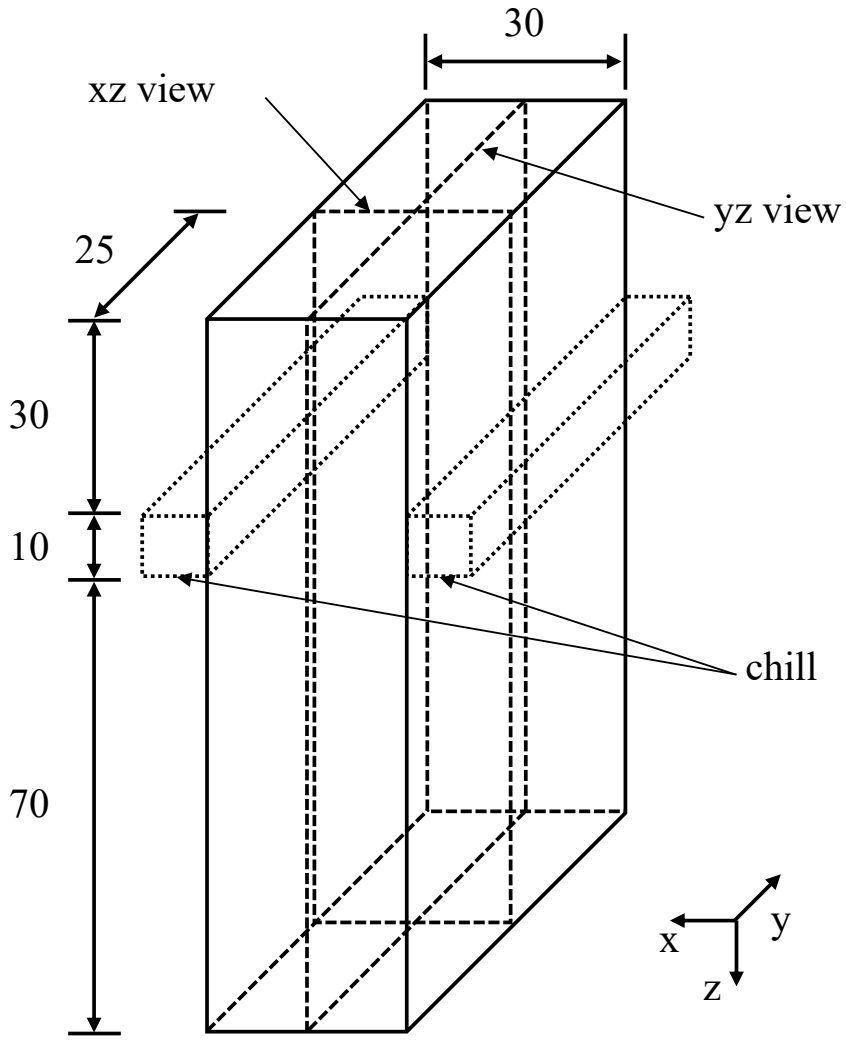

Fig. 2.1.1. Schematic drawing of observation part in the ingot. (unit: mm)

2.1.3 Results and discussion

2.1.3.1 Morphology of solidification structure and defects

The areas of the longitudinal section (xz view in Fig. 2.1.1) of two samples, etched by saturated picric acid aqueous solution, were observed. From the etched print of samples, as shown in Fig. 2.1.2, some large shrinkage porosities were observed in the high superheating sample No.1 (Fig. 2.1.2 (a)), and shrinkage porosities were observed in the low superheating sample No.2, (Fig. 2.1.2 (e)). The shrinkage porosity is more significant in part closer to the bottom of the bridging zone. Columnar dendrites with significantly different morphologies and coarsened dendrites were observed in the high superheating sample No.1, as shown in Fig. 2.1.2 (b-d). However, equiaxed dendrites with similar morphology, except for a minimal amount of columnar dendrites, could be observed in low superheating sample No.2, as shown in Fig. 2.1.2 (f-i). In sample No.1, there were many defects, such as porosities shown in Fig. 2.1.2 (c) and extremely fine dendrites shown in Fig. 2.1.2 (d). As the solidification structure, it could be observed that the higher casting temperature can form well-developed columnar dendrites, and the branched columnar dendrites are also obvious. There are also equiaxed grains in the central and lower part of the ingot. However, the solidification structure of the sample cast at lower casting temperatures is relatively uniform equiaxed dendrites.

Preferential growth and bridging occurred because of partial cooling for the upper part of the sample with the chill plates installed over the entire width. Higher superheating would make a higher temperature gradient around the chill plate, making forced growth of columnar dendrite easier. When the direction of growth is opposite to the direction of heat flow, it is often referred to as forced growth which is the case with directional solidification or columnar crystal growth. That is, the rate of advancement of the isotherm

limits the dendrites to grow at a given speed, thereby forcing the dendritic tip to have an undercooling. The equiaxed dendrites solidify if the heat flows from the crystal to the melt. Dendrites grow freely in the radial direction at a rate allowed by the undercooling until they meet the dendrites that grow from other nuclei. In the directional growth, the crystal is in contact with the chill, and heat is led through the crystal in a direction parallel to the crystal growth direction. Therefore, the melt is the hottest part. When the equiaxed dendrite grows, the heat generated by the solidification process must pass through the melt, and the crystal is the hottest part, and the heat flux q is in the radial direction and coincides with the growth direction. Therefore, a high cooling rate created by a high casting temperature can form columnar dendrite bridging. Regardless of whether this phenomenon occurs in the continuous casting or the ingot casting process, huge shrinkage porosity may be generated, thereby affecting the quality of the material.

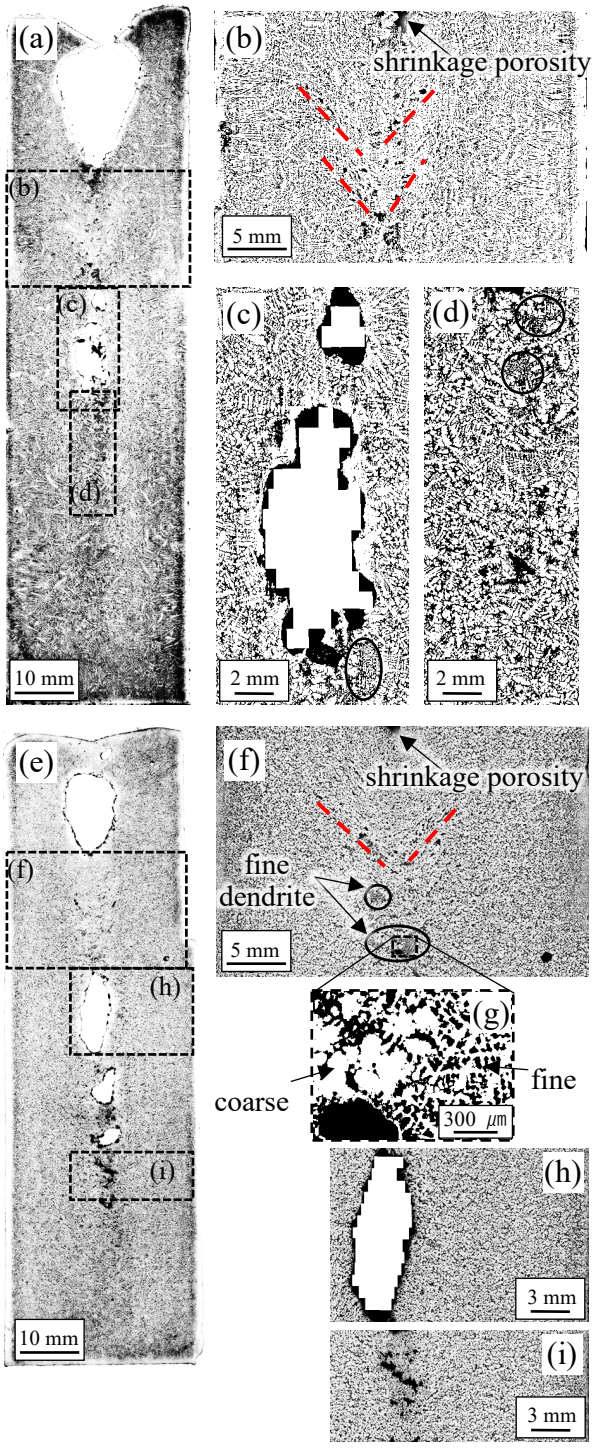

Fig. 2.1.2. Solidification microstructure in longitudinal section (xz view shown in Fig. 2.1.1). (a)(e) The etched prints of samples No.1 and No.2, respectively. (b)(f) The bridging zone in (a) and (e). Area (c) in the vicinity of shrinkage and area (d) under shrinkage of sample No.1. And area (h), (i) in the vicinity of shrinkage of sample No.2.

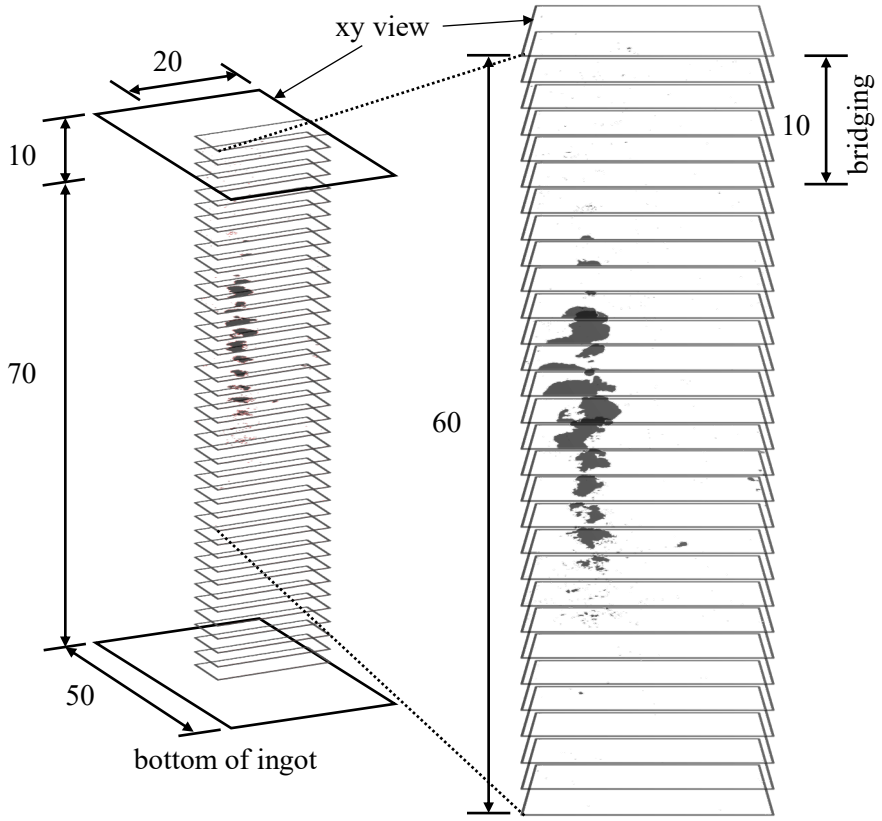

Fig. 2.1.3. Shrinkage porosity morphology in the observed area (xy view shown in Fig. 2.1.1) gained by serial sectioning method, of samples No.1. (unit: mm)

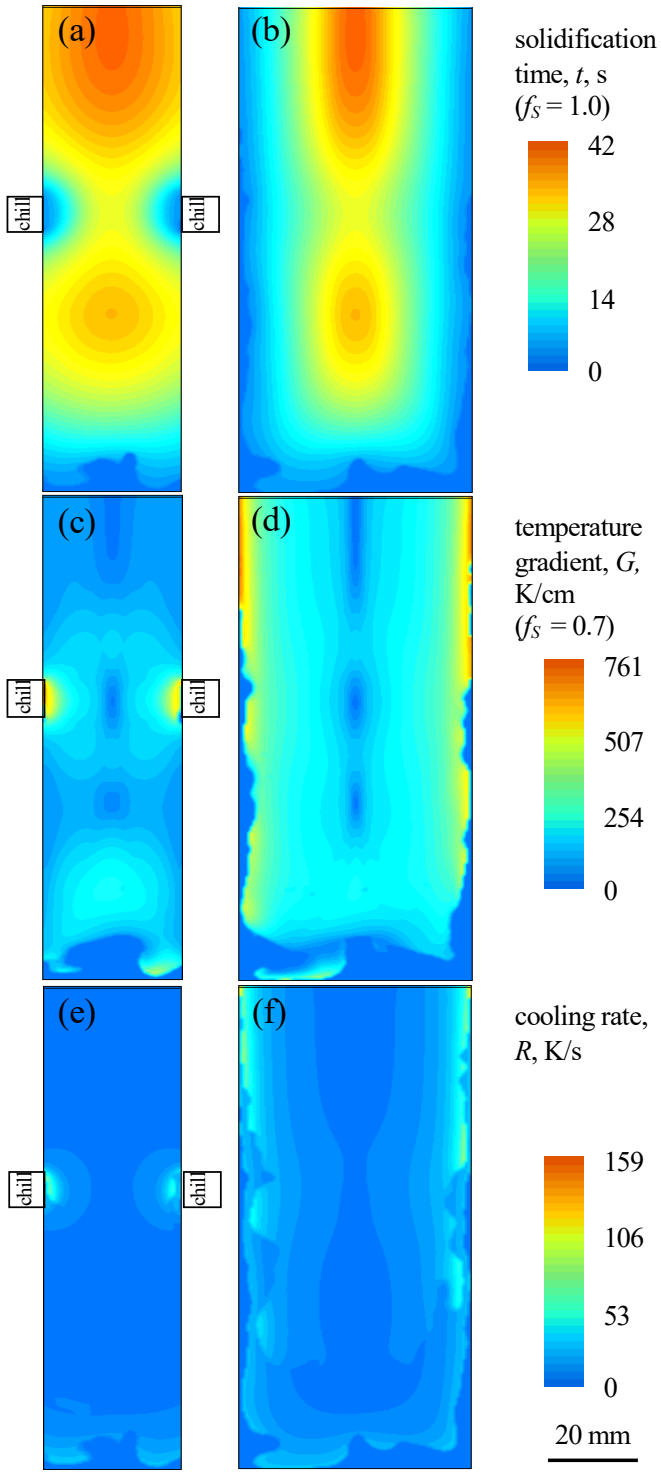

Fig. 2.1.4. (a)(b) Solidification time, (c)(d) the temperature gradient, (e)(f) cooling rate of the simulation case of sample No.1. Graphs (a), (c), and (e) are in the xz view, (b), (d), and (f) are in the yz view, as shown in Fig. 2.1.1.

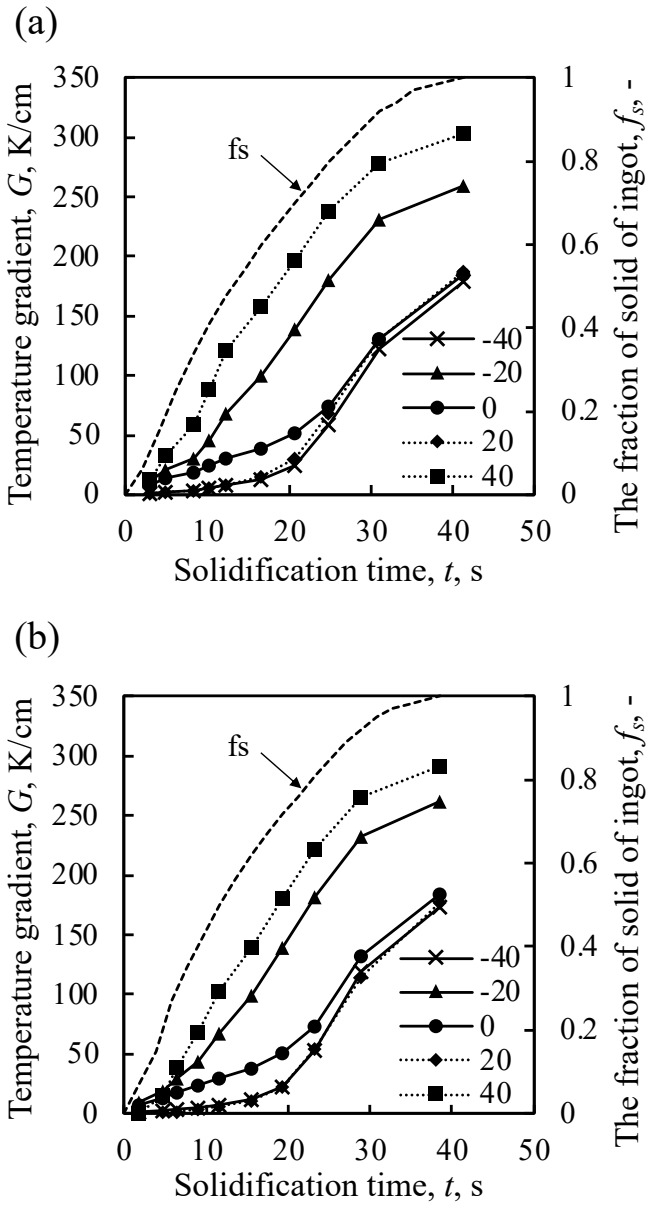

Fig. 2.1.5. The relationship between temperature gradient in the centerline and solidification time of the simulated case of the sample (a) No.1 and (b) No.2, respectively. 0 in the legend presents the lower side of the chill plate. -20 and -40 present 20 and 40 mm above the lower side of the chill plate, and 20 and 40 present 20 and 40 mm below the lower side of the chill plate, respectively.

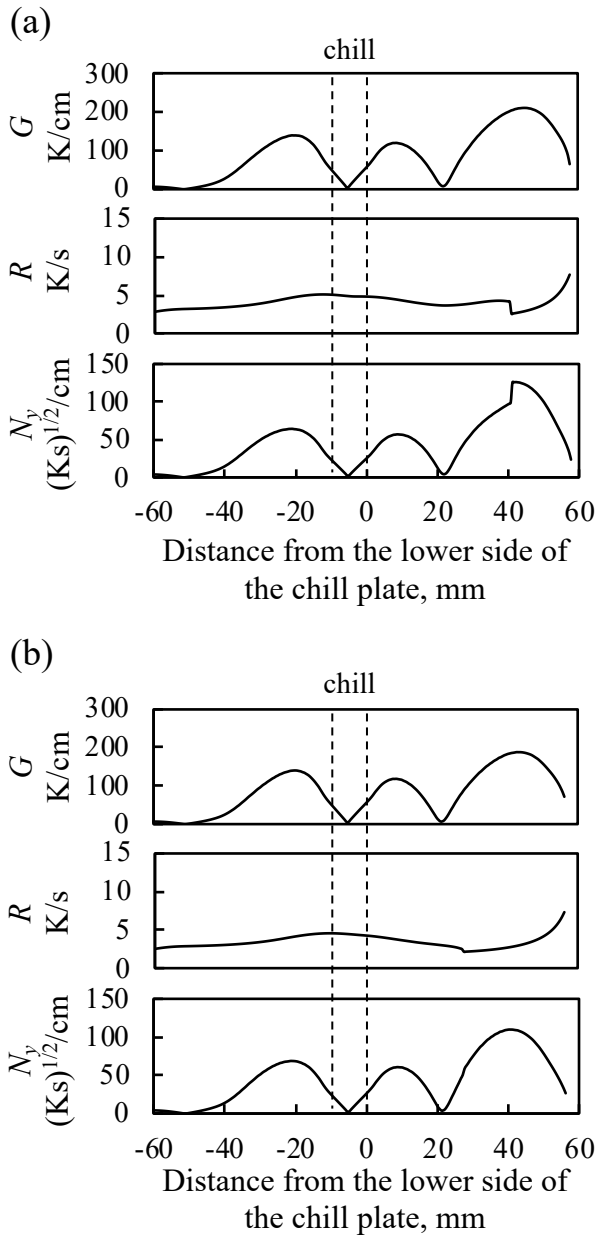

Fig. 2.1.6. Temperature gradient, cooling rate, and Niiyama criterion in the centerline when f_s equal 0.7 of the simulated case of the sample (a) No.1 and (b) No.2, respectively. -20, -40, and -60 present 20, 40, and 60 mm above the lower side of the chill plate, and 20, 40, and 60 present 20, 40, and 60 mm below the lower side of the chill plate, respectively.

To obtain the morphology of the shrinkage porosity more clearly, the serial sectioning method was used. And the porosity morphology is shown in Fig. 2.1.3. In the resulting 10 mm bridging area, there are some very fine shrinkage porosities. Also, there is a huge penetrating shrinkage porosity about 25 mm long below the bridging area. By an approximate calculation, the volume fraction of the shrinkage porosity is about 4.19% in the area from the top of the chill to the bottom of the ingot. Those defects below the bridging zone were attributed to the lack of molten metal since bridging occurred, resulting from the preferential growth of columnar dendrite near the chill plates.

The solid fraction was calculated. As shown in Fig. 2.1.4, the solidification time, the temperature gradient, and the cooling rate was calculated, and the solidification sequence can be qualitatively understood. From Fig. 2.1.4, the relationship between temperature gradient and solidification time of the simulated case of samples No.1 and No.2 is picked up and shown in Fig. 2.1.5 (a), (b). The lower side of the chill plate was set as the zero of the z-axis. -20 and -40 present 20 and 40 mm above the lower side of the chill plate, and 20 and 40 present 20 and 40 mm below the lower side of the chill plate, respectively. As shown in Fig. 2.1.6, temperature gradient, cooling rate, and Niiyama criterion[19] in the centerline when f_s equal 0.7 of the simulated case of the sample (a) No.1 and (b) No.2 were calculated from Fig. 2.1.4. According to the results of simulations, near the chill plates, the temperature gradient is larger, and the cooling rate is much faster. And the solidification process is significantly faster than the upper and lower part of the bridging area near the chill plates. The Niiyama criterion[19], N_y, a local thermal parameter, is defined as the ratio of the temperature gradient to the square root of the cooling rate, (Eqs. (2.1.3)), which is used for the prediction of shrinkage porosity. Shrinkage porosities are expected to form in the areas where Niiyama values are below a certain threshold.

$$N_y = \frac{G}{\sqrt{R}} \tag{2.1.3}$$

Where G is the temperature gradient and R is the cooling rate. As shown in Fig. 2.1.6 (a), the Niiyama criterion in the centerline of the simulated case of sample No.1 was calculated. The average cooling rate for the entire casting was 5.3 K/s, and the average cooling rate along the centerline was 4.2 K/s. Comparing the computed results with the actual casting observations, it could be concluded that when the overall solid fraction was 0.7, the threshold was about 5 $(Ks)^{1/2}$/cm, and it was about 30 $(Ks)^{1/2}$/cm when the fraction of solid equaled 1.

Generally, when the solid fraction in the cross-section of the casting exceeds about 70 vol.%, it was considered that the melt could hardly flow. However, some dendrites bridged, causing casting defects, such as huge shrinkages. It was observed that the columnar dendrite grew to about 5 mm from the surface of the mold, but it was about 8 mm in the bridging zone of sample No.1. It was considered the lower casting temperature dominated the formation of equiaxed dendrites in sample No.2. In sample No.2, those shrinkage porosities below the chill plates were attributed to the lack of molten metal, resulting from the higher nucleation rate of equiaxed dendrite near the chill plates.

In sample No.1, very fine dendrites and very large dendrites were observed below the shrinkage, as shown in Fig. 2.1.2 (d). According to the morphology of dendrite, the bridging zone can be divided into four areas from surface to center: developed fine columnar dendrite area, messy coarse dendrite area, messy and smaller equiaxed and columnar dendrite area, and coexisting area of the smallest one and the coarsen one. This separation results from the bridging zone producing a negative pressure in the lower part of the ingot, which enhances the effect of suction from the lower part. It can also be proved by the V-shape tendency of those regions with very fine dendrites.

2.1.3.2 Segregation analysis

It was considered that macrosegregation had occurred. An increase in the solute concentration of the sample predicts the result of an increase in liquid phase concentration with the growth of dendrites and suction flow between dendrites. The concentration of composition is attributed to the Scheil-Gulliver equation (Eqs. (2.1.4) and (2.1.5)) and lever rule (Eqs. (2.1.4) and (2.1.6)) according to the solid-phase diffusion. [1,20-26)]

$$C_S^* = k_0 C_L^* \tag{2.1.4}$$

$$C_L^* = C_0(1 - f_S)^{(k_0 - 1)} \tag{2.1.5}$$

$$C_L^* = C_0(f_S \cdot k_0 + 1 - f_S)^{-1} \tag{2.1.6}$$

Where C_L^* and C_S^* are the interface concentrations in the liquid phase and solid phase, k_0 is the equilibrium partition coefficient, and f_s is the fraction of solid. The liquid phase concentration of each element was predicted using the initial composition and partition coefficient. As shown in Table 2.1.1, the k_0 of C is 0.35-0.50[27,28)], and the carbon concentration of melt is 0.51 in the peritectic reaction and 4.32 in the eutectic reaction. The elements contained in relatively large amounts are Mn and Si, but the partition coefficient is also as large as 0.5[29)] (Si) and 0.75[30)] (Mn). Therefore, assuming that f_s equals 0.6, the concentration of Si and Mn in the liquid phase is about 0.8 mass% and 1 mass%, respectively, as shown in Fig. 2.1.7. And the k_0 of P and S is 0.06[29)] and 0.02[29)], respectively. On the other hand, P and S have small partition coefficients, and they were as high as 0.14 mass% P and 0.07 mass% S when f_s equals 0.6, despite the initial compositions of 0.06 mass% and 0.03 mass%, respectively.

Table 2.1.1 Parameter for lever rule and Scheil equation

	C_0 (mass%)	k_0	Composition	ref.
C	0.45	0.35-0.50	0.51-4.32	27,28)
Si	0.5	0.5	-	29)
Mn	0.8	0.75	-	30)
P	0.06	0.06	-	29)
S	0.03	0.02	-	29)

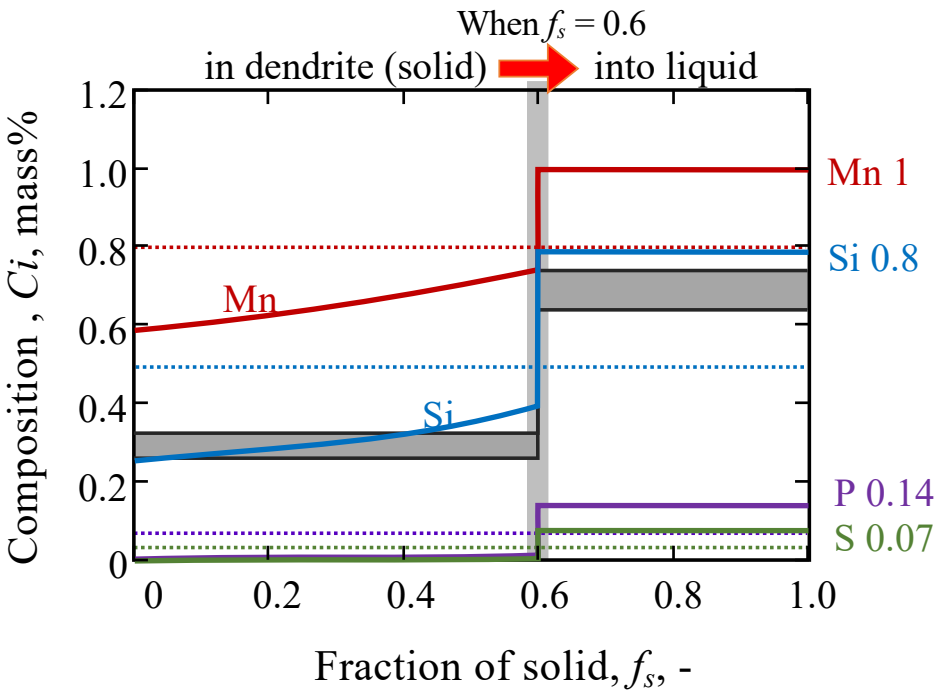

Fig. 2.1.7. Estimation of pile up composition by lever rule and Scheil-Gulliver equation at *fs*=0.6.

EPMA line analyses present the composition changes with positions along the selected lines. Segregation can be measured along the chosen line crossing some secondary dendrite arms. Any abnormal segregation features, such as saw-tooth profiles, can be shown by line analysis. However, the line analysis method is based on 2-D data, and it may lose some segregation features of dendrite structures, such as the maximum element concentration in the most segregated region. Therefore, line analysis parallels to the casting direction and perpendicular to the casting direction was set, respectively, as shown in Fig. 2.1.8, to demonstrate the relative concentration difference of the elements in different areas of the sample. Results of the composition of alloying elements determined from EPMA line analyses are shown in Fig. 2.1.9 - Fig. 2.1.12. Line analysis of the concentration of carbon, phosphorus, and manganese in the vertical direction in samples No.1 and No.2 is shown in Fig. 2.1.9. Microsegregation of alloying elements occurring between the interdendritic region and dendritic could be observed by saw-tooth profiles that were demonstrated by line analysis. The solid circle dots in the figure represent the mean concentration per 1 mm. The blank part in results (1) and (11) shown in Fig. 2.1.9 is where the shrinkage porosity is located. Viewed from the longitudinal section of sample No.1, carbon and phosphorus were diluted along the centerline and concentrated in the area near the interface between the columnar dendrite and the equiaxed dendrite. Also, carbon was concentrated in the area near the surface of the bottom. In addition, manganese was concentrated below the porosity and the area near the bottom of the centerline. From sample No.2, carbon was concentrated under porosity in the equiaxed dendrite area. Phosphorus was concentrated below the bridging zone, and manganese was homogeneously distributed macroscopically. Line analysis of carbon, phosphorus, and manganese concentration in the horizontal direction in sample No.1 was performed, as

shown in Fig. 2.1.10, Fig. 2.1.11, and Fig. 2.1.12, respectively. Some scattered segregation areas marked by circles can be observed. Especially in the bridging area and the area under the shrinkage porosity, apparent positive segregation occurred.

The solidified structure of the cross-section at the corresponding position of the line analysis was observed to demonstrate the mechanism of the formation of the segregation. As shown in Fig. 2.1.13, the solidification microstructure and the SDAS on the horizontal (yz) section of sample No.1, (a) 5 mm above the lower side of the chill plate, (b) 23 mm below the lower side of the chill plate, (c) 38 mm below the lower side of the chill plate, was observed. The line analysis on the longitudinal section corresponding to the three cross-sections shown in Fig. 2.1.13 is Fig. 2.1.8 (a) (5), (8), and (9), respectively. The dashed lines marked in the solidification micrograph, as shown in Fig. 2.1.13, represent the interfaces between dendrites with different morphologies, as mentioned above. In sample No.1, the length of the columnar dendrite is about 4 mm from the surface of the ingot in the area near the bottom of the ingot, about 5 mm in the area below porosity, and about 8 mm in the bridging area. The SDAS in those areas is less than 100 μm. Coarser secondary dendrites can be observed in the region along the centerline, and the SDAS is about 160 μm. In addition, fine dendrites can also be observed in this area, and the SDAS is similar to the dendrites near the mold. The region where these fine dendrites exist was considered to be the final solidification region, and it was also considered to be the enriched region of alloying elements with a small equilibrium partition coefficient.

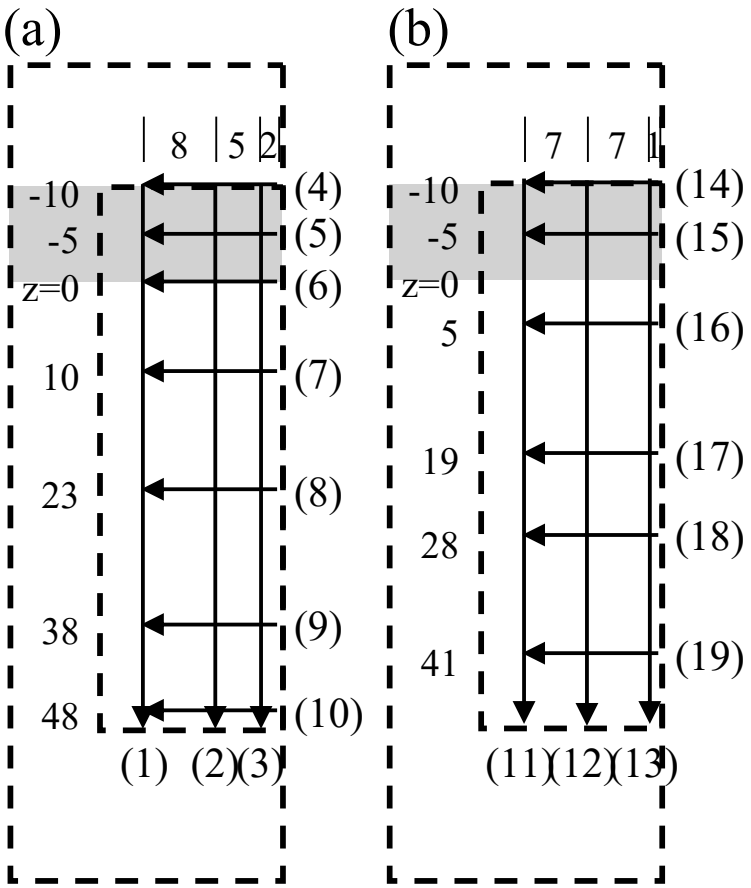

Fig. 2.1.8. Position of EPMA line analysis on the longitudinal section (xz view in Fig. 2.1.1) of (a) sample No.1 and (b) sample No.2. The shaded area in the schematic drawing is the bridging area. (unit: mm)

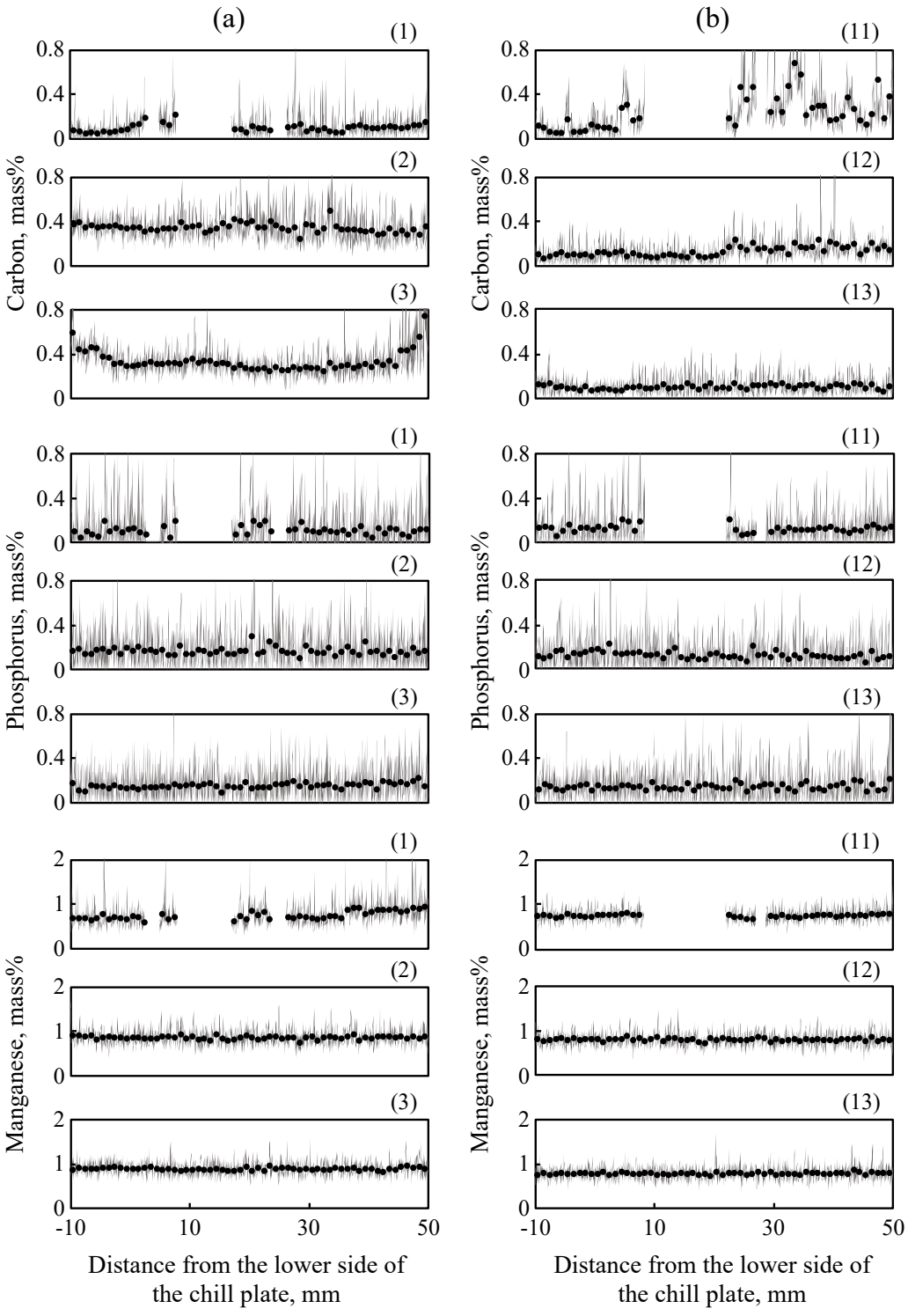

Fig. 2.1.9. Line analysis of the concentration of carbon, phosphorus, and manganese in the vertical direction in samples (a) No.1 and (b) No.2, as shown in Fig. 2.1.8 (a), (b), respectively.

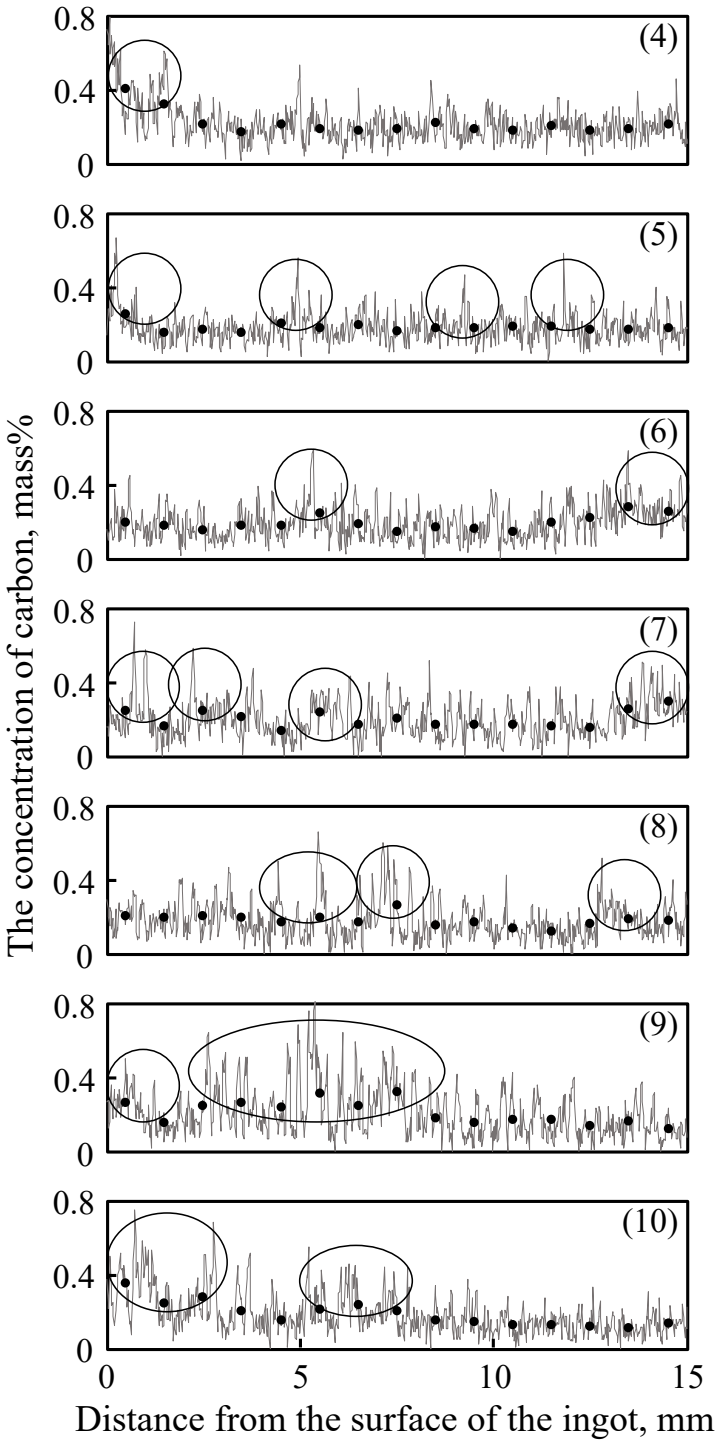

Fig. 2.1.10. Line analysis of the concentration of carbon in the horizontal direction in sample No.1, as shown in Fig. 2.1.8 (a).

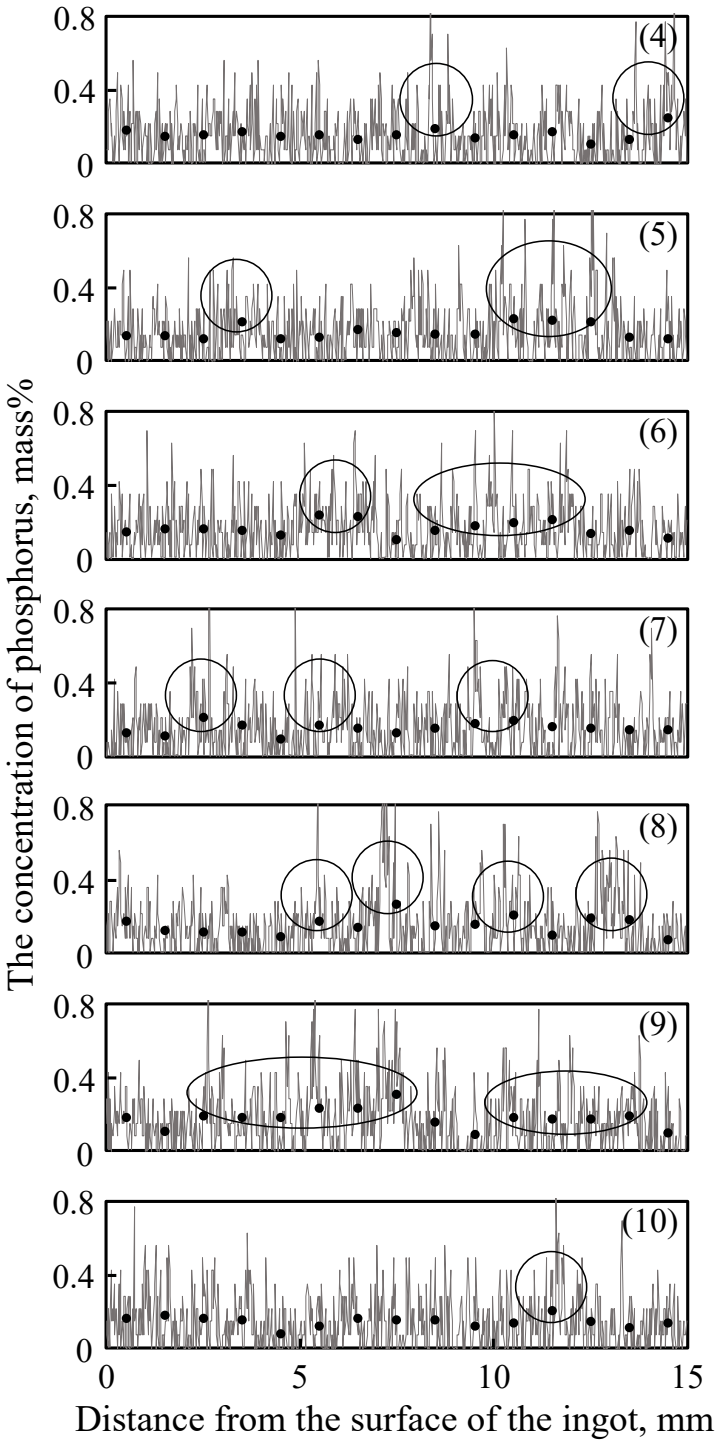

Fig. 2.1.11. Line analysis of the concentration of phosphorus in the horizontal direction in sample No.1, as shown in Fig. 2.1.8 (a).

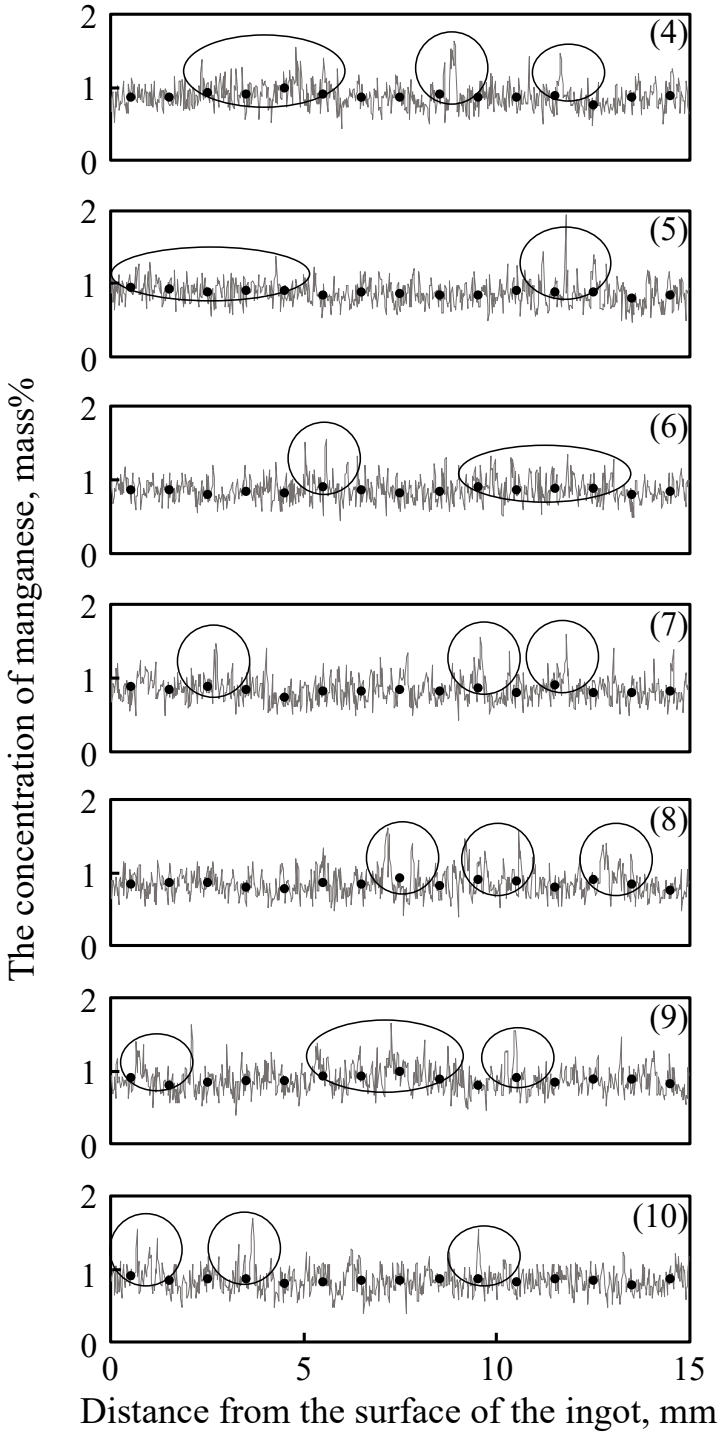

Fig. 2.1.12. Line analysis of the concentration of manganese in the horizontal direction in sample No.1, as shown in Fig. 2.1.8 (a).

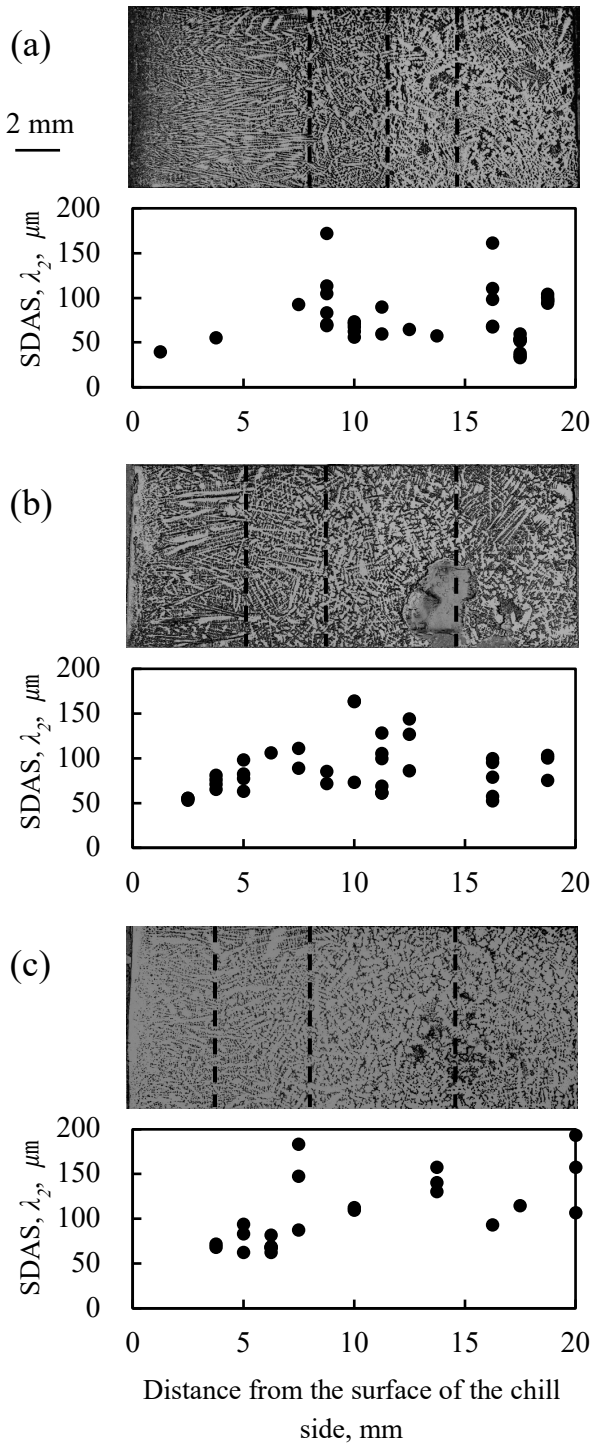

Fig. 2.1.13. Solidification microstructure and the SDAS in the horizontal section (xy view) in sample No.1, (a) 5 mm above the lower side of the chill plate, (b) 23 mm below the lower side of the chill plate, and (c) 38 mm below the lower side of the chill plate, respectively.

2.1.3.3 Formation mechanism of macrosegregation

Combining the line analysis results and the images of the solidified structure, in the area below the bridging of the casting, point-like or band-like, or channel-type[31] positive macrosegregation occurred at the interface between columnar dendrites and equiaxed dendrites. An overview of the analysis results of sample No.1 is shown in Fig. 2.1.14 (e). And in the final solidification region near the shrinkage porosity, a point-like distribution of positive segregation occurred, as shown in Fig. 2.1.14 (f).

As shown in Fig. 2.1.14 (a), solidification progressed from the surface of the chill. The solidification rate was higher around the chill plate, where thermal conductivity was higher than that in other areas. In the middle stage of solidification, as shown in Fig. 2.1.14 (b), there was a tendency to form bridging because of the rapid growth of dendrites near the chill plates. As shown in Fig. 2.1.14 (c), the liquid phase was separated by the bridging zone. As the solidification progressed, negative pressure was formed at the bottom, suction occurred, and the concentrated melt flowed into the bottom from the solid-liquid coexistence region, as indicated by the black arrow in the figure. In addition, the liquid phase flowed into the solid-liquid coexistence region of the bridging from the upper part. After the solidification contraction flow stopped, point-like positive and negative segregation along the V-shaped distribution and tiny shrinkage porosities were formed in the bridging zone. In the lower part of the mold, coarse shrinkage porosity was formed, as shown in Fig. 2.1.14 (d). The concentrated liquid phase remained in this region, and finally, the macrosegregation occurred mainly at the bottom of the shrinkage porosity. In addition, in sample No.2, the massy solidification occurs because of low superheating, and the V-shaped segregation near the bridging zone might be small.

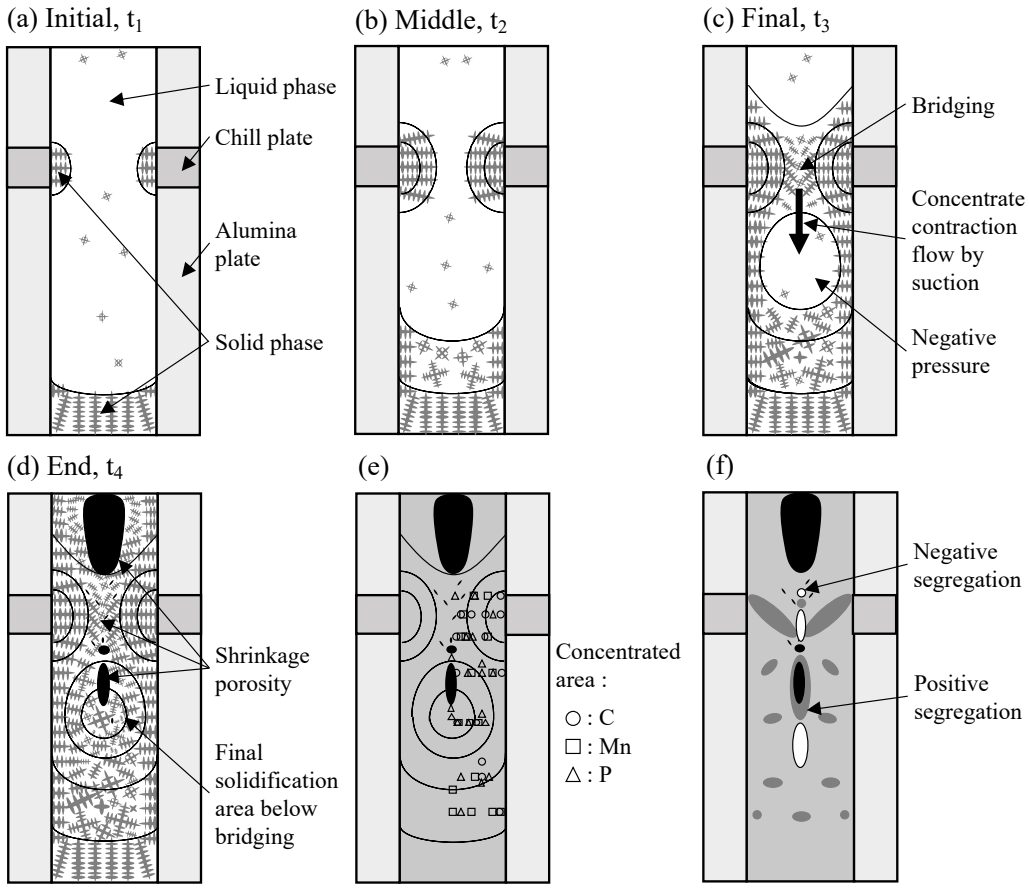

Fig. 2.1.14. Schematic drawing of (a-d) solidification and formation of (f) casting defects in the local-chilled mold used in this study. (e) Overview of analysis results of sample No.1.

2.1.4 Conclusions

A model casting experiment was adopted to understand the formation mechanism of macrosegregation of steel casting that occurred by local bridging during solidification with a laboratory-scale local-chilled mold. The obtained results are as follows.

(1) Columnar dendrites and equiaxed dendrites with extremely different morphologies were observed in the sample with a high superheating of 100 °C, however, equiaxed dendrites with similar morphology, except a very small amount of columnar dendrites, could be observed in the sample with a low superheating of 30 °C.

(2) Chill plates successfully formed the columnar dendrite bridging area and the columnar dendrite shell in the sample with high superheating by the laboratory-scale local-chilled mold.

(3) V segregation was formed at the bridging area, and large shrinkage porosities were formed under a high casting temperature, while a lower casting temperature increased the grain density and formed shrinkage porosities that were smaller in size but larger in number and more dispersed.

(4) In the sample with high superheating of 100 °C, fine and coarse dendrites appeared near the large shrinkage porosity. In the area below the bridging of the casting, point-like or band-like positive macrosegregation occurred in the interdendritic region between columnar dendrites and equiaxed dendrites. And in the final solidification region around the shrinkage porosity, positive macrosegregation occurred.

References

1) M. C. Flemings: *Metall. Trans. B*, **5** (1974), 2121. https://doi.org/10.1007/BF02643923
2) M. C. Flemings: *ISIJ Int.*, **40** (2000), 833. https://doi.org/10.2355/isijinternational.40.833
3) E. J. Pickering: *ISIJ Int.*, **53** (2013), 935. https://doi.org/10.2355/isijinternational.53.935
4) M. C. Flemings: Solidification Processing, McGraw-Hill, NY, (1974).
5) R. Mehrabian, M. Keane, and M. C. Flemings: *Metall. Mater. Trans. B*, **1** (1970), 1209. https://doi.org/10.1007/BF02900233
6) T. Murao, T. Kajitani, H. Yamamura, K. Anzai, K. Oikawa, and T. Sawada: *Tetsu-to-Hagané*, **99** (2013), 94. (in Japanese). https://doi.org/10.2355/tetsutohagane.99.94
7) S. K. Choudhary, and S. Ganguly: *ISIJ Int.*, **47** (2007), 1759. https://doi.org/10.2355/isijinternational.47.1759
8) Y. Natsume: *Tetsu-to-Hagané*, **103** (2017), 738. (in Japanese). https://doi.org/10.2355/tetsutohagane.TETSU-2017-062
9) F. Satou, H. Esaka, and K. Shinozuka: *Tetsu-to-Hagané*, **99** (2013), 101. (in Japanese). https://doi.org/10.2355/tetsutohagane.99.101
10) E. Aritaka, H. Esaka, and K. Shinozuka: *Tetsu-to-Hagané*, **104** (2018), 293. (in Japanese). https://doi.org/10.2355/tetsutohagane.TETSU-2017-096
11) T. Kawawa, and Y. Tsuchida: Materials of the 21st Conference on Solidification Phenomena, (Solidification 156), Japan Society for the Promotion of Science, (1974).
12) H. Esaka, and S. Ogibayashi: *Tetsu-to-Hagané*, **84** (1998), 49.

13) B. Weisgerber, M. Hecht, and K. Harste: *Steel Res.*, **70** (1999), 403. https://doi.org/10.1002/srin.199905659

14) M. Bobadilla, J. M. Jolivet, J. Y. Lamant, and M. Larrecq: *Mater. Sci. Eng. A*, **173** (1993), 275. https://doi.org/10.1016/0921-5093(93)90229-8

15) D. W. Guo, Z. B. Hou, Z. Q. Peng, Q. Liu, Y. Chang, and J. H. Cao: *ISIJ Int.*, **61** (2021), 844.

16) K. A. Jackson, J. D. Hunt, D. R. Uhlmann, and T. P. Seward: *Trans. Metall. Soc. AIME*, **236** (1966), 149.

17) K. P. Young, and D. H. Kerkwood: *Metall. Mater. Trans. A*, **6** (1975), 197. https://doi.org/10.1007/BF02673688

18) JSCAST. http://www.iesol.com (accessed 2019-10-01).

19) E. Niyama, T. Uchida, M. Morikawa, and S. Saito: *AFS Cast Met. Res. J.*, **7** (1982), 52.

20) E. Scheil: *Z. Metallkd.*, **34** (1942), 70.

21) G. H. Gulliver: *J. Inst. Met.*, **9** (1913), 70.

22) H. D. Brody: Ph.D. thesis, Massachusetts Institute of Technology, (1965). https://dspace.mit.edu/bitstream/handle/1721.1/13371/25362444-MIT.pdf?sequence=2

23) H. D. Brody, and M. C. Flemings: *Trans. Metall. Soc. AIME*, **236** (1966), 615.

24) T. F. Bower, H. D. Brody, and M. C. Flemings: *Trans. Metall. Soc. AIME*, **236** (1966), 624.

25) T. W. Clyne, and W. Kurz: *Metall. Trans. A*, **12** (1981), 965. https://doi.org/10.1007/BF02643477

26) M. C. Flemings: *Metall. Trans. A*, **22** (1991), 957. https://doi.org/10.1007/BF02661090

27) M. G. BENZ, and J. F. ELLIOTT: *Trans. Metall. Soc. AIME*, **221** (1961), 323.

28) R. Tanaka: *Tetsu-to-Hagané*, **53** (1967), 1586. (in Japanese). https://doi.org/10.2355/tetsutohagane1955.53.14_1586

29) J. Chipman: *Basic Open Hearth Steelmaking, Physical Chemistry of Steelmak ing Committee, Iron and Steel Division, AIME*, (1951), 632.

30) C. E. Sims: *Electric Furnace Steelmaking*, **2** (1962), 99.

31) N. Mori and K. Ōgi: *Metall. Mater. Trans. A*, **22** (1991), 1663. https://doi.org/10.1007/BF02667378

2.2 Influence of bridging on macrosegregation in the medium-carbon steel cast with a laboratory-scale middle-chilled mold

2.2.1 Introduction

Currently, steel is manufactured by continuous casting or large-sized ingot casting,[1)] and macrosegregation[1-5)] that occurs during the manufacturing process significantly impacts product quality in terms of cracks and deterioration of mechanical properties[1)]. Therefore, it is required to eliminate macrosegregation in castings as much as possible.[6)] Macrosegregation occurs due to the local accumulation of rejected solute by transport over relatively long distances through the casting. Numerical calculation methods based on analytical formulas[7-10)] and mathematical models[11-14)] have been proposed for research on microsegregation. The development of defect prediction methods using numerical simulation is remarkable, but the prediction of macrosegregation is still in the developmental stage since macrosegregation is a complex phenomenon caused by convection and other factors in microsegregation, so it is not easy to analyze and predict the segregation position[15)]. The main types of macrosegregation in the continuous casting process or ingot casting are centerline segregation, A segregation, and V segregation.[1,4,16-21)] Regarding the centerline segregation, the liquid phase is concentrated due to the redistribution of solutes during solidification, and the concentrated liquid phase accumulates due to the flow of molten alloy at the final stage of solidification.[15)] And the concentration in the segregated part is about 2.5 times higher for carbon and about five times higher for sulfur, *etc.*, compared to the initial concentration in the continuous casting process.[22)] And the solidification microstructures in castings are often locally quite different due to the occurrence of bridging[17)] and contraction flow during solidification.[23)] At the bridging region, the developed dendrites are bridged, concentrated

melt between dendrites flows along the casting direction by suction due to solidification shrinkage, and severe segregation is formed[6,24].

In recent years, research has been conducted to understand the essence of macrosegregation. Aritaka *et al.*[25] investigated the flow of the residual liquid phase in the interstices of dendrites by observing the movement of bubbles in the final stage of solidification. In addition, Satou *et al.*[26] conducted a laboratory-scale model experiment in which bridging was intentionally caused by locally enhanced cooling in a simple mold to investigate the relationship between solidified structure and macrosegregation using Al-10mass%Cu alloy. Since it successfully formed bridges during the solidification of Al-10mass%Cu alloys and caused macrosegregation, which has important reference significance for the study on macrosegregation of steel.

To clarify the principle of casting defects, such as shrinkage porosity and macrosegregation, due to the formation of bridging during the solidification of steel, the samples were cast by a laboratory-scale local-chilled mold in which the upper part was forcedly cooled to cause bridging, and the bridging, shrinkage porosities, and macrosegregation were observed successfully. However, due to the small size of the mold, the upper part of the bridging area does not have enough melt to supplement the effect of solidification shrinkage. Therefore, the mold was improved, and the height of the mold was increased so that the bridging area was set in the center of the casting. In this study, the solidification structure morphology was observed, concentration analysis of alloying elements was performed, and the effect of bridging on macrosegregation was investigated.

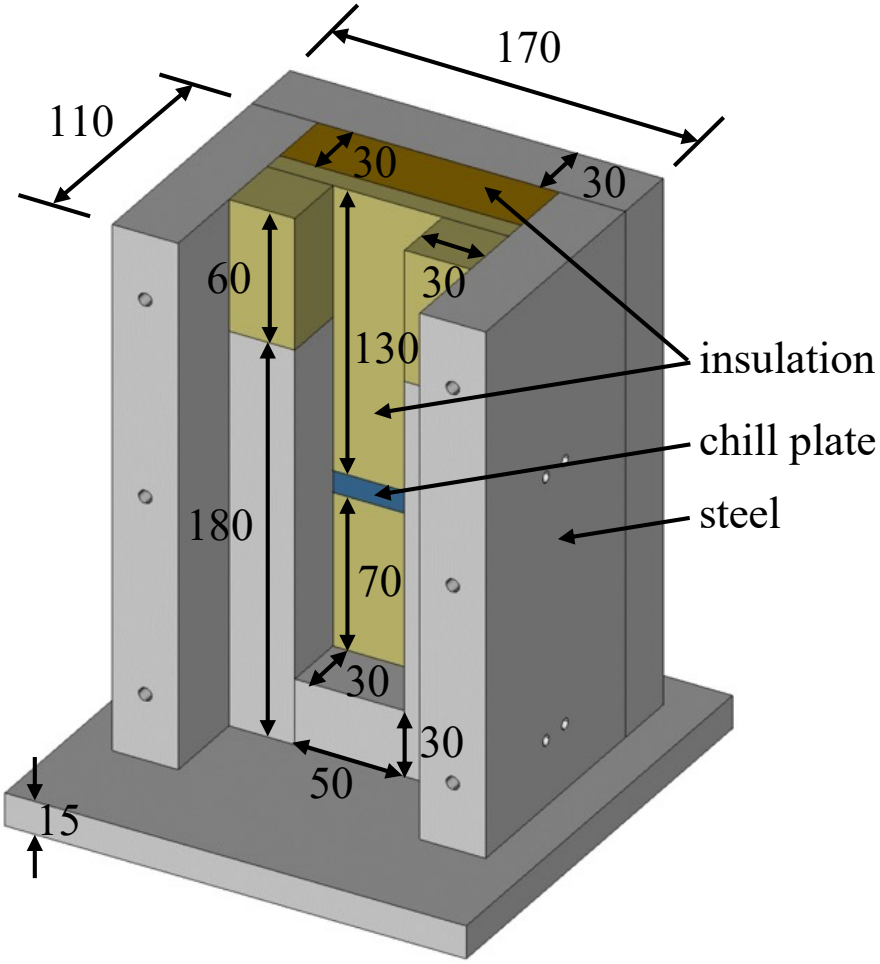

Fig. 2.2.1. Schematic drawing of the mold. (unit: mm)

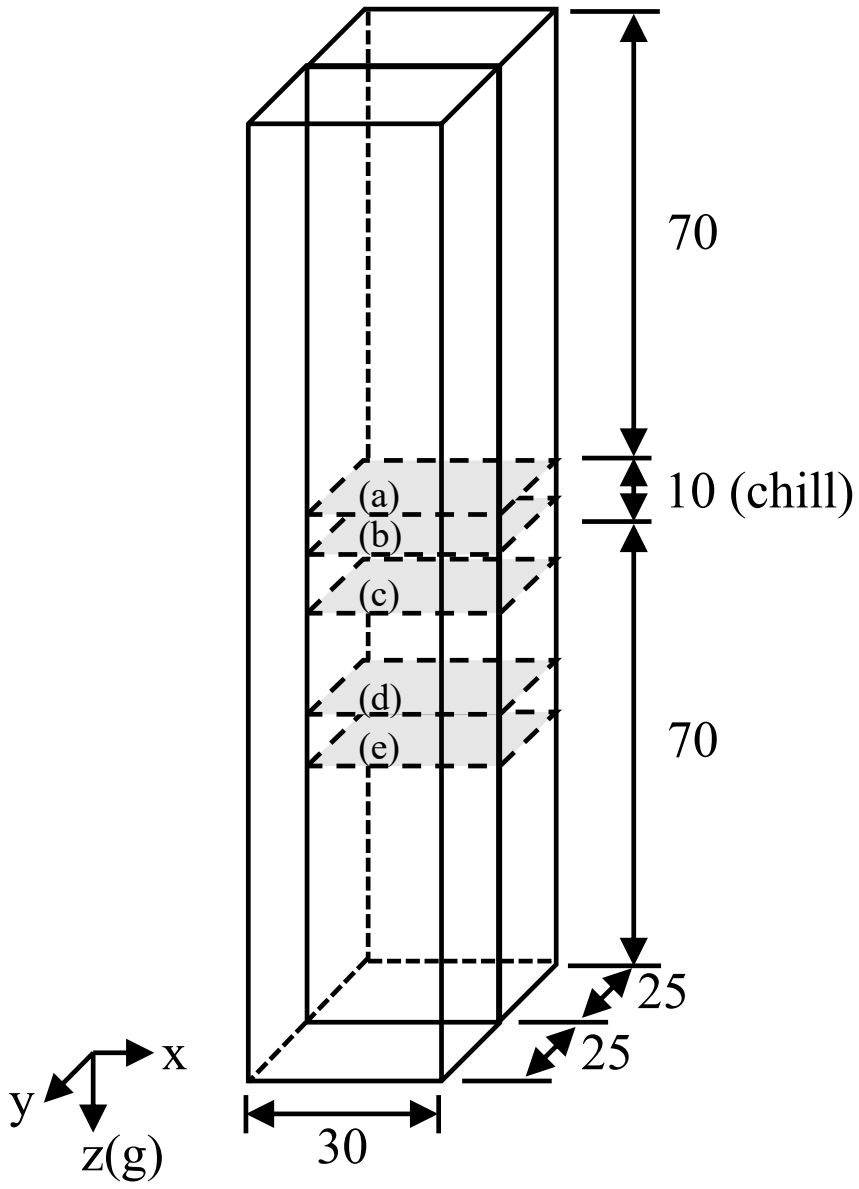

Fig. 2.2.2. Schematic drawing of observation part in the ingot. (unit: mm)

2.2.2 Experimental procedure

Medium-carbon steel was used in this study. The chemical composition (in mass%) of the sample was 0.45% Carbon, 0.5% Silicon, 0.8% Manganese, 0.06% Phosphorus, and 0.03% Sulfur. A schematic diagram of the mold is shown in Fig. 2.2.1. The inner dimension of the mold was 30 mm (T) × 50 mm (W) × 210 mm (H). A pair of chill plates with a thickness of 10 mm, which caused bridging in the ingot, were installed in the mold at 70 mm from the bottom of the mold to increase the cooling rate locally, as shown in blue in Fig. 2.2.1. The inside part of the mold was thermally insulated with porous alumina ceramic plates, as shown in yellow and yellow-brown in Fig. 2.2.1. The outside part of the mold and the U-shaped support structure including the bottom was made of SUS304 to give strength, as shown in grey in Fig. 2.2.1. And a BN-based mold release agent was used. The casting temperature of samples No.1, No.2, and No.3 was 1670 °C, 1539 °C, and 1670 °C, respectively. Sample No.1 and No.2 were cast using the mold with the chill plates, and sample No.3 was cast using a mold without the chill plates, which was set as a control group, to investigate the effect of bridging on macrosegregation with and without chill plates. In the mold without chill plates, the material of the chill plate was replaced with insulation.

The cutting procedure of samples is shown in Fig. 2.2.2. First, the sample was cut vertically at the center of the width. Next, after observations on the longitudinal section were performed, the sample was cut into 25 mm × 30 mm × 1 mm. After grinding with emery paper and mirror polishing by diamond paste (1 μm and 0.25 μm), samples were etched with the saturated picric acid aqueous solution. The microstructural morphology of etched samples was observed using an optical microscope (Nikon ECLIPSE L150) and a stereomicroscope (Nikon system stereomicroscope SMZ1500). The secondary dendrite

arm spacing (SDAS) was also measured.

The concentration of the alloying elements in the area near the chill in the longitudinal section of sample No.1 and sample No.2 was analyzed by an electron probe micro-analyzer (EPMA, Shimadzu EPMA 1720) on polished surfaces with an acceleration voltage of 20 kV. In addition, quantitative mapping analysis was performed using scanning electron microscopy – energy dispersive x-ray spectroscopy (SEM-EDX, SU3500, Hitachi High-Tech Co., Ltd.) to measure macrosegregation of sample No.1 and sample No.3. The analysis conditions for SEM-EDX were an acceleration voltage of 15 kV, a magnification of 100 times, and a matrix of 256 × 200. And 15 areas of each piece of the sample were analyzed.

2.2.3 Results and discussion

2.2.3.1 Solidification structure and defects

Samples were etched with the saturated picric acid aqueous solution, and the microstructural morphology was observed. The solidification structure in the longitudinal section of the ingot without sprue is shown in Fig. 2.2.3. The columnar dendrite and a small number of equiaxed dendrites were observed in sample No.1 (Fig. 2.2.3 (a)) and sample No.3 (Fig. 2.2.3 (c)), which were cast at a higher casting temperature. And only the equiaxed dendrite was observed in sample No.2 (Fig. 2.2.3 (b)), which was cast at a lower casting temperature, although this sample was cast by the mold equipped with chill plates. Therefore, the large temperature gradient produced by high casting temperature has a great influence on the morphology of solidified structure, which can promote the formation of columnar dendrite. In addition, since the growth direction of the columnar dendrite is opposite to the direction of heat flow, and the temperature of the melt was

higher than that of the mold, the columnar dendrites grew from the surface of the mold toward the center of the ingot.

A few large shrinkage porosities below the bridging area formed by chill plates were observed in sample No.1 (Fig. 2.2.3 (a)). In addition, some tiny shrinkage porosities scattered around the centerline of the ingot in the V shape were observed in the low superheating sample No.2 (Fig. 2.2.3 (b)), and several shrinkage porosities smaller than those in sample No.1 were observed in both upper and lower regions of sample No.3 (Fig. 2.2.3 (c)). The shrinkage porosities in the three samples were significantly different in number, size, morphology, and position. The huge shrinkage porosities in sample No.1 were considered to be caused by the bridging that occurred in the middle of the ingot since the local cooling was strengthened by chill plates, which prevents the upper melt from compensating for solidification shrinkage in the lower part of the ingot. In sample No.2, those tiny shrinkage porosities were attributed to the lack of molten metal, resulting from the higher nucleation rate of equiaxed dendrite in the entire ingot and the natural convection during solidification. In sample No.3, those small shrinkage porosities scattered in the central equiaxed dendrite region were smaller and located more upward. This result was similar to that of ordinary ingot casting, but during the solidification process, the shrinkage porosities were affected by locally developed columnar dendrites and dispersed into multiple smaller ones.

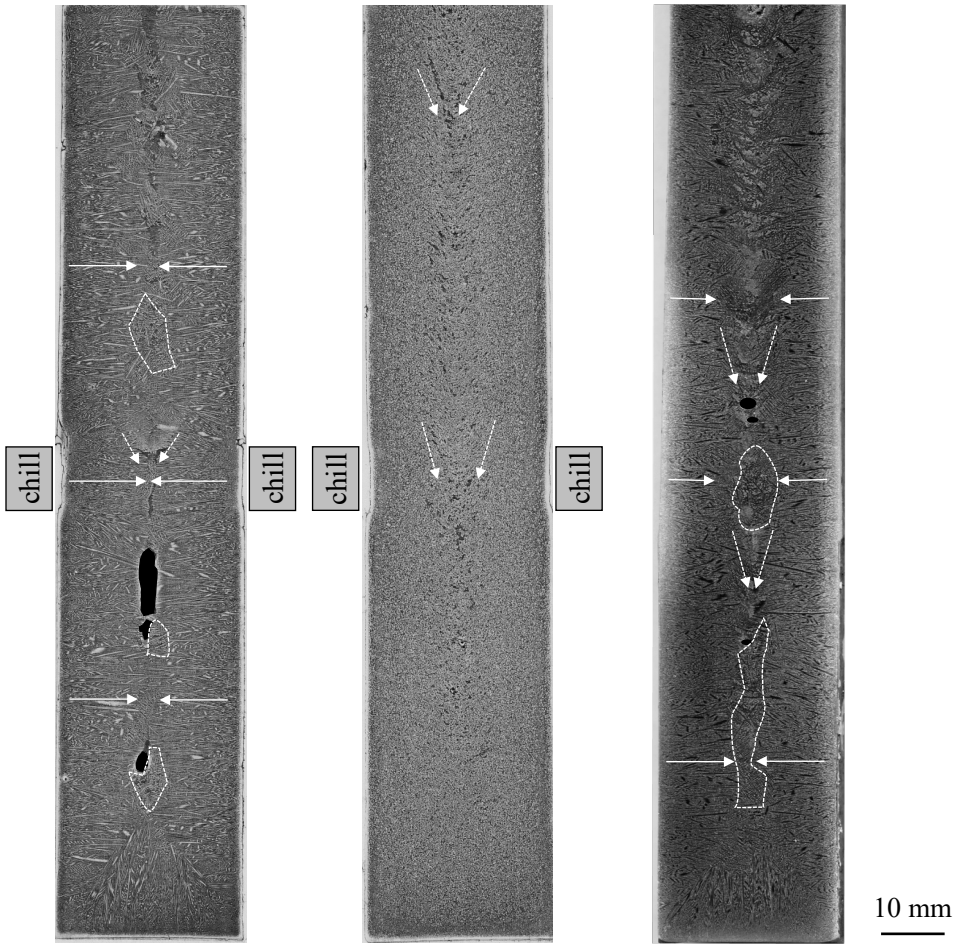

Fig. 2.2.3. Solidification structure in the longitudinal section of the sample (a) No.1, (b) No.2, and (c) No.3.

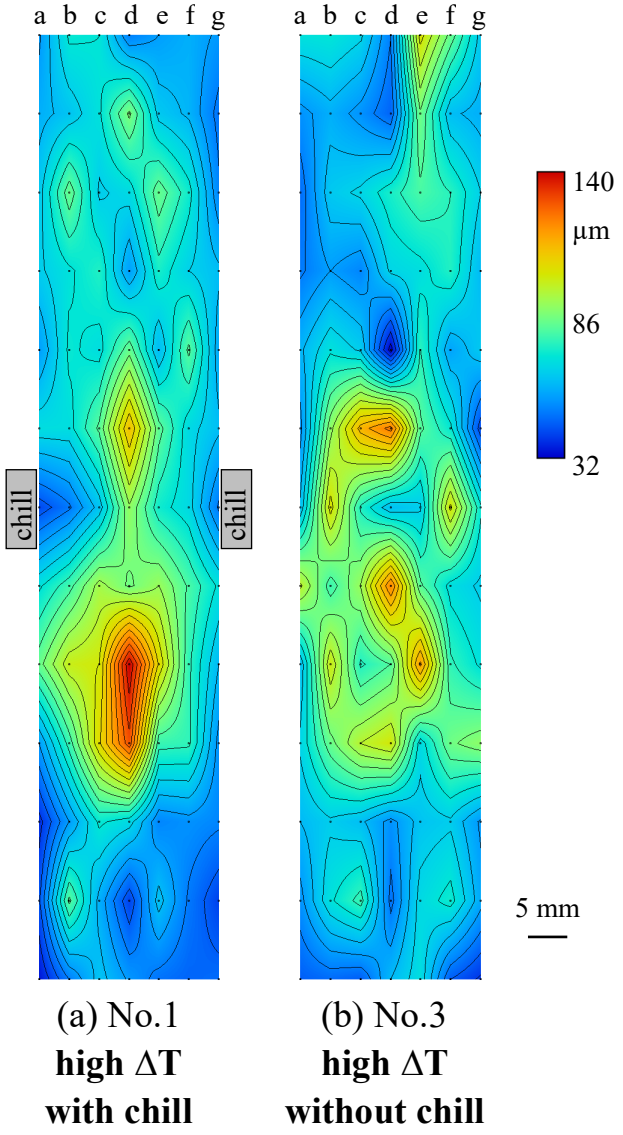

Fig. 2.2.4. Secondary dendrite arm spacing (SDAS, λ_2, μm) in the longitudinal section of the sample (a) No.1, and (b) No.3, respectively. a, 3.7 mm, b, 7.5 mm, c, 11.3 mm from the left surface of the ingot, d, centerline of the ingot, e, 11.3 mm, f, 7.5 mm, g, 3.7 mm from the right surface of the ingot.

The SDAS in the longitudinal section of sample No.1 and sample No.3 was also measured, and where there was a shrinkage porosity, the dendrite in the nearest area was measured. The measurement results of sample No.1 and sample No.3 are shown in Fig. 2.2.4 (a) and Fig. 2.2.4 (b), respectively. The SDAS of the dendrite near the chill plate and the bottom is the smallest at about 32 μm, while the SDAS of the dendrite in the lower middle region of the ingot exceeds 100 μm. It is worth noting that there are two regions with large SDAS in the bottom region of both samples cast at high casting temperature, and those regions are symmetrical about the center line. This was considered to be caused by the growth of dendrites that settled to the bottom with natural convection, and it proves that convection existed in this casting experiment, and the influence of convection needs to be considered when considering the formation mechanism of the solidification structure.

Comparing the results of solidification structure morphology shown in Fig. 2.2.3 and the SDAS shown in Fig. 2.2.4, the equiaxed dendrite area near the shrinkage porosity has smaller SDAS, which is considered to be the final solidification area. In sample No.1, the solidification structure near the chill plates and its upper and lower areas are almost developed columnar dendrites, as shown by the white solid arrow in Fig. 2.2.3 (a), where the direction of the arrow indicates the growth direction of the columnar dendrites. The areas enclosed by the white dotted lines are the equiaxed dendrite regions, and the V-shaped distribution tendency of the fine shrinkage porosities is pointed out by the dotted arrows. It can be observed that in the center of the bridging area, oppositely growing columnar dendrites intersect, and there is a huge shrinkage porosity below it, while the area immediately to the bottom of the shrinkage porosity is an equiaxed dendrite region with fine dendrite arm spacing. As shown in Fig. 2.2.3 (c), in sample No. 3, because there

is no chill plate, the solidification structure shows a columnar dendrite area near the surface, and there are some larger equiaxed dendrite areas and smaller solidification shrinkage porosities in the middle part of the casting. In addition, in the lower right areas near the middle of casting as shown in Fig. 2.2.4 (a) and (b), the results of SDAS are relatively small, which was consistent with the observed solidification structures shown in Fig. 2.2.3 (a) and (c). Considering that the concentration of solute will lead to the reduction of the SDAS, it can be speculated that the equiaxed dendrite region near the bottom of the shrinkage porosity is the final solidification area in the lower part of the casting, and it is the region where segregation might occur.

2.2.3.2 Segregation analysis

It is generally believed that centerline segregation as a problem in the continuous casting of steel is mainly caused by solidification contraction flow, bridging caused by solidification structure, and forced flow caused by roll extrusion. The EPMA mapping analysis of the concentration of silicon, manganese, and sulfur in the area near the chill in the longitudinal section of samples was carried out, and the macroscopic display of the segregation near the chill plate was obtained, the results of sample No.1 and sample No.2 are shown in Fig. 2.2.5 (a) and (b), respectively. The analysis was performed in two adjacent square areas with a side length of 25 mm. The results of manganese and sulfur clearly show the formation of segregation, and the positions of the positive and negative segregation of manganese and sulfur coincide with each other, which indicates that compounds of manganese and sulfur, such as manganese sulfide, may be formed during the solidification process. As shown in Fig. 2.2.5 (a), in the results of manganese of sample No.1, there is a significant negative segregation area at the position marked by

the solid black line (1), and this area is located directly above the bridging, while there is positive segregation below it. In addition, there is a long and narrow positive segregation area at the center of the bridging marked by the solid black line (2), and positive segregation also exists around the lower shrinkage porosity. From the results above, it could be inferred that before the bridging was formed entirely and the melt flow was blocked, the solidification contraction flow generated by the negative pressure created by the volume reduction caused by the difference in solid-liquid phase density during solidification might have been generated in this region, and the differentiation of segregation was strengthened. In the early stage of solidification, the columnar dendrites in the bridging region grew rapidly, and at the same time, the solute was discharged into the surrounding melt. Under the influence of natural convection and solidification contraction flow, the concentrated melt flowed downward and passed through the center of the bridging, and positive segregation was formed in the center of the bridging and the final solidification area, while negative segregation was formed above the bridging. However, as shown in Fig. 2.2.5 (b), in the results of sample No.2, segregation also occurred, but the positive segregation in this sample was scattered in the area near the chill plate.

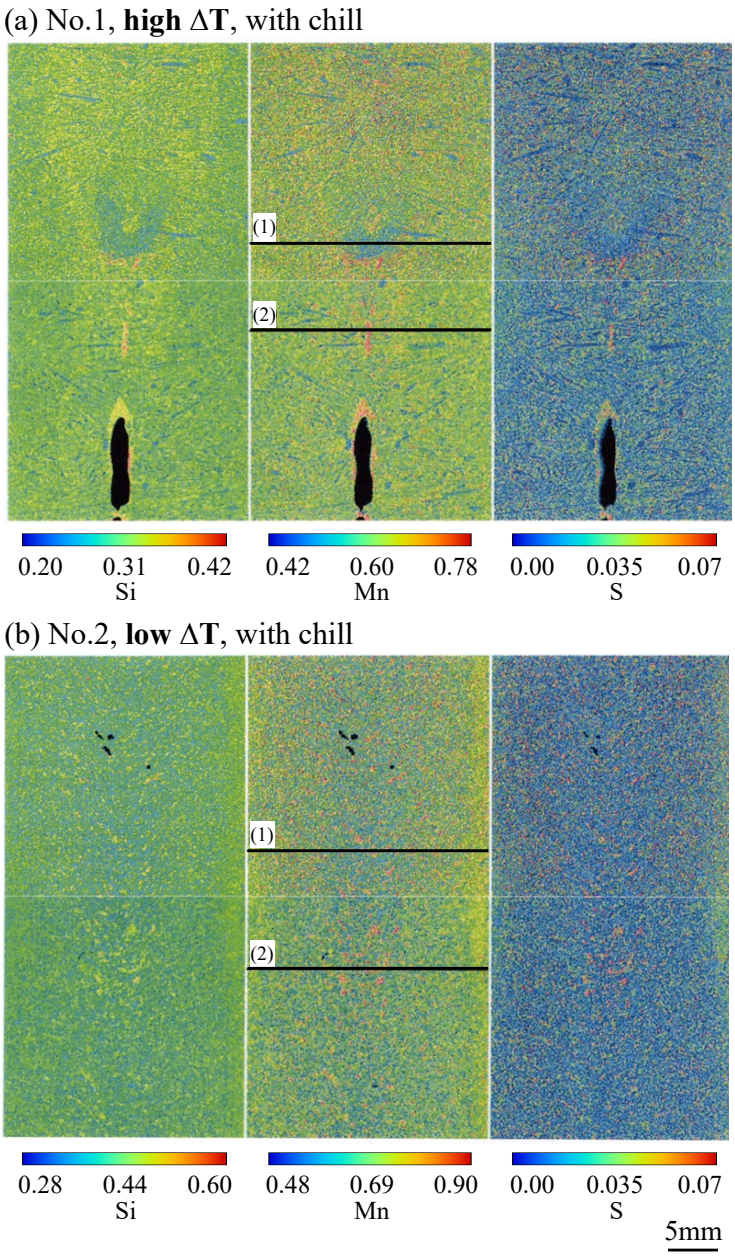

Fig. 2.2.5. EPMA mapping analysis of the concentration (mass%) of silicon, manganese, and sulfur in the area near the chill in the longitudinal section in samples (a) No.1 and (b) No.2, respectively.

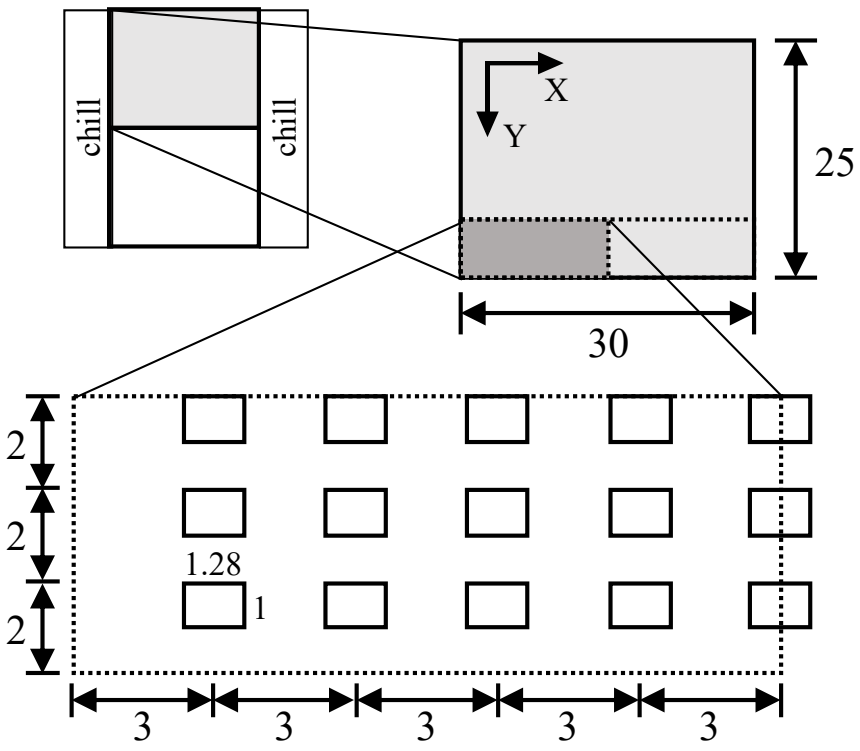

Fig. 2.2.6. Schematic drawing of the position of concentration distribution analysis in the cross-section shown in Fig. 2.2.2. (unit: mm)

The serial sectioning method was used to obtain the result of concentration distribution more clearly and clarify the effect of bridging on segregation. As shown in Fig. 2.2.6, the schematic drawing shows the position of concentration distribution analysis in the cross-section shown in Fig. 2.2.2. Concentration distribution graphs of silicon, manganese, sulfur, and phosphorus in the cross-section of sample No.1 are shown in Fig. 2.2.7. The average values of each analyzed section are shown in Fig. 2.2.8. And (a) z=0 represents the section of the upper side of the chill plate, (b) z=6 represents 6 mm below the upper side of the chill plate, (c) z=16 is between the bridging area and the porosity, 16 mm below the upper side of the chill plate, (d) z=32 represents 32 mm below the upper side of the chill plate, and (e) z=38 represents 38 mm below the upper side of the chill plate in the sample No.1. The results of sample No.3 are shown in Fig. 2.2.9 and Fig. 2.2.10. Each point in Fig. 2.2.7 and Fig. 2.2.9 represents the mean value of the rectangular analysis area at the corresponding location shown in Fig. 2.2.6. The leftmost point of the graph represents the result of the area closest to the side surface of the ingot, the rightmost point represents the result of the region on the center line, and the color scale below the graph represents the extreme value that the element was measured in the sample. In addition, the solidification structure of the areas (marked by the dashed box (30 mm × 6 mm) in Fig. 2.2.6) in the cross-section of sample No.1 and sample No.3 are shown in Fig. 2.2.11 and Fig. 2.2.12, respectively. The arrow direction in the figure indicates the growth direction of columnar dendrites, the dashed line indicates the interface between dendrites with different growth orientations, and the solid ellipse line indicates the equiaxed dendrite region.

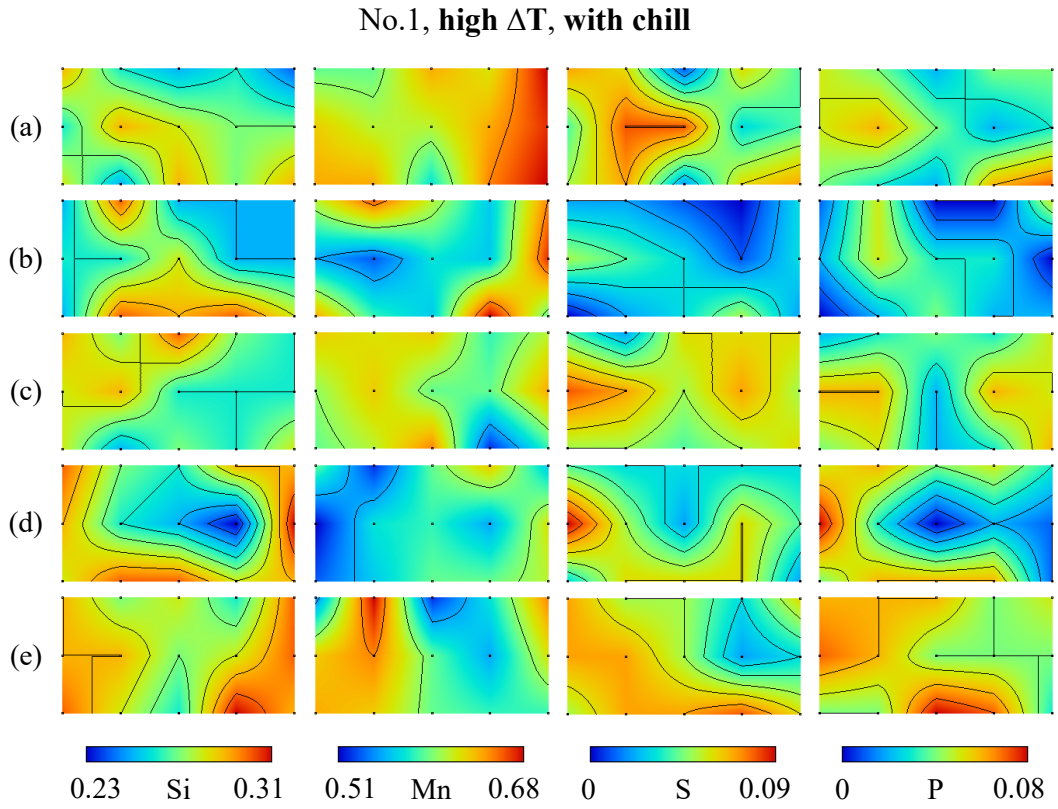

Fig. 2.2.7. Concentration (mass%) distribution graphs of silicon, manganese, sulfur, and phosphorus in the cross-section of sample No.1, (a) z=0, the section of the upper side of the chill plate, (b) z=6, 6 mm below the upper side of the chill plate, (c) z=16, between the bridging area and the porosity, 16 mm below the upper side of the chill plate, (d) z=32, 32 mm below the upper side of the chill plate, and (e) z=38, 38 mm below the upper side of the chill plate.

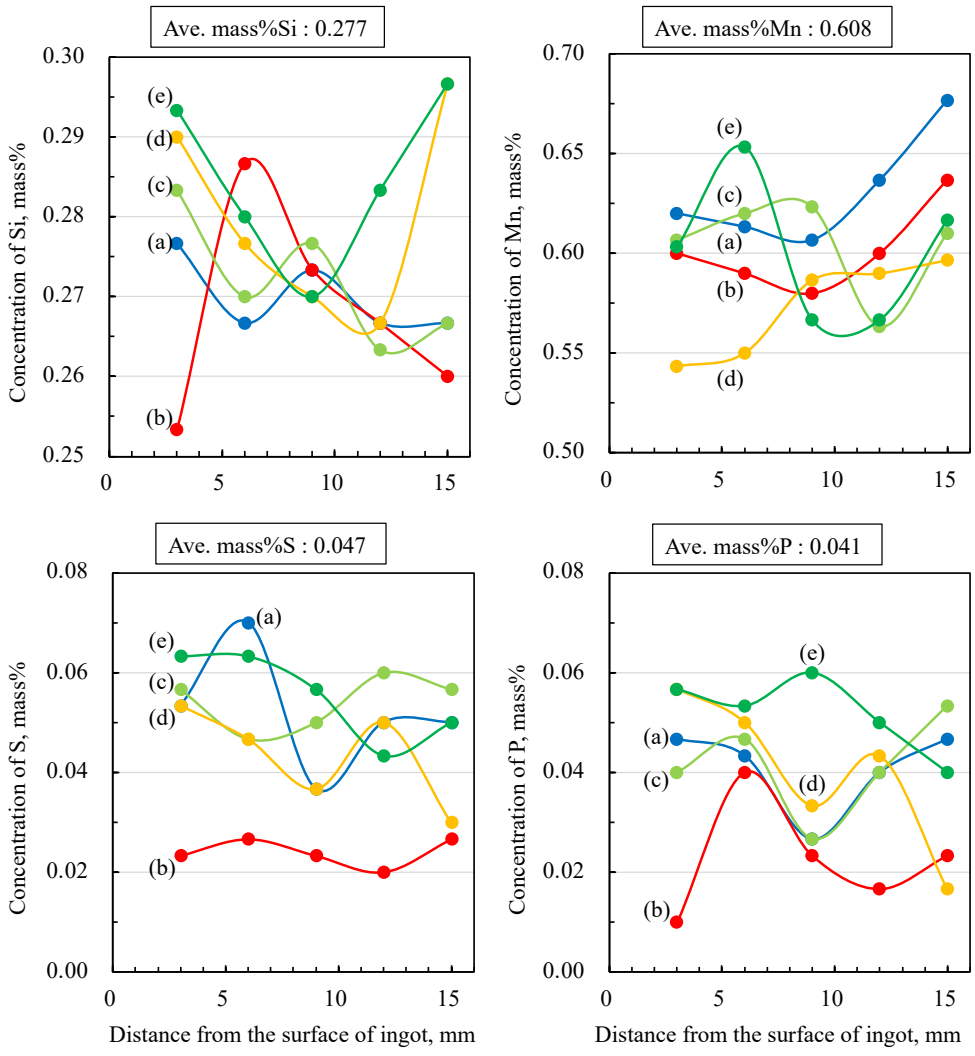

Fig. 2.2.8. Concentration (mass%) of alloying element in the cross-section of sample No.1, (a) z=0, the section of the upper side of the chill plate, (b) z=6, 6 mm below the upper side of the chill plate, (c) z=16, between the bridging area and the porosity, 16 mm below the upper side of the chill plate, (d) z=32, 32 mm below the upper side of the chill plate, and (e) z=38, 38 mm below the upper side of the chill plate, as shown in Fig. 2.2.7.

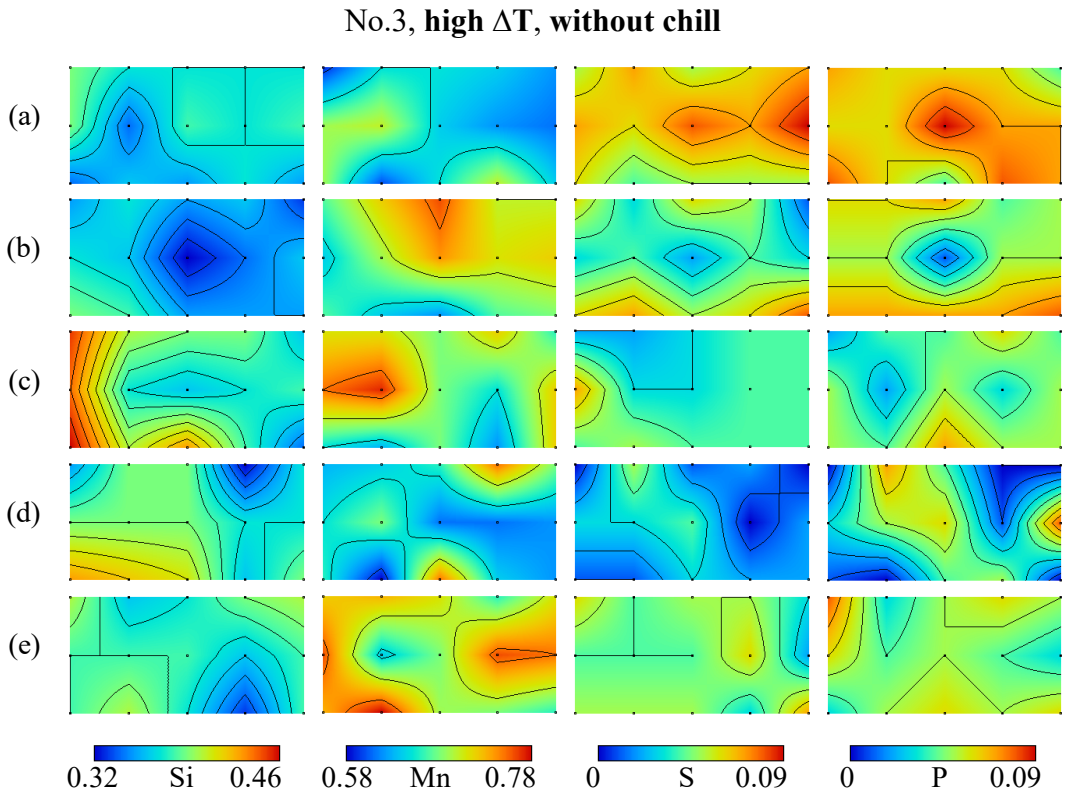

Fig. 2.2.9. Concentration (mass%) distribution graphs of silicon, manganese, sulfur, and phosphorus in the cross-section of sample No.3, (a) z=0, the section of the upper side of the chill plate, (b) z=6, 6 mm below the upper side of the chill plate, (c) z=16, between the bridging area and the porosity, 16 mm below the upper side of the chill plate, (d) z=30, 30 mm below the upper side of the chill plate, and (e) z=42, 42 mm below the upper side of the chill plate.

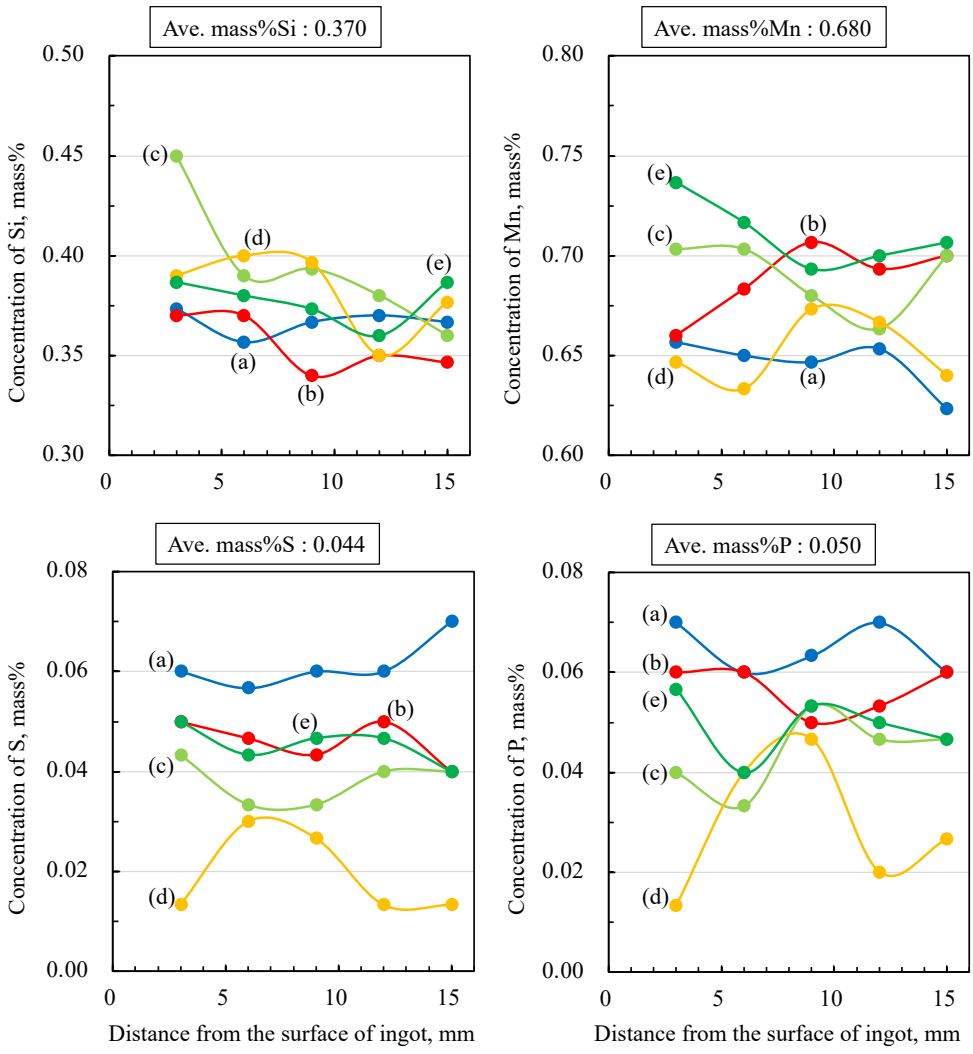

Fig. 2.2.10. Concentration (mass%) of alloying element in the cross-section of sample No.3, (a) z=0, the section of the upper side of the chill plate, (b) z=6, 6 mm below the upper side of the chill plate, (c) z=16, between the bridging area and the porosity, 16 mm below the upper side of the chill plate, (d) z=30, 30 mm below the upper side of the chill plate, and (e) z=42, 42 mm below the upper side of the chill plate, as shown in Fig. 2.2.9.

Since the equilibrium partition coefficients of P and S are small, those alloying elements tend to concentrate in the residual melt during solidification and finally cause severe segregation. For sample No.1 cast with chill plates, as shown in Fig. 2.2.7 (a), (c), and (e), Mn, S, and P were concentrated in the areas above bridging, z=0, between the bridging and the porosity, z=16, and below the large porosity, z=38, but diluted in the areas of bridging, z=6. However, for sample No.3 cast without chill plates, as shown in Fig. 2.2.9, Mn was concentrated in the regions where z=6, z=16, and z=42, but diluted in the areas where z=0. S and P were concentrated in the regions where z=0 and z=6. In summary, the positive segregation of Mn in sample No.1 was slightly higher than that in sample No.3, while the positions of S and P in sample No.1 were lower than those in sample No.3, suggesting the formation of bridging affects the distribution of elements, blocking the sinking of heavy elements and the floating of light elements, and finally increased the difference between positive and negative segregation.

In the bridging areas of sample No.1, the solidified structure was almost all columnar dendrite, as shown in Fig. 2.2.11. There were equiaxed dendrite areas formed below the shrinkage porosity. Columnar dendrites grew from the surface to the center in all parts, except for those in the region between bridging and the shrinkage porosity, which grew in random directions. And this particular growth orientation was considered to be affected by the accelerated solidification contraction flow before the upper bridging was totally formed, and the local convection disturbed the growth orientation of dendrites in this region. As shown in Fig. 2.2.12, columnar dendrites grew from the surface to the center in all parts, but there were some equiaxed dendrite regions in the middle of the ingot, and the area fraction increased gradually from the bottom to the top. In addition, the morphology of the solidification structure can also prove that the formation of bridging

impacts the types and distribution of solidification defects.

As mentioned above, the compound of manganese and sulfur might be formed during the solidification process. Therefore, mapping and line analysis were performed after the sample in the bridging area of sample No.1 had been re-polished and etched with Nital. As shown in Fig. 2.2.13 (a), the SEM-SE image of microstructure etched by Nital in the longitudinal section that z=0 of sample No.1 was observed. Fig. 2.2.13 (b) shows the SEM-SE image of the selected area for concentration distribution mapping analysis. SEM-EDX maps of the distribution of (c) Fe, (d) C, (e) Mn, (f) Si, (g) S, and (h) P were obtained. The result of SEM-EDX line analysis, as marked in (b), is shown in atomic percent, as shown in Fig. 2.2.13 (i). According to the analysis results, the metallographic structures of sample No.1 are ferrite and pearlite, and there are inclusions of manganese sulfide in the ferrite.

No.1, **high ΔT**, **with chill**

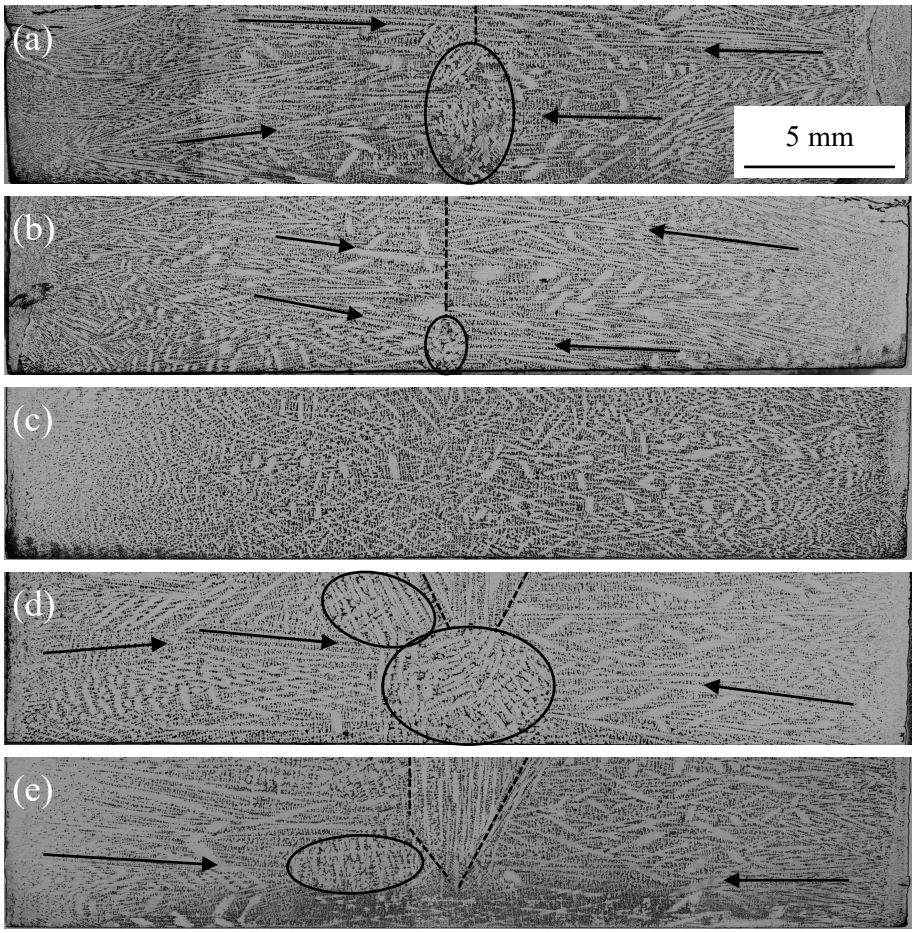

Fig. 2.2.11. Solidification structure in the cross-section of sample No.1. (a) z=0, the section of the upper side of the chill plate, (b) z=6, 6 mm below the upper side of the chill plate, (c) z=16, between the bridging area and the porosity, 16 mm below the upper side of the chill plate, (d) z=32, 32 mm below the upper side of the chill plate, and (e) z=38, 38 mm below the upper side of the chill plate.

No.3, **high ΔT**, **without chill**

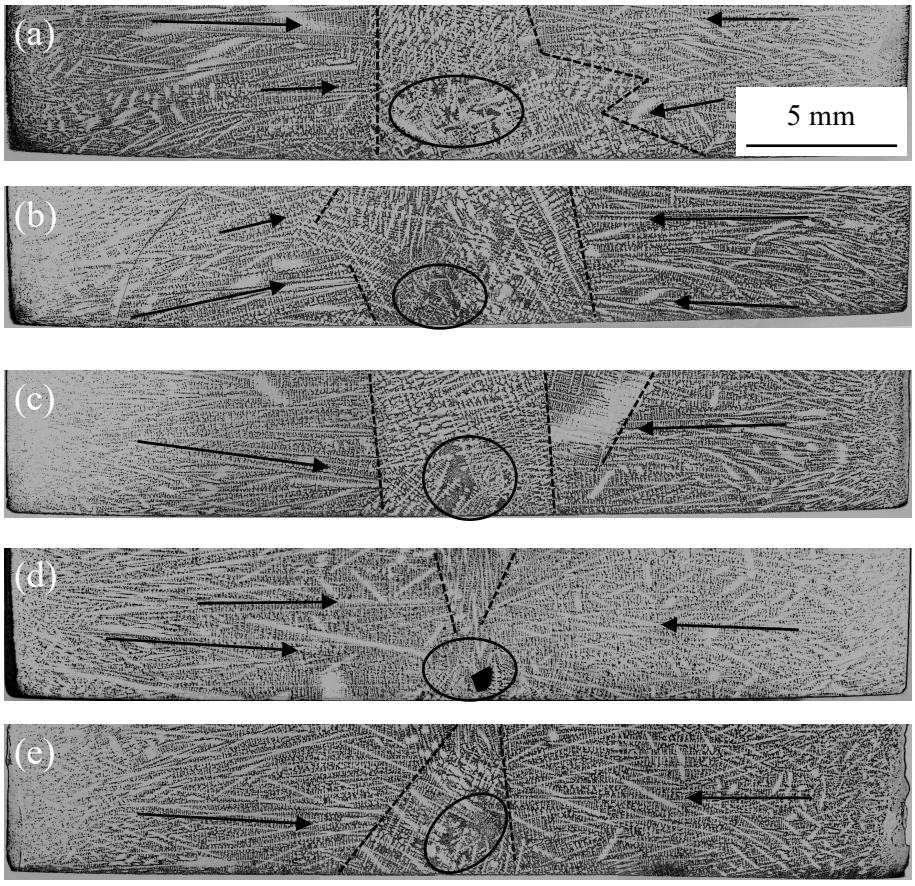

Fig. 2.2.12. Solidification structure in the cross-section of sample No.3. (a) z=0, the section of the upper side of the chill plate, (b) z=6, 6 mm below the upper side of the chill plate, (c) z=16, between the bridging area and the porosity, 16 mm below the upper side of the chill plate, (d) z=30, 30 mm below the upper side of the chill plate, and (e) z=42, 42 mm below the upper side of the chill plate.

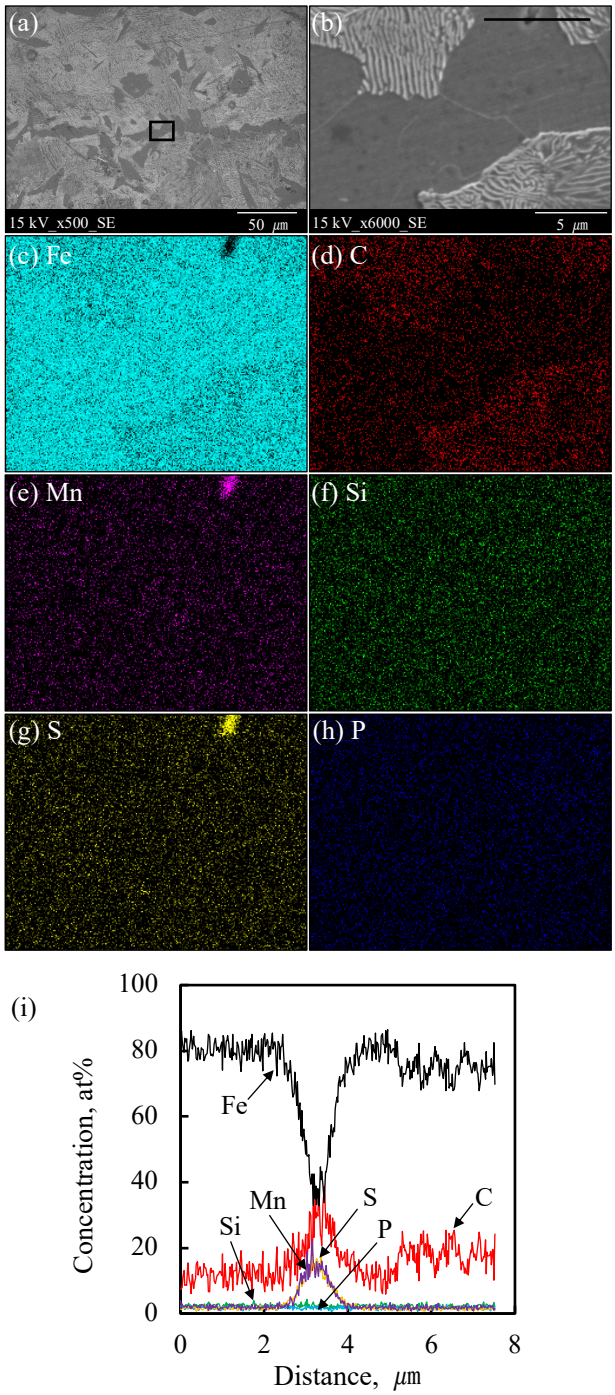

Fig. 2.2.13. (a) SEM-SE image of microstructure etched by Nital in the longitudinal section that z=0 of sample No.1. (b) SEM-SE image of the selected area for concentration distribution mapping analysis as marked in (a). SEM-EDX maps of the distribution of (c) Fe, (d) C, (e) Mn, (f) Si, (g) S, and (h) P. (i) Result of SEM-EDX line analysis as marked in (b).

2.2.3.3 Formation mechanism of macrosegregation

Schematic drawings of the solidification process and the formation mechanism of macrosegregation in sample No.1 and sample No.3 are shown in Fig. 2.2.14 (a)(c) and (b)(d), respectively. As shown in Fig. 2.2.14 (a)(c), in the case of casting with chill plates at a high casting temperature, solidification proceeded from the surface of the chill plate and the bottom of the mold at t_1. Then, as a result of the rapid growth of dendrites near the chill plates, there was a tendency to form bridging of columnar dendrites at t_2. As the solidification proceeded, shrinkage occurred, negative pressure was formed in the lower region, suction occurred, and the contraction flow of concentrated melt flowed into the lower part from the solid-liquid coexistence region, as indicated by the black dashed arrow in the figure. In addition, the liquid phase flowed into the solid-liquid coexistence region of the bridging from the upper part. After the bridging was formed at t_3, solidification contraction flow was stopped, and positive and negative segregation were formed above the bridging. And in the lower part of the ingot, coarse shrinkage porosity was formed. Positive segregation was also formed in the center of bridging and the areas around the shrinkage porosity, which were considered as the final solidification area in the lower side of the ingot. Finally, the solidification proceeded from t_4 to t_5, which was similar to the case of normal ingot casting, as shown in Fig. 2.2.14 (b).

In the case of casting without chill plates at a high casting temperature, solidification proceeded from the surface of the mold at t_1. Since the solidification proceeded equally from each side of the mold, columnar dendrite grew from the surface, and the melt zone containing some equiaxed dendrite nuclei in the center of the casting was inverted conical until t_4. As the solidification proceeded, some alloying elements diffused into the liquid phase, and the concentration near the gradually rising solid-liquid phase interface

increased. Light elements with small equilibrium partition coefficients (k_0) in the melt, such as sulfur (0.02)[27] and phosphorus (0.06)[27], moved upward with the solid-liquid interface, while the solute from the upper columnar dendrite region settled downward with natural convection. Eventually, the concentration of the melt in the central part of the casting increased, and positive segregation might occur. In the middle stage of solidification, the solidification shrinkage occurred, but it had been filled with the melt from the upper side without the influence of bridging. Therefore, huge shrinkage porosity was not formed in the middle stage of solidification. At the final stage of solidification, t_5, the residual concentrated or diluted liquid phase finally solidified, but some small shrinkage porosities remained, and positive or negative segregation occurred scattered in the ingot. Comparing the solidification cases with and without the formation of bridging, it can be concluded that macrosegregation was formed by the bridging, and the difference in the degree between positive and negative segregation was increased due to the formation of bridging.

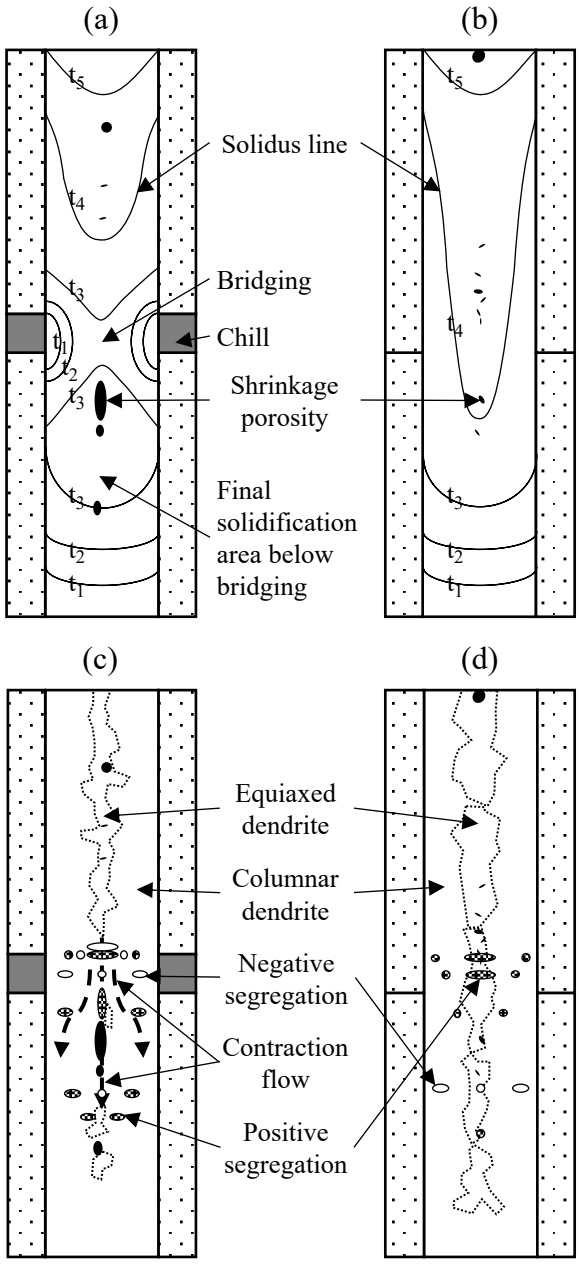

Fig. 2.2.14. Schematic drawing of solidification process and the formation mechanism of macrosegregation in the sample (a)(c) No.1 and (b)(d) No.3, respectively.

2.2.4. Conclusions

A model casting experiment was adopted to understand the formation mechanism of macrosegregation that occurred by local bridging during casting. The solidification structure morphology was observed, concentration analysis of alloying elements was performed, and the effect of bridging on macrosegregation was investigated. The obtained results are as follows.

(1) Solidification proceeded preferentially from the chill plate, and the bridging was formed successfully at a high casting temperature. High casting temperature could cause bridging, but large shrinkage porosities would be formed as well, while lower casting temperature could increase the grain density and form shrinkage porosities that are smaller in size but larger in number and more dispersed, compared with the case cast with no chill plate mold.

(2) Alloying elements were concentrated below the bridging near the mold, which was due to the convection caused by the difference in solidification speed between the chilled part and the others, and the concentrated molten steel from the chilled part flowed into the lower part and solidified.

(3) Around the shrinkage porosity, the concentration of alloying elements was most significant. It was considered that the area around the shrinkage porosity is the final solidified part.

(4) Due to the formation of bridging, macrosegregation was formed, and the difference between positive and negative segregation was increased.

References

1) E. J. Pickering: *ISIJ Int.*, **53** (2013), 935. https://doi.org/10.2355/isijinternational.53.935

2) M. C. Flemings: *Metall. Trans. B*, **5** (1974), 2121. https://doi.org/10.1007/BF02643923

3) M. C. Flemings: *ISIJ Int.*, **40** (2000), 833. https://doi.org/10.2355/isijinternational.40.833

4) M. C. Flemings: Solidification Processing, McGraw-Hill, NY, (1974).

5) R. Mehrabian, M. Keane, and M. C. Flemings: *Metall. Mater. Trans. B*, **1** (1970), 1209. https://doi.org/10.1007/BF02900233

6) M. Kawamoto, and T. Nagira: *Tetsu-to-Hagané*, **100** (2014), 472. (in Japanese). https://doi.org/10.2355/tetsutohagane.100.472

7) H. D. Brody, and M. C. Flemings: *Trans. Metall. Soc. AIME*, **236** (1966), 615.

8) T. W. Clyne, and W. Kurz: *Metall. Trans. A*, **12A** (1981), 965. https://doi.org/10.1007/BF02643477

9) I. Ohnaka: *Trans. Iron Steel Inst. Jpn*, **26** (1986), 1045. https://doi.org/10.2355/isijinternational1966.26.1045

10) S. Kobayashi: *Trans. Iron Steel Inst. Jpn*, **28** (1988), 728. https://doi.org/10.2355/isijinternational1966.28.728

11) T. Matsumiya, H. Kajioka, S. Mizoguchi, Y. Ueshima, and H. Esaka: *Trans. Iron Steel Inst. Jpn*. **24** (1984), 873. https://doi.org/10.2355/isijinternational1966.24.873

12) H. Combeau, J.-M. Drezet, A. Mo, and M. Rappaz: *Metall. Mater. Trans. A*, **27A** (1996), 2314. https://doi.org/10.1007/BF02651886

13) D. Tourret, and Ch.-A. Gandin: *Acta Mater.*, **57** (2009), 2066. https://doi.org/10.1016/j.actamat.2009.01.002

14) Y. Natsume, M. Shimamoto, and H. Ishida: *ISIJ Int.*, **50** (2010), 1867. https://doi.org/10.2355/isijinternational.50.1867

15) K. Oikawa, N. Hirata, and K. Anzai: *Tetsu-to-Hagané*, **103** (2017), 747. (in Japanese). https://doi.org/10.2355/tetsutohagane.TETSU-2017-024

16) T. Kawawa, H. Sato, S. Miyahara, T. Koyano, and H. Nemoto: *Tetsu-to-Hagané*, **60** (1974), 486. https://doi.org/10.2355/tetsutohagane1955.60.5_486

17) T. Murao, T. Kajitani, H. Yamamura, K. Anzai, K. Oikawa, and T. Sawada: *Tetsu-to-Hagané*, **99** (2013), 94. (in Japanese). https://doi.org/10.2355/tetsutohagane.99.94

18) A. Suzuki: *Tetsu-to-Hagané*, **60** (1974), 774.

19) K. Kumai, K. Asano, T. Ohhashi, E. Nomura, and H. Fujii: *Tetsu-to-Hagané*, **60** (1974), 894. (in Japanese). https://doi.org/10.2355/tetsutohagane1955.60.7_894

20) S. Takaishi, T. Komai, K. Noro, and Y. Akita: *Tetsu-to-Hagané*, **60** (1974), 915. (in Japanese). https://doi.org/10.2355/tetsutohagane1955.60.7_915

21) S. Ogibayashi: *Sanyo Tech. Rep.*, **19** (2012), 2. (in Japanese).

22) Solidification in Casting, Japan Institute of Metals, 156.

23) S. K. Choudhary, and S. Ganguly: *ISIJ Int.*, **47** (2007), 1759. https://doi.org/10.2355/isijinternational.47.1759

24) Y. Natsume: *Tetsu-to-Hagané*, **103** (2017), 738. (in Japanese). https://doi.org/10.2355/tetsutohagane.TETSU-2017-062

25) E. Aritaka, H. Esaka, and K. Shinozuka: *Tetsu-to-Hagané*, **103** (2017), 688. (in Japanese). https://doi.org/10.2355/tetsutohagane.TETSU-2017-038

26) F. Satou, H. Esaka, and K. Shinozuka: *Tetsu-to-Hagané*, **99** (2013), 101. (in Japanese). https://doi.org/10.2355/tetsutohagane.99.101

27) J. Chipman: *Basic Open Hearth Steelmaking, Physical Chemistry of Steelmak ing Committee, Iron and Steel Division, AIME*, (1951), 632.

Chapter 3. Simulation of solidification in laboratory-size mold

In the continuous casting process and ingot casting, macrosegregation and casting defects are known to occur when the thickness of the solidified layer becomes non-uniform due to bridging during solidification. Macrosegregation directly affects the cracking of slabs and the deterioration of mechanical properties. For example, in the continuous casting process, central segregation is a problem in which solute-enriched molten steel flows due to solidification shrinkage flow. However, macrosegregation accompanied by convection is greatly influenced by the mold and casting conditions, and it is difficult to perform quantitative and highly reproducible analysis.

Recently, a method has been proposed in which a part of the mold is forcibly cooled to form a non-uniform solidified area and analyze the macrosegregation. In the small-scale casting experiment, a mold that can form a non-uniform solidification structure in the center of the sample with high reproducibility was used, the dendrite structure was observed, and the distribution of casting defects and the distribution of solute concentration was analyzed. And the effect of heterogeneous structure on the process of structure formation was discussed. Although the structure after solidification can be observed from casting experiments, in order to obtain the optimal method to reduce segregation, it is necessary to understand the entire solidification process as much as possible. Therefore, the solidification process with bridging was simulated by JSCAST Ver.13 software. In addition, the in-situ observation of simulated solidification of metals using ammonium chloride aqueous solution is a widely used method for studying the movement of convection during solidification. However, there have been no reports of in-situ observation in water model experiments for the case with bridging.

Therefore, in this study, the solidification process by local cooling was simulated,

various changes in the solidification process were analyzed, and the accuracy of simulation calculations to reproduce casting defects due to actual small-scale casting experiments and bridging was evaluated. Also, the movement of convection was investigated through in-situ observation for the reproduction of macrosegregation using an ammonium chloride aqueous solution.

3.1 Calculation of casting with local bridging

3.1.1 Introduction

In the work presented in the previous chapter, the model casting experiments were adopted to understand the formation mechanism of macrosegregation that occurred by local bridging during casting. In order to obtain the optimal method to reduce segregation, it is necessary to understand the entire solidification process as much as possible. Therefore, the solidification process with bridging was simulated by JSCAST Ver.13 software.

In this study, the solidification process by local cooling[1-3] was simulated, various changes in the solidification process were analyzed, and the accuracy of simulation calculations to reproduce casting defects due to actual small-scale casting experiments and bridging was evaluated.

3.1.2 Thermodynamic parameters and calculation conditions

The solidification process in which bridging occurs was simulated using JSCAST Ver.13. The schematic drawing of the mold used for the simulation is the same as the mold shown in Fig. 2.2.1. The thermodynamic parameters used for the simulation are shown in Table 3.1.1. The thermal conductivity coefficients are shown in Table 3.1.2. The

basic composition of the S45C is Fe-0.45%C-0.5%Si-0.8%Mn-0.03%S-0.06%P.

Table 3.1.1 Thermodynamic parameters of each material in the simulation

Material	S45C	Chill plate	Ceramics (TEP)	Ceramics (LAP)
Initial temperature (℃)	1670	-	20	20
Liquidus temperature (℃)	1491	-	-	-
Solidus temperature (℃)	1420	-	-	-
Density (g/cm^3)	7.84	7.50	3.35	0.90
Specific heat capacity (cal/(g·℃)	0.11703	0.16000	0.28123	0.24123
Thermal conductivity (cal/(cm·s·℃))	0.10748	0.08000	0.00859	0.00084
Latent heat (cal/g)	65	-	-	-
Kinematic viscosity coefficient (cm^2/s)	0.005	-	-	-

Table 3.1.2 Thermal conductivity coefficients between the various materials

	S45C	Chill plate	Ceramics (TEP)	Ceramics (LAP)	External atmosphere
S45C	-	0.2	0.01	0.01	0.0005
Chill plate	0.2	-	0.2	0.2	0.0005
Ceramics (TEP)	0.01	0.2	-	0.01	0.0005
Ceramics (LAP)	0.01	0.2	0.01	-	0.0005

Changes in solidification temperature, fraction of solid, pressure, and liquid phase flow velocity during solidification were calculated. The casting temperature was predicted using the following equation (3.1.1).

$$T_i = T_S + (T_L - T_S) \times (1 - f_S)^n \quad (3.1.1)$$

Where T_i is the temperature of the element in the simulation, T_S is the solidus temperature, T_L is the liquidus temperature, f_S is the fraction of solid, and n is the solidification index. In this simulation, to simplify the calculation model, the relationship between temperature and the fraction of solid was set as a linear relationship, so the value of n was set to 1. And the simulation calculation conditions are shown in Table 3.1.3.

Table 3.1.3 Simulation calculation conditions

Shape of elements	Orthogonal element
Minimum division width	0.5 (mm)
Calculation condition	With temperature calculation
Gravity designation	Fixed in the direction of gravity, parallel to the axis
Direction of gravity	z axis (down)
Gravitational acceleration	980 (cm/s^2)
Exit conditions for casting	Calculate up to a filling factor of 100%
Courant-Friedrichs-Lewy Condition	0.5
Exit conditions for solidification	Calculate up to a fraction of solid of 100%

3.1.3 Results and discussion

3.1.3.1 Various parameters during the solidification process

The locations of the recording points in the sample cast without or with local chilled are the same, as shown in Fig. 3.1.1. Cooling curves of recorded points on the casting centerline of the case cast without or with the chill plate are shown in Fig. 3.1.2 and Fig. 3.1.3, respectively. According to the results of the cooling curve of the record point 7 in Fig. 3.1.2 and Fig. 3.1.3, and the solidification time when the fraction of solid reaches 1 on each section shown in Fig. 3.1.4 and Fig. 3.1.5, it was considered that bridging was formed successfully due to rapid cooling near the chill plates. The variation of pressure and velocity with the solidification time of five positions on the central line of the case cast without the chill plate is shown in Fig. 3.1.6. Negative pressure was generated in the relatively lower area, resulting in increased flow velocity in the upper area. The variation of pressure and velocity with the solidification time of the case cast with the chill plate is shown in Fig. 3.1.7. In addition, the pressure change and the liquid phase velocity in the three regions of upper of bridging, central of bridging, and lower of bridging were calculated, respectively. Fig. 3.1.8 shows the variation of pressure and velocity with solidification time for three positions, 47 mm, 75 mm, and 105 mm from the bottom of the case cast with the chill plate. Around 28 seconds after the start of solidification, the negative pressure at the bottom of the bridging reaches its maximum of 0.665 g/cm^2, and the flow velocity at the center of the bridging also reaches its maximum of 0.130 cm/s at about 25 seconds after the start of solidification. That indicated the shrinkage contraction flow was generated. It could be considered that it would be positively segregated in the final solidification zone at the bottom of the bridging, and negatively segregated above the bridging.

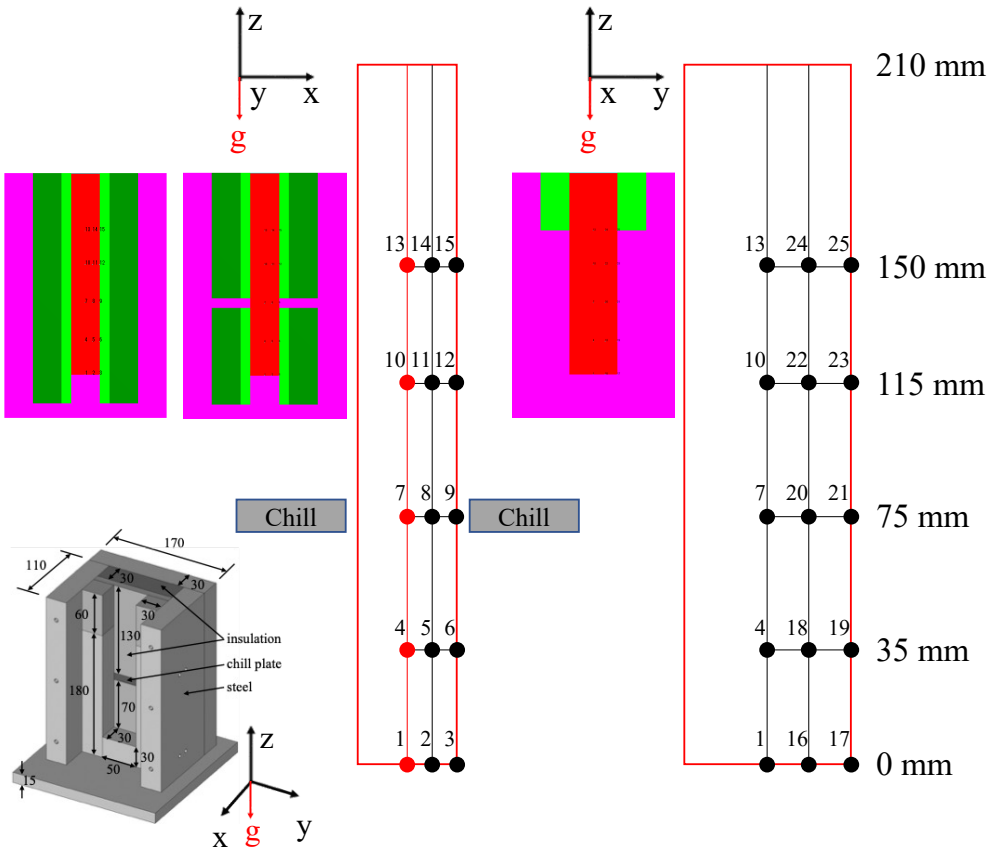

Fig. 3.1.1. Schematic drawing of the mold without or with chill plates, and the positions of the recording points.

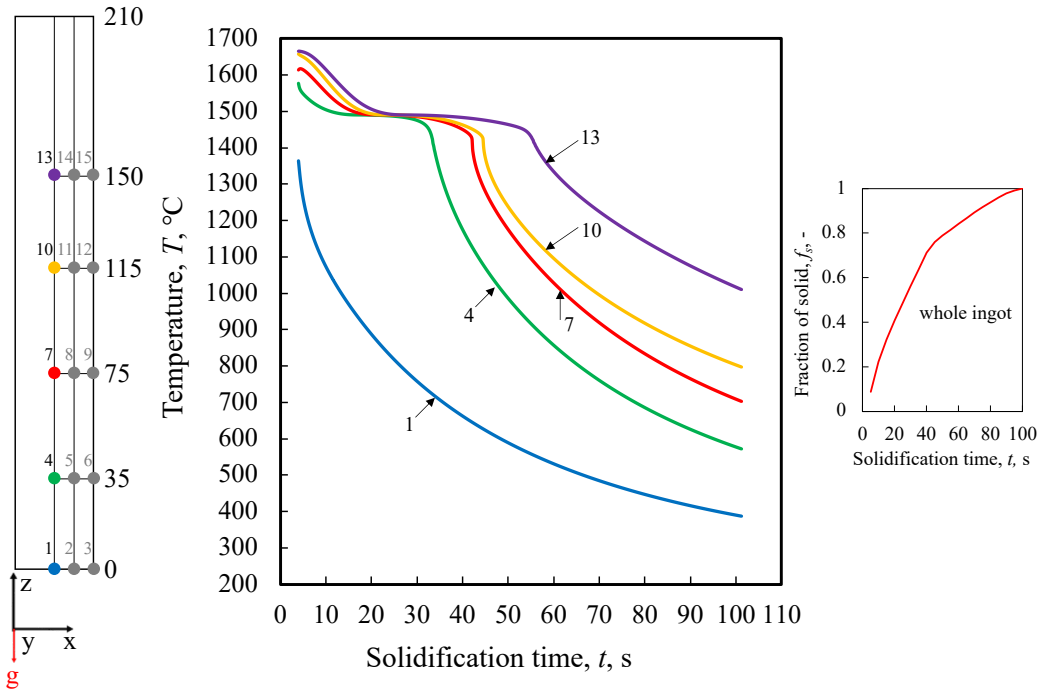

Fig. 3.1.2. Cooling curves of recorded points on the casting centerline of the case cast without the chill plate.

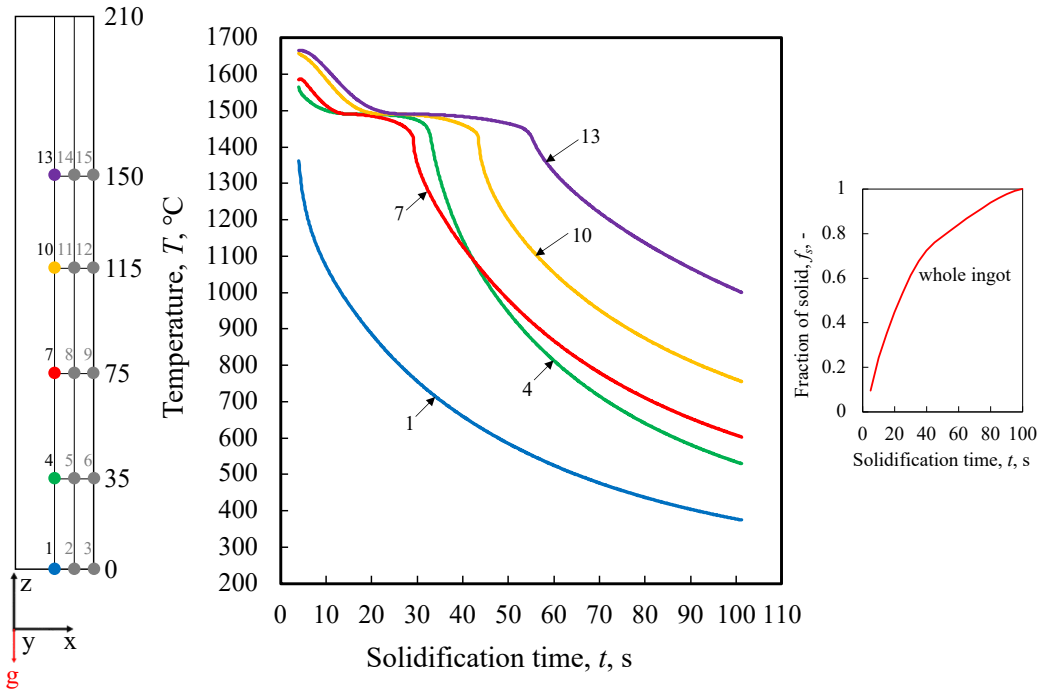

Fig. 3.1.3. Cooling curves of recorded points on the casting centerline of the case cast with the chill plate.

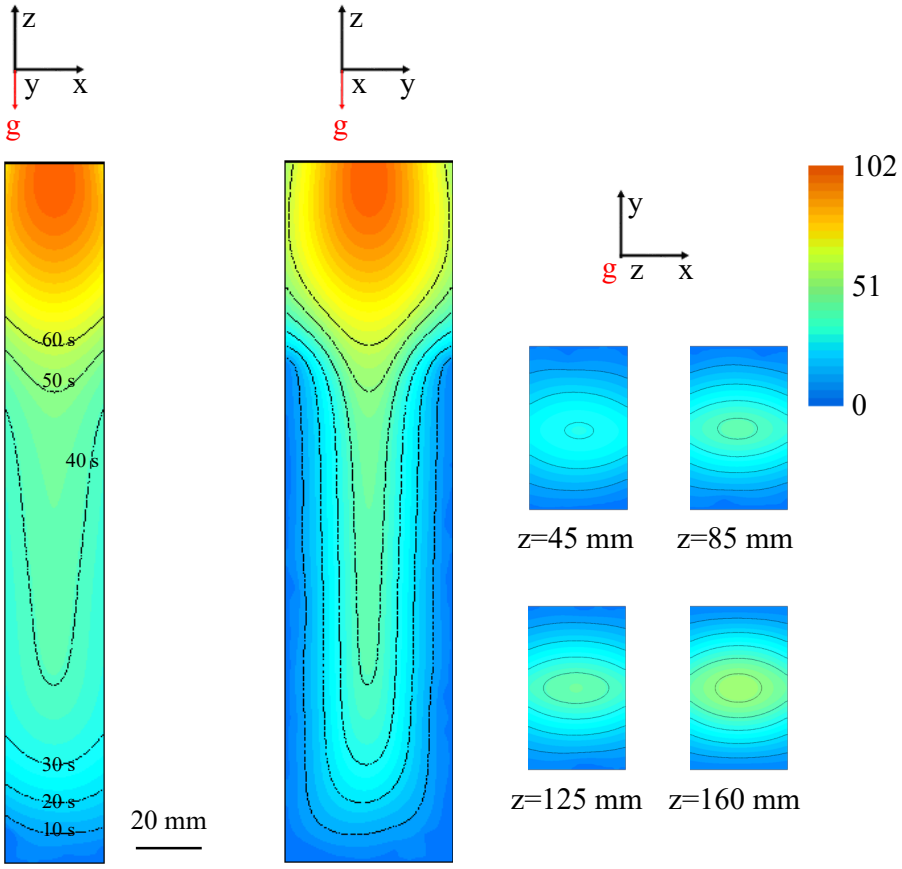

Fig. 3.1.4. Solidification time (f_s=1) on each section of the case cast without the chill plate. (unit: s)

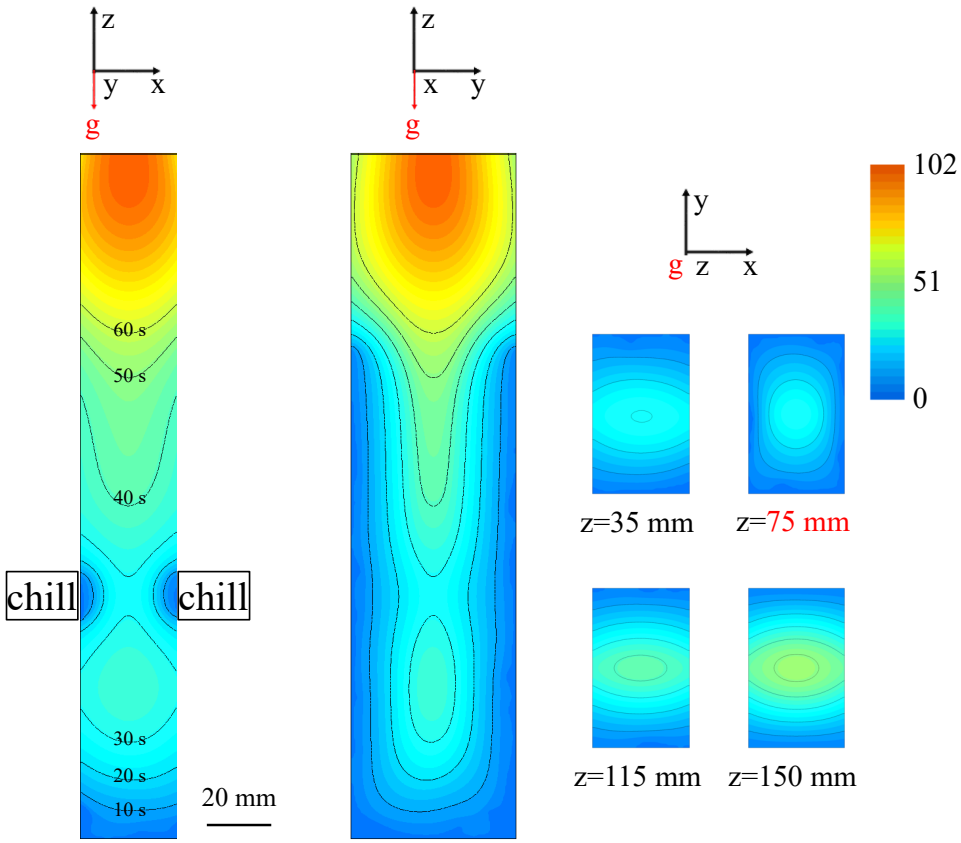

Fig. 3.1.5. Solidification time (f_s=1) on each section of the case cast with the chill plate. (unit: s)

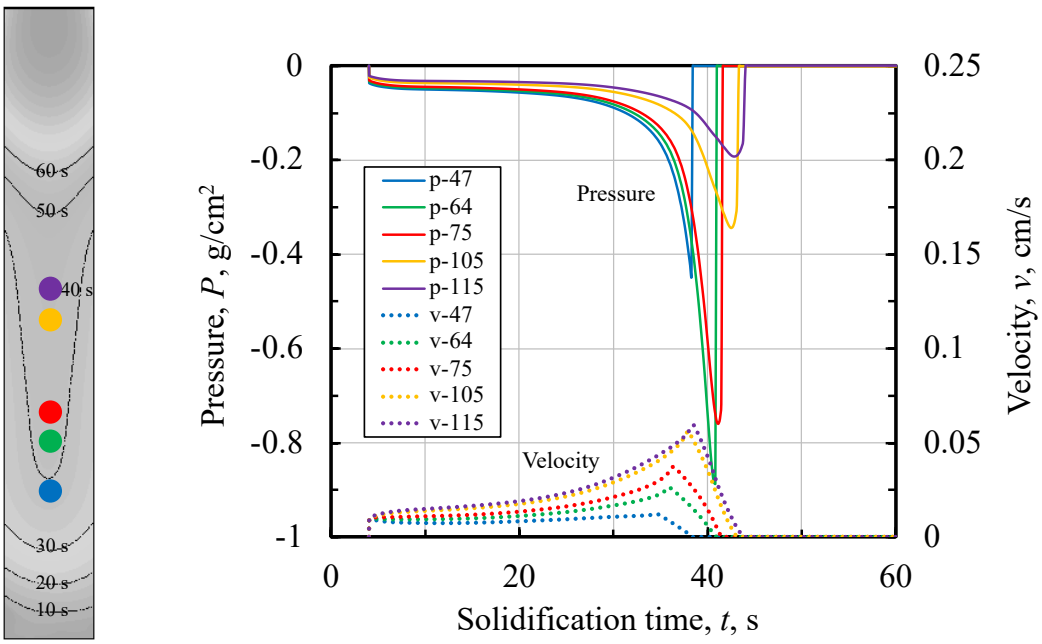

Fig. 3.1.6. Variation of pressure and velocity with solidification time of the case cast without the chill plate.

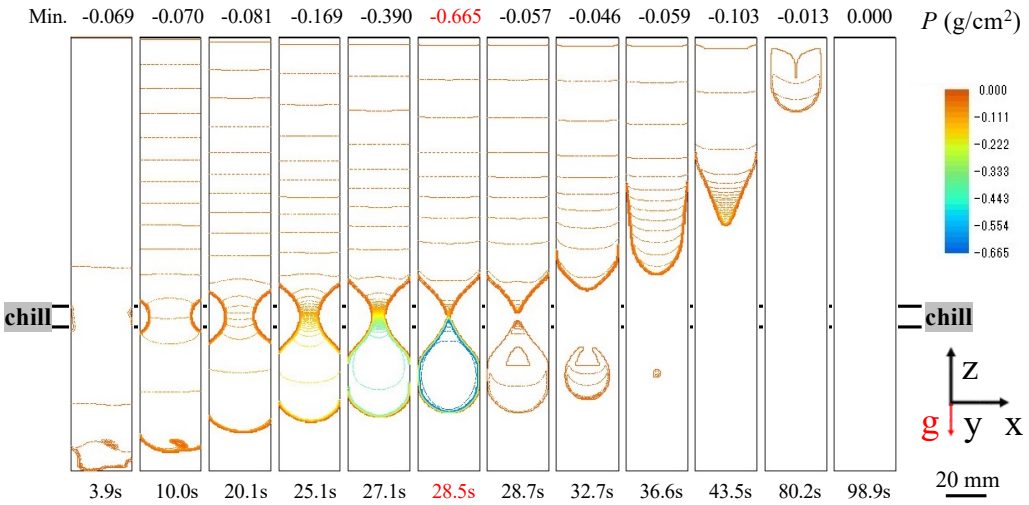

(a) P (g/cm^2)

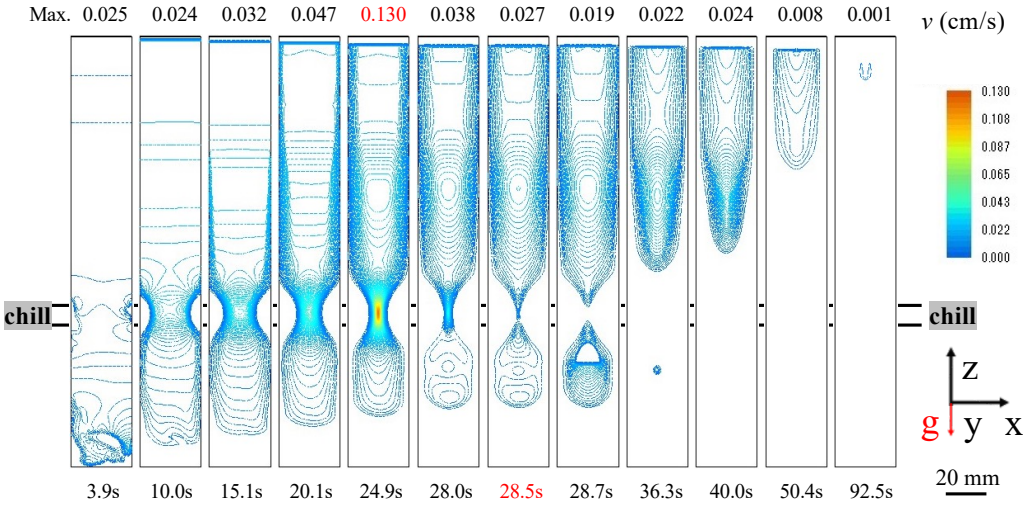

(b) v (cm/s)

Fig. 3.1.7. Variation of (a) pressure and (b) velocity with solidification time on the longitudinal (xz) section of the case cast with the chill plate.

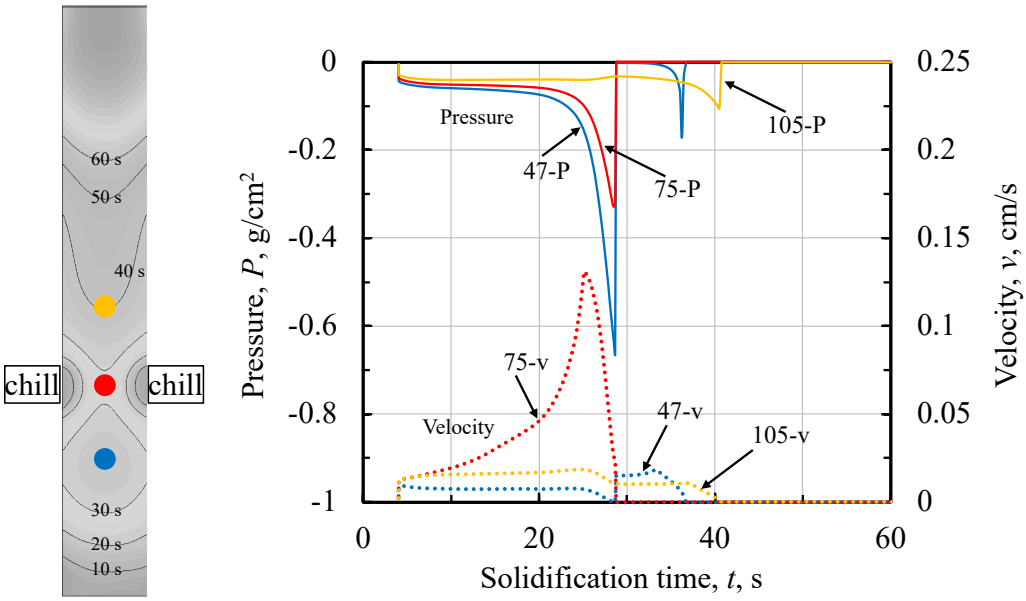

Fig. 3.1.8. Variation of pressure and velocity with solidification time of the case cast with the chill plate.

3.1.3.2 Predictive calculations of the location of casting defects

The Niiyama parameter is used to predict the locations of solidification shrinkage. Furthermore, the Niiyama values were calculated using the ratio of the temperature gradient and the square root of the cooling rate, (Eqs. (2.1.3)), as shown in Fig. 3.1.9 and Fig. 3.1.10. When the fraction of solid reaches 0.7, in the case of that cast without the chill plate, shrinkage porosities were predicted in the central area of the casting. And in the case of that cast with the chill plate, the maximum value of the temperature gradient on the longitudinal (xz) section was 818 K/cm, and the maximum value of the cooling rate was 142 K/s. Shrinkage porosities were predicted in the central and lower regions of the bridging, while the threshold of the Niiyama value was about 1 $(Ks)^{1/2}$/cm. Thus, it could be concluded that the simulation results in this experiment were in good agreement with the actual casting experiments, showing shrinkage porosities in the central and lower regions of the bridging, as shown in Fig. 3.1.11.

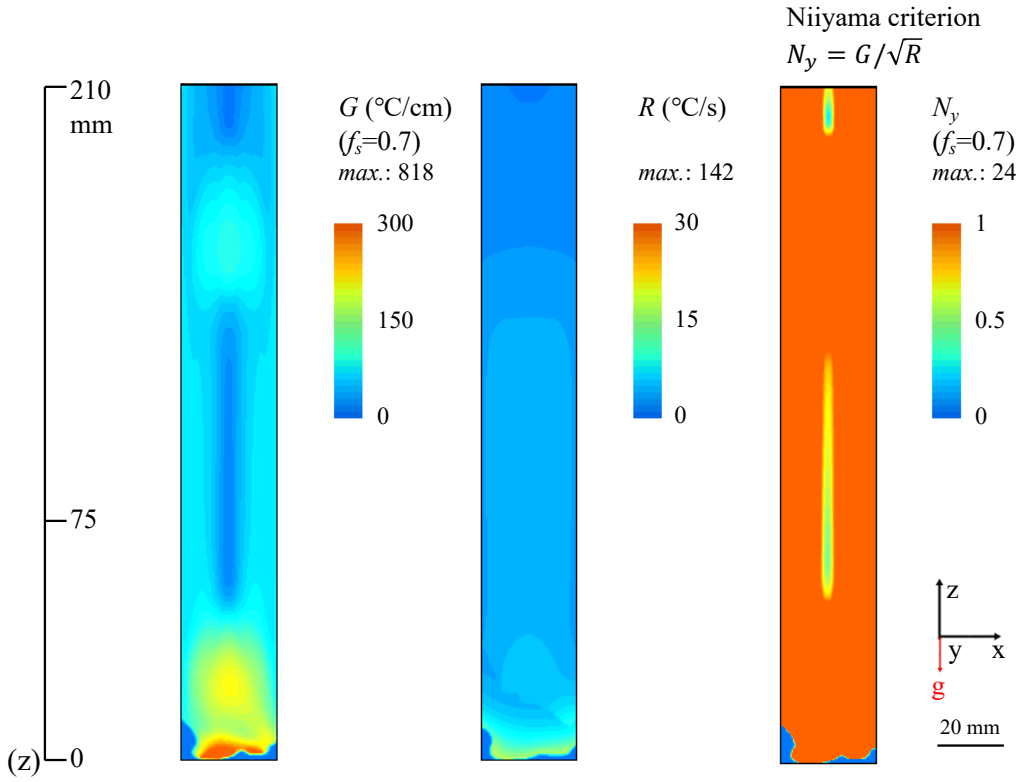

Fig. 3.1.9. The temperature gradient, the cooling rate, and the Niiyama values of the case cast without the chill plate when the fraction of solid equals 0.7.

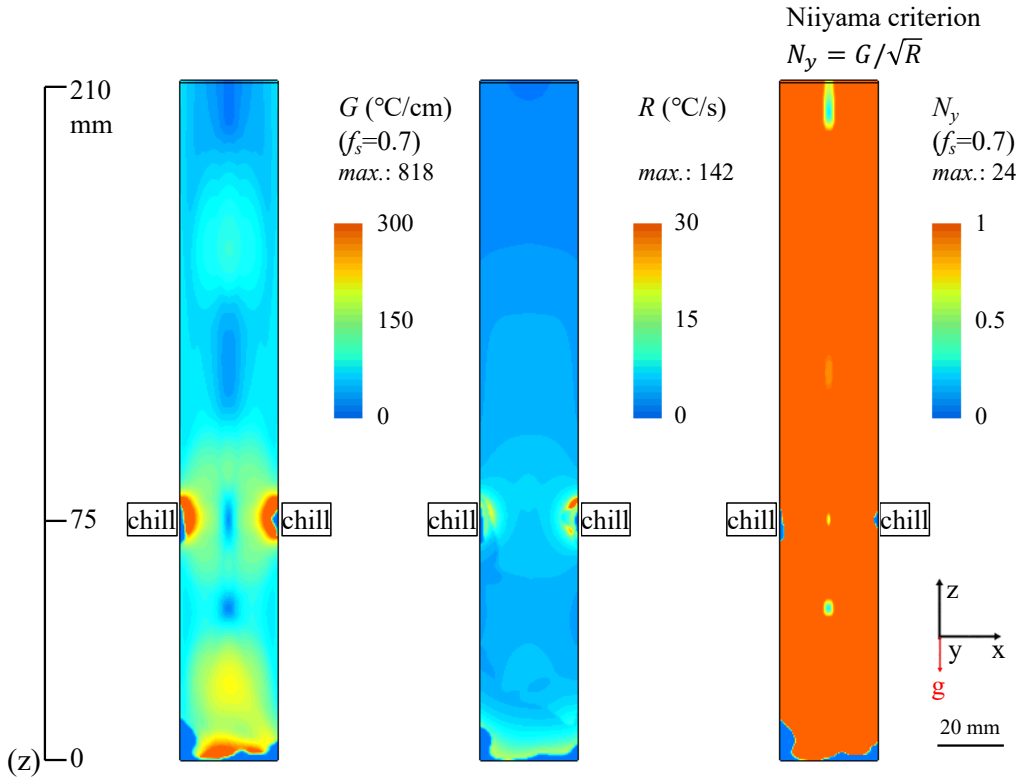

Fig. 3.1.10. The temperature gradient, the cooling rate, and the Niiyama values of the case cast with the chill plate when the fraction of solid equals 0.7.

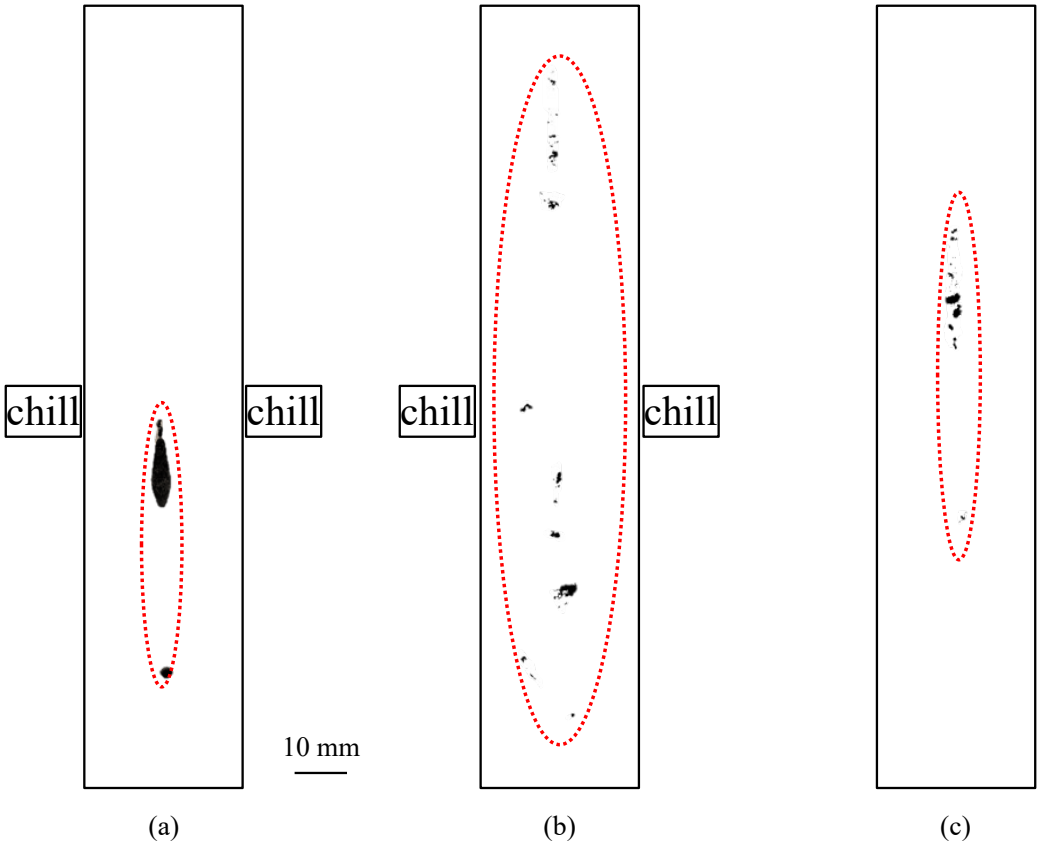

Fig. 3.1.11. Binarization figures of the shrinkage porosity position in the model casting experiments samples, as shown in Fig. 2.2.3.

3.1.3.3 The change of each parameter in the case with two parts of bridging

The effect of bridging on the generation of solidification defects and segregation during solidification was obtained through the experiments and simulations presented above. However, due to the use of simple models, more complex cases were not fully resolved. Therefore, based on successfully simulating the simple model, a simulation calculation was carried out for the case where two parts of bridging exist.

Variation of pressure and velocity with solidification time in the case with two parts of bridging is shown in Fig. 3.1.12. Similar to the previous experiments, solidification was preferential near the chill plates, but a more significant negative pressure was generated between the two bridging regions. In the case of two bridging areas, the maximum negative pressure was about 34 times that of one bridging, and the flow velocity was about 1.6 times. Moreover, the results of the two recording points between the bridging areas were significant, the negative pressure increased sharply at about 40 seconds after the start of solidification, and the flow velocity curve presented a sawtooth shape, which shows that the suction effect was powerful, and could significantly increase the degree of segregation.

In addition, the temperature gradient, the cooling rate, and the Niiyama values when the fraction of solid equals 0.7 in the case with two bridging areas are shown in Fig. 3.1.13. According to the results, the area between the two bridging areas also formed a plate-shaped solidification shrinkage porosity area. If this happens in the actual continuous casting process, with the light pressure of the rolls, the central area of the ingot will form a plate-shaped central segregation. Therefore, in order to reduce the generation of macrosegregation, the formation of excessive bridging regions should be avoided, or bridging should be eliminated in the early stage of solidification.

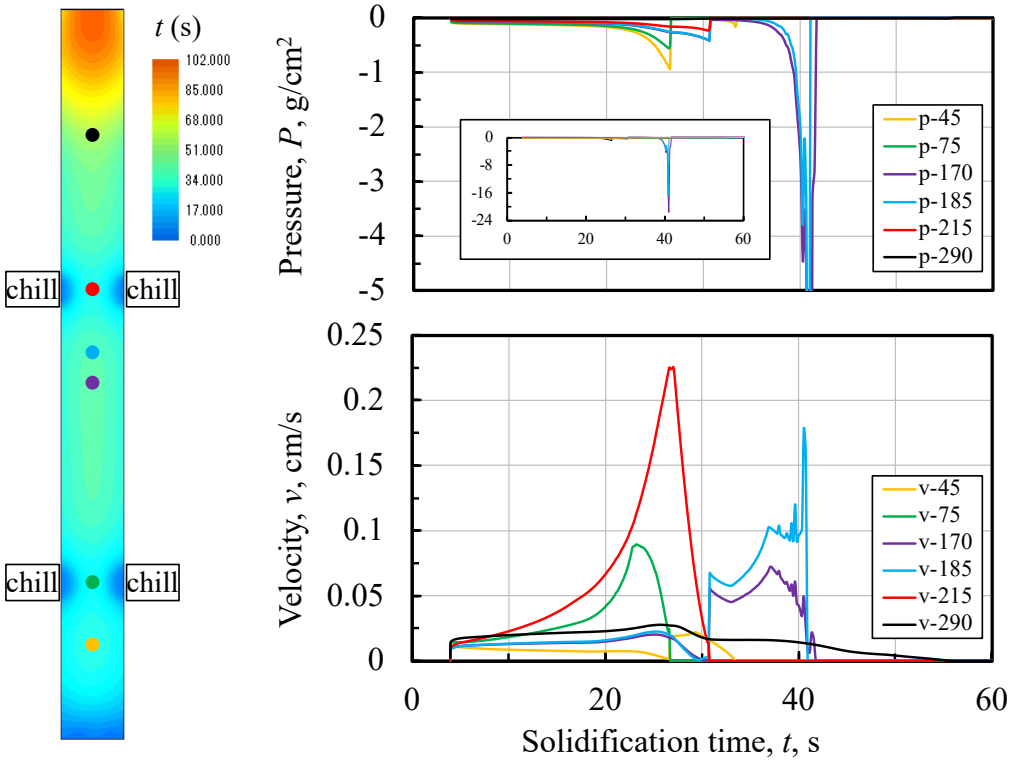

Fig. 3.1.12. Variation of pressure and velocity with solidification time in the case with two parts of bridging.

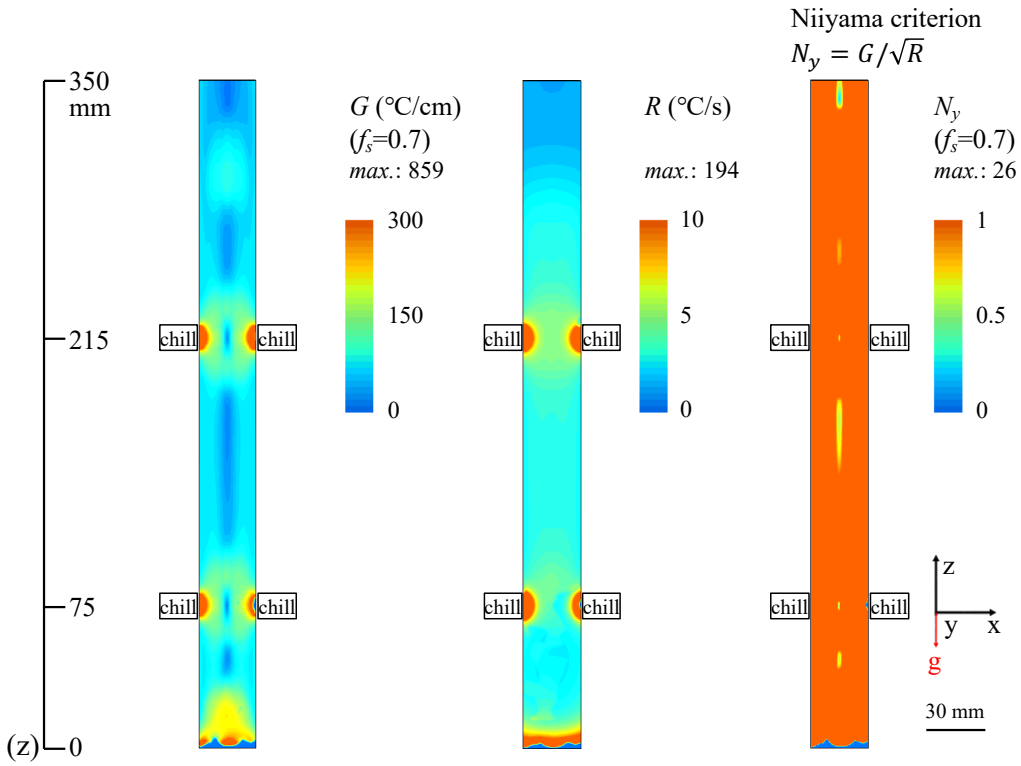

Fig. 3.1.13. The temperature gradient, the cooling rate, and the Niiyama values when the fraction of solid equals 0.7 in the case with two parts of bridging.

3.1.4 Conclusions

The simulation of the solidification process by local cooling was evaluated. Various changes in the solidification process, such as solidification temperature, fraction of solid, pressure, and flow velocity during solidification, were calculated. And the accuracy of simulation calculations to reproduce casting defects due to actual small-scale casting experiments and bridging was evaluated.

(1) It succeeded in reproducing the solidification process that forms bridging by local cooling by simulation, confirmed the suction effect due to bridging, and understood that bridging promotes segregation.

(2) In the case of two bridging areas, the maximum negative pressure was about 34 times that of one bridging, and the flow velocity was about 1.6 times. The suction effect could be enhanced, significantly increasing the degree of segregation.

References

1) T. Murao, T. Kajitani, H. Yamamura, K. Anzai, K. Oikawa, and T. Sawada: *Tetsu-to-Hagané*, **99** (2013), 94. https://doi.org/10.2355/tetsutohagane.99.94

2) F. Satou, H. Esaka, and K. Shinozuka: *Tetsu-to-Hagané*, **99** (2013), 101. https://doi.org/10.2355/tetsutohagane.99.101

3) Y. Natsume: *Tetsu-to-Hagané*, **103** (2017), 738. https://doi.org/10.2355/tetsutohagane.TETSU-2017-062

3.2 Simulation experiments of metal solidification process using water-ammonium chloride solution

3.2.1 Introduction

A number of methods have been used to elucidate and discuss macrosegregation. The representative techniques include the method of considering segregation by measuring solute concentration by T. Motegi *et al.*[1], the method of mathematically analyzing macrosegregation by M. Ohno *et al.*[2], and the method of in situ observation using X-rays by I. Uwabe *et al.*[3], *etc*. In addition, in recent years, numerical simulations[4] and experiments with small special molds[5] have been conducted to investigate the effects of bridging formed by dendrites on central segregation. It was also reported that spot-like positive segregation was also generated by solidification contraction flow.

In a study on numerical simulation of macrosegregation formation, Y. Natsume[6] reported the results of simulating the flow velocity and direction of liquid phase flow during solidification of an Al-10wt%Cu alloy. In addition, in experiments with small simple molds for steel, it is difficult to directly observe the formation of bridging and the existence of solidification contraction flow. Therefore, it is still being determined whether the liquid phase flows according to the direction and magnitude of the flow velocity vector as shown in the simulation during actual solidification.

The solidification process with bridging by local chilled was successfully simulated by JSCAST Ver.13 software. In this study, in order to better understand the effects of columnar bridging on central segregation, the effects of bridging, solidification contraction flow, and natural convection on macrosegregation were investigated through in-situ observation for the reproduction of macrosegregation using an ammonium chloride aqueous solution[7,8] with a local chilled mold.

3.2.2 Experimental apparatus and methods

The H_2O-35mass%NH_4Cl aqueous solution was selected as an experimental sample since the solidification of the ammonium chloride and water mixtures is similar to the metallic alloys at ambient temperature and because of their transparency property which is suitable for direct observation. The equilibrium state phase diagram of the water-ammonium chloride system is shown in Fig. 3.2.1. The phase diagram shows that the liquidus temperature is about 60 °C when the concentration of ammonium chloride is 35mass%. At this temperature, the primary crystals begin to crystallize. Note that at room temperature, the fraction of solid is only about 11%, which could be assumed to be the initial stage of solidification in the actual casting process of steel.

A local chilled mold with a pair of chill plates was fabricated. The schematic drawing of the local chilled mold is shown in Fig. 3.2.2. The chill plates were used to strengthen cooling and intentionally cause bridging. The molds were fabricated with internal dimensions of 30 mm (width) × 140 mm (height) × 5 mm (thickness). A pair of copper chill plates with a width of 20 mm was placed at a position 70 mm from the bottom of the mold. The width of the stainless steel plate is 10 mm, 5 mm, and 3 mm, respectively. The H_2O-35mass%NH_4Cl solution was heated to 90 ℃ and cast into the mold. The growth of dendritic microstructure and liquid phase flow inside the mold was observed in situ with a digital microscope.

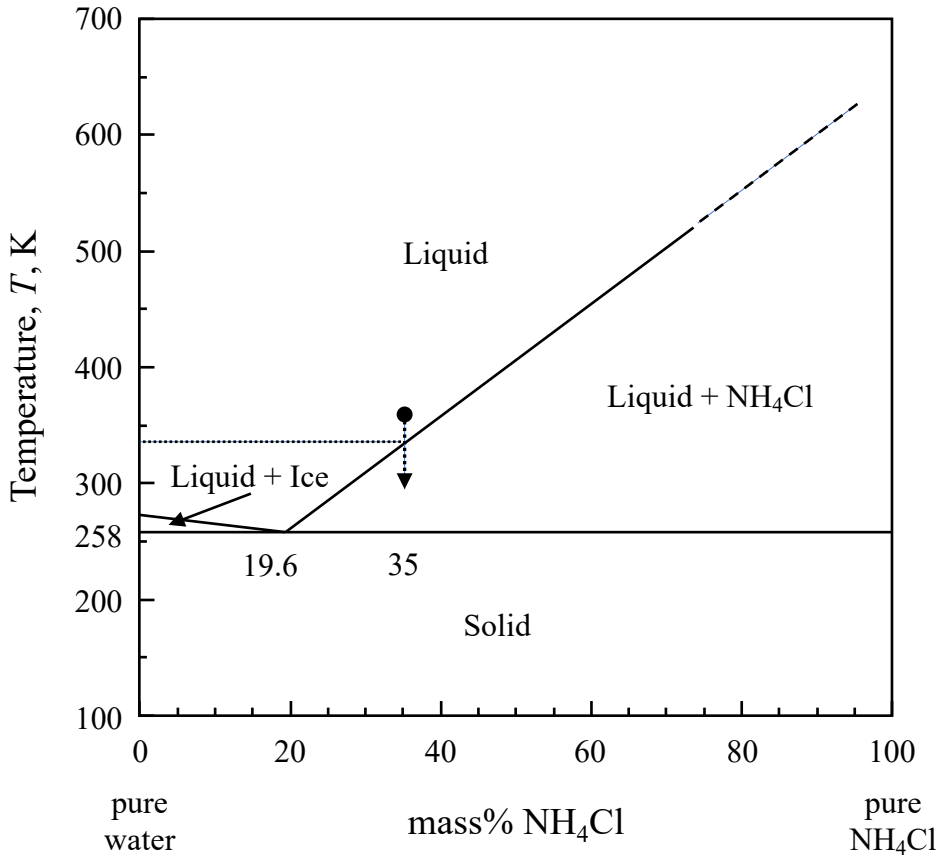

Fig. 3.2.1. Phase diagram of the NH_4Cl-H_2O.[7,8)]

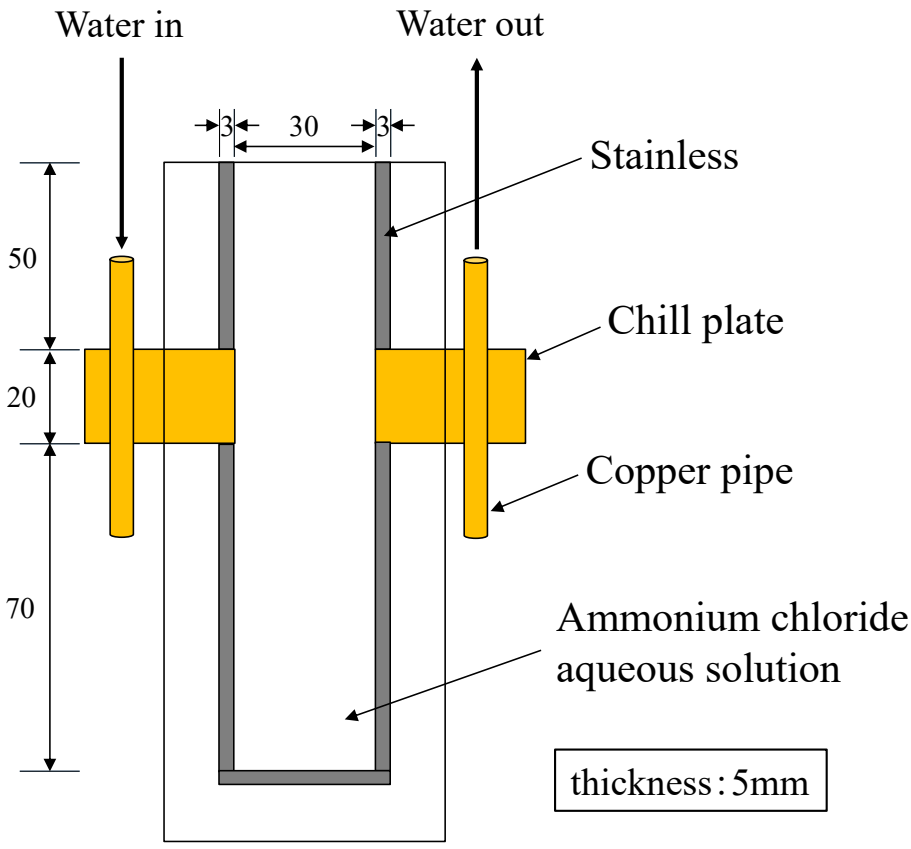

Fig. 3.2.2. Schematic drawing of the local chilled mold. (unit: mm)

3.2.3 Analysis of flow velocity and flow track during solidification

In-situ observations were carried out to evaluate the progress of solidification and the convection flow in the mold with and without local cooling.

As shown in Fig. 3.2.3, the solidification structure of H_2O-35mass%NH_4Cl cast in the mold without the chill plate was obtained. Some small shrinkage porosities were observed in the lower part near the bottom of the mold, marked with black circles. V-shaped shrinkage was observed in the upper part, while inverse V-segregation was observed in the vicinity of the mold, marked with red circles in the figure. The solidification structure of this case was similar to that of common large-scale ingot casting. Columnar dendrites grew from the side of the mold, and equiaxed dendrite regions with shrinkage porosities were formed in the middle and lower regions of the sample.

In the case cast in the mold with the chill plate, the width of the stainless steel plate is 10 mm. The velocity of movement of free dendrites was measured by Flownizer2D software[9)], and the solidification structure was observed. Since the width of the stainless steel plate is large, the cooling rate near it was also large, so the bridging was partially formed near the chill plate. In the area below the chill plate, a large number of equiaxed dendrites precipitated and settled from the upper part forming an equiaxed dendrite area containing larger shrinkage porosities. As shown in Fig. 3.2.4, the maximum velocity of dendrites was over 8000 μm/s at t_1 and t_2, especially in the area near the dendrite tips. This high velocity could be dominated by the result of a combination of water expelled during solidification and natural convection in the liquid phase. In the results at t_3, it was observed that the free dendrites moved to the interdendritic regions and the shrinkage porosity, the trajectories are shown by the black lines in the figure, and the velocity is

significantly higher near the narrow region. Also, the velocity of free dendrites inside the shrinkage porosity was observed to be smaller, according to the results at t_4 in Fig. 3.2.4.

In order to obtain a complete bridging area, the width of the stainless steel plate was reduced to reduce the cooling rate around it. Thus, the H_2O-35mass%NH_4Cl was cast again in the mold with the chill plate, and the width of the stainless steel plate was reduced to 5 mm. In this case, a perfect bridging area was obtained. The columnar dendrite growth was maintained in the upper and lower areas of the chill plate, which met the requirements for the simulation of bridging formed by local chilled in the continuous casting process, as shown in Fig. 3.2.5. Since the fraction of solid is only about 11% at the room temperature, this case could be assumed to be the initial stage of solidification in the actual casting process of steel.

As shown in Fig. 3.2.5, at the initial stage of solidification, the moving track of the free dendrites was consistent with the conclusion given in the schematic drawing of solidification and the formation mechanism of macrosegregation in Fig. 2.2.14, which proved the accuracy of the relevant conclusions obtained in the actual small-scale casting experiments. The velocity of movement of free dendrites in the area (a) above the bridging, (b) in the center of the bridging, and (c) below the bridging is shown in Fig. 3.2.6. The graphs show the velocities of all free dendrites in each region during solidification. The mean value of the area above the bridging, in the center of the bridging, and below the bridging is 2093 μm/s, 2252 μm/s, and 1993 μm/s, respectively. Before the bridging area was blocked, the flow velocity in the center of the bridging area was the largest, which is also consistent with the simulation results shown in Fig. 3.1.4. After the bridging area was blocked, the flow velocity in the area above the bridging and below the

bridging was increased slightly, which was considered as the result of the formation of the contraction flow.

In addition, the case with 3 mm stainless steel plates was carried out, and the result is shown in Fig. 3.2.7. Regarding the results of the center of the chilled part, the growth direction of the secondary dendrite arms was upward. This was thought to be due to the large temperature difference between the root side of the columnar crystal and the high temperature at the tip side of the columnar dendrite in the chill part, which caused convection from top to bottom in the columnar dendrite and caused the secondary dendrite arm to grow upward. At 20 mm below the chilled part, the growth direction of the secondary dendrite arms changes from top to bottom, with the columnar dendrite length of about 5 mm as the boundary. The convection due to the temperature difference was dominated up to about 5 mm from the side of the mold as described above, but above 5 mm, the convection was dominated by the difference in solute concentration.

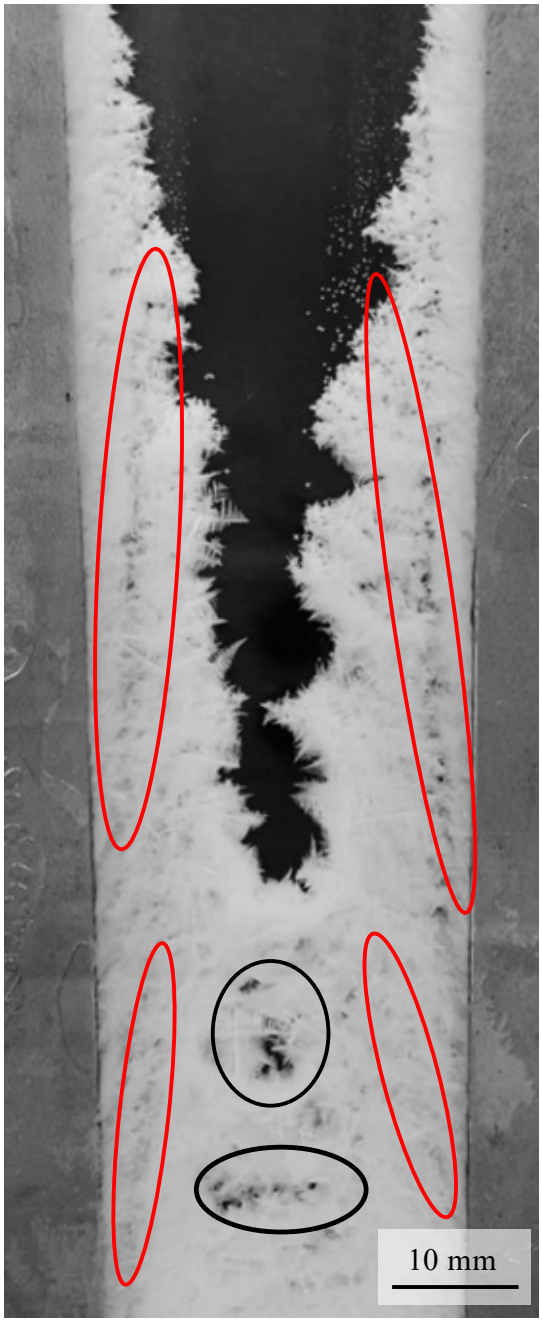

Fig. 3.2.3. Solidification structure of H_2O-35mass%NH_4Cl cast in the mold without the chill plate.

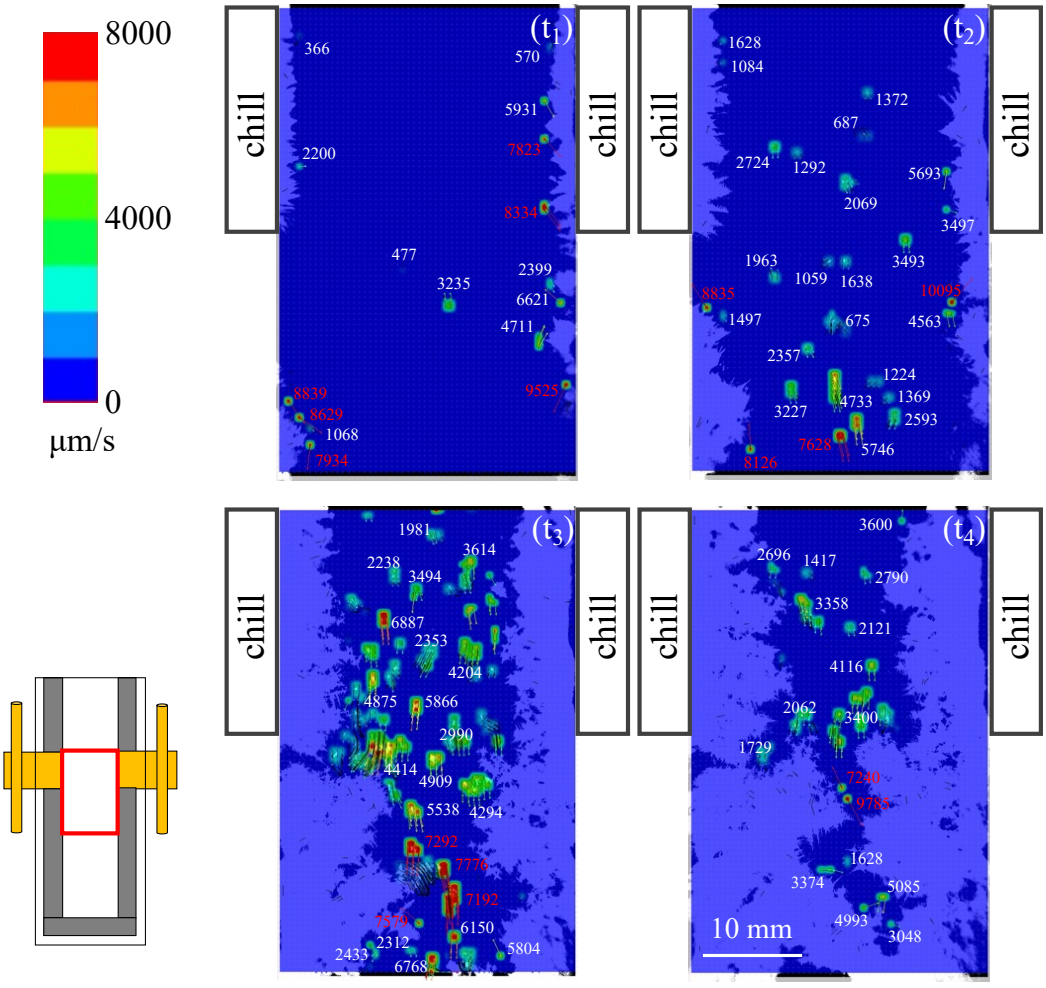

Fig. 3.2.4. The velocity of movement of free dendrites and the solidification structure of H_2O-35mass%NH_4Cl cast in the mold with the chill plate, and the width of the stainless steel plate is 10 mm.

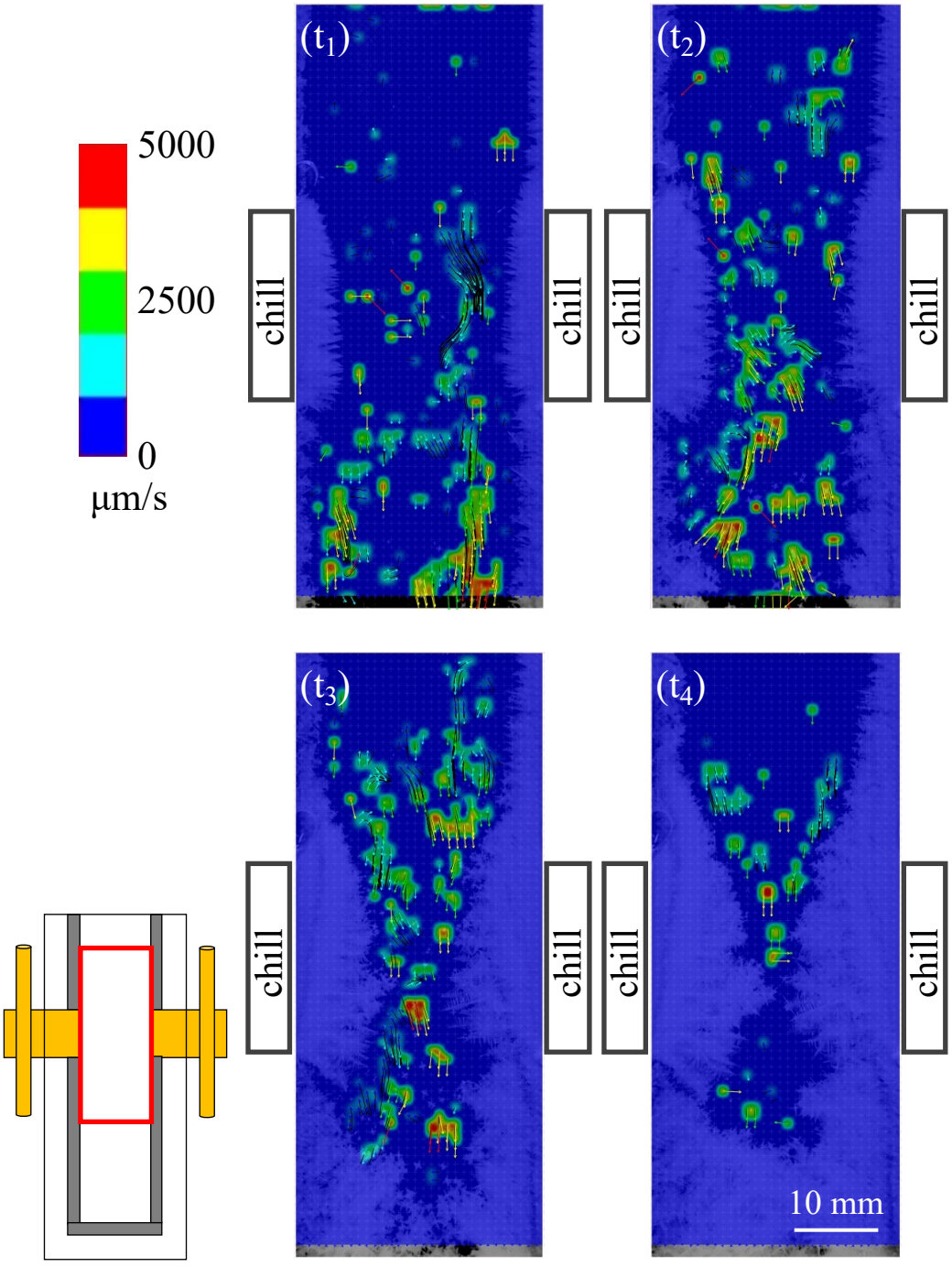

Fig. 3.2.5. The velocity of movement of free dendrites and the solidification structure of H_2O-35mass%NH_4Cl cast in the mold with the chill plate, and the width of the stainless steel plate is 5 mm.

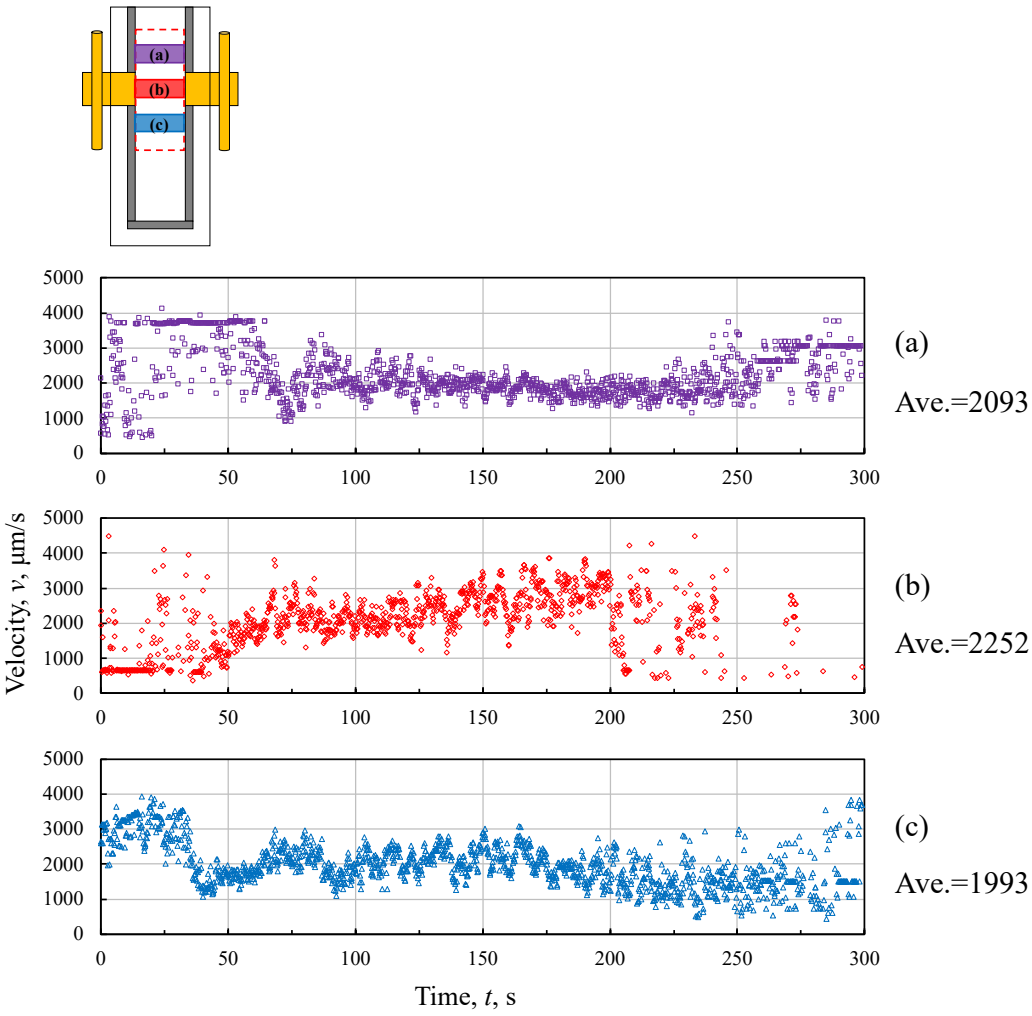

Fig. 3.2.6. The velocity of movement of free dendrites in the area (a) above the bridging, (b) in the center of the bridging, (c) below the bridging in the case cast in the mold with the chill plate, and the width of the stainless steel plate is 5 mm, as shown in Fig. 3.2.5.

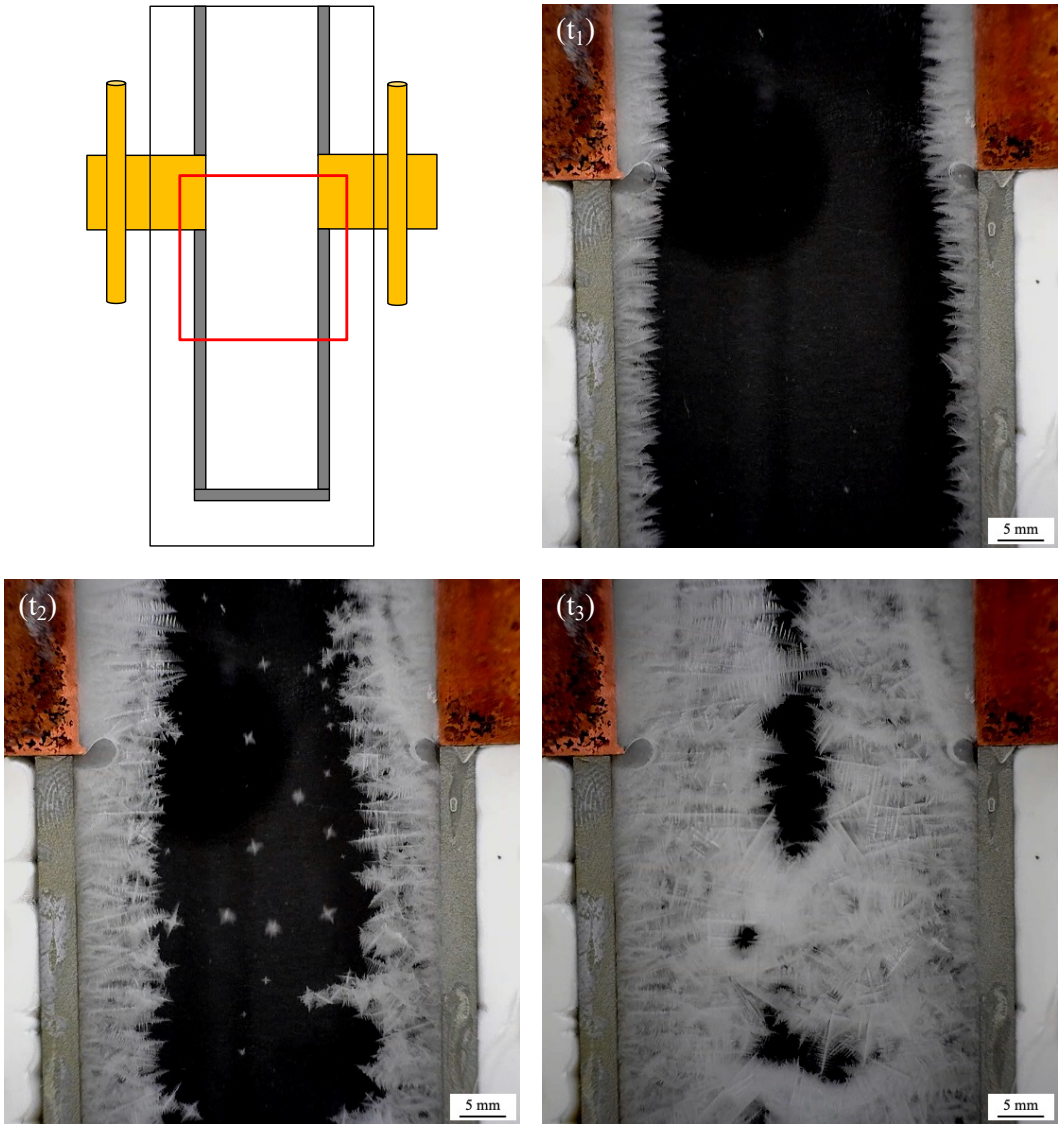

Fig. 3.2.7. Solidification structure of H_2O-35mass%NH_4Cl cast in the mold with the chill plate, and the width of the stainless steel plate is 3 mm.

3.2.4 Conclusions

In-situ observations of the solidification of ammonium chloride aqueous solution were carried out to evaluate the progress of solidification and the convection flow in the mold with and without local cooling to better understand the effects of columnar bridging on macrosegregation.

(1) In the case that H_2O-35mass%NH_4Cl was cast in the mold with the chill plate, and the width of the stainless steel plate was 5 mm, a perfect bridging area was obtained, and the columnar dendrite growth was maintained in the upper and lower areas of the chill plate. Since the fraction of solid is only about 11% at room temperature, this case could be assumed to be the initial stage of solidification in the actual casting process of steel.

(2) Before the bridging area was blocked, the flow velocity in the center of the bridging area was the largest. After the bridging area was blocked, the flow velocity in the area above the bridging and below the bridging was increased slightly, and it was considered as the result of the formation of the contraction flow.

(3) The convection due to the temperature difference was dominated up to about 5 mm from the side of the mold, but above 5 mm, the convection was dominated by the difference in solute concentration.

References

1) T. Motegi, and A. Ohno: *Trans. Japan Inst. Met.*, **25** (1984), 122. https://doi.org/10.2320/matertrans1960.25.122

2) M. Ohno, D. Kimura, and K. Matsuura: *Tetsu-to-Hagané*, **103** (2017), 711. https://doi.org/10.2355/tetsutohagane.TETSU-2017-028

3) I. Uwabe, K. Dobara, K. Moroshita, T. Nagira, and H. Yasuda: *Tetsu-to-Hagané*, **103** (2017), 678. https://doi.org/10.2355/tetsutohagane.TETSU-2017-077

4) T. Murao, T. Kajitani, H. Yamamura, K. Anzai, K. Oikawa, and T. Sawada: *Tetsu-to-Hagané*, **99** (2013), 94. https://doi.org/10.2355/tetsutohagane.99.94

5) F. Satou, H. Esaka, and K. Shinozuka: *Tetsu-to-Hagané*, **99** (2013), 101. https://doi.org/10.2355/tetsutohagane.99.101

6) Y. Natsume: *Tetsu-to-Hagané*, **103** (2017), 738. https://doi.org/10.2355/tetsutohagane.TETSU-2017-062

7) B. Appolaire, V. Albert, H. Combeau, and G. Lesoult: *ISIJ Int.*, **39** (1999), 263. https://doi.org/10.2355/isijinternational.39.263

8) S. A. Lowry, T. D. McCay, and M. H. McCay: Micro/Macro Scale Phenomena in Solidification, HTD-Vol. 218, AMD-Vol. 139, *The Am. Soc. Mech. Eng.*, New York, N.Y., (1992), 1.

9) Flownizer2D. https://www.ditect.co.jp/products/software/flownizer2d.html (accessed 2022-04-05).

Chapter 4. Experiments of equiaxed crystallization by applying external energy during solidification to reduce segregation - Formation of the equiaxed dendrite of Al-Cu alloy by applying direct current during solidification

4.1 Introduction

Continuous casting technology has been improved for the diversification of needs and stricter steel quality requirements.[1)] However, central segregation is a problem that needs to be solved.[2-8)] A large temperature gradient is generated by water cooling from the side surface during the continuous casting, forming the columnar structure. As the solidification progresses, the solute is concentrated in the liquid phase, and the solute is localized in the final solidified part of the slab, resulting in central segregation. As a result, the maximum concentration of solute elements in the segregated part is about 2.5 times the initial concentration for carbon and about five times for phosphorus and sulfur. The central segregation affects the uniformity of transformation temperature and hardenability and causes casting, rolling, and hydrogen cracks.[9)] Central segregation has been improved by the low-temperature casting methods[2,10)], wire addition method[11)], the ultrasonic application method[12)], soft reduction method[13)], *etc.* In recent years, with the stricter quality requirements of materials, it is necessary to reduce even minute segregation, which has not been a problem in the past. Melting dendrites by electromagnetic stirring, lowering the casting temperature, and adding nucleating agents[14-18)] are efficient methods for gaining equiaxed crystals that could inhibit liquid flow between solid phases at the end stage of solidification even if the solidification conditions change slightly. However, there are still some problems, including white band or spot segregation caused by

electromagnetic stirring, inclusions under low-temperature casting conditions, and contamination of slabs when nucleating agents are added.

As a new method other than those described above, equiaxed crystal formation by Joule heat or Lorentz force by applying a large current during solidification can be considered. According to the result reported by Jie Li *et al.*, which applied an AC to pure Al, fine equiaxed crystals were generated on the upper part of the molten metal by the Lorentz force and Joule heat with high efficiency.[19] Tadashi Momono *et al.* reported that when the Al-3mass%Cu alloy was stirred by Lorentz force during solidification, the equiaxed crystal zone was expanded, and the crystal grains were refined.[20-22] It was reported that it caused remarkable grain refinement by fusing and dispersing the dendrite arm and reducing the temperature gradient in the melt. According to the report by Nakatani *et al.*, the equiaxed crystal ratio was increased by applying a direct current to the S45C.[23] And Aritaka *et al.* reported that the more refined the equiaxed crystals, the lower the macrosegregation.[16] However, no studies have reported that the dendrite arm is fused and released, and the equiaxed crystal zone is expanded only by applying the direct current (DC). In addition, the solidification microstructure of Al-15mass%Cu alloy has clear primary α (Al) phase and eutectic phase. Therefore, in this study, DC was applied to Al-15mass%Cu alloy during solidification, and the effectiveness for melting and equiaxed crystallization of dendrite dominated by Joule heat was investigated.

4.2 Experimental Procedure

In this study, Al-15mass%Cu was used as the target composition. Al-15mass%Cu was cast in a Φ15 rod-shaped mold in a high-frequency vacuum melting furnace under an Ar atmosphere. As shown in Fig. 4.1, the mold used was a cuboid (10 mm×26 mm×20 mm). The carbon rods with a diameter of 7 mm and a length of 200 mm were used as the electrode rods, and one K-type sheath-type thermocouple was used for the temperature measurement. A DC power supply (PWR1600L manufactured by Kikusui Electronics Co., Ltd.) was used. The Al-15mass%Cu alloy sample was melted by raising the temperature to about 740 ℃ with the mold in the muffle furnace to minimize the heat transfer between the molten metal and the mold. After sufficiently holding the sample in a molten state, the mold was taken out from the muffle furnace, and the electrode rod and the thermocouple fixed to the frame were immersed in the molten metal for about 15 mm, and cooled in the air. Firstly, the liquidus temperature and eutectic temperature were measured by the installed thermocouple without current applied. Subsequently, the same preparation procedure as before was performed on the sample to which the current was applied, and then a DC of 70 A was applied to the sample during cooling. Temperature-time cooling curves of samples with no DC and ten times applied were shown in Fig. 4.2.

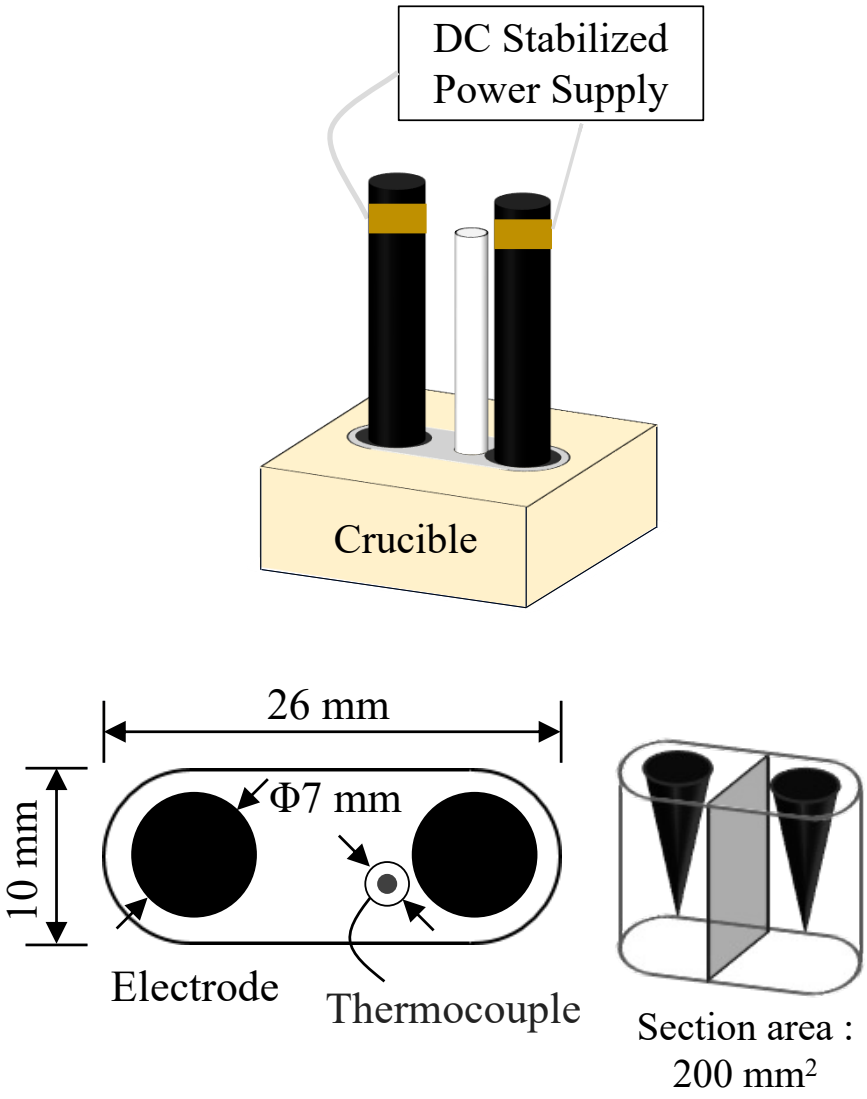

Fig. 4.1. A schematic drawing of the mold.

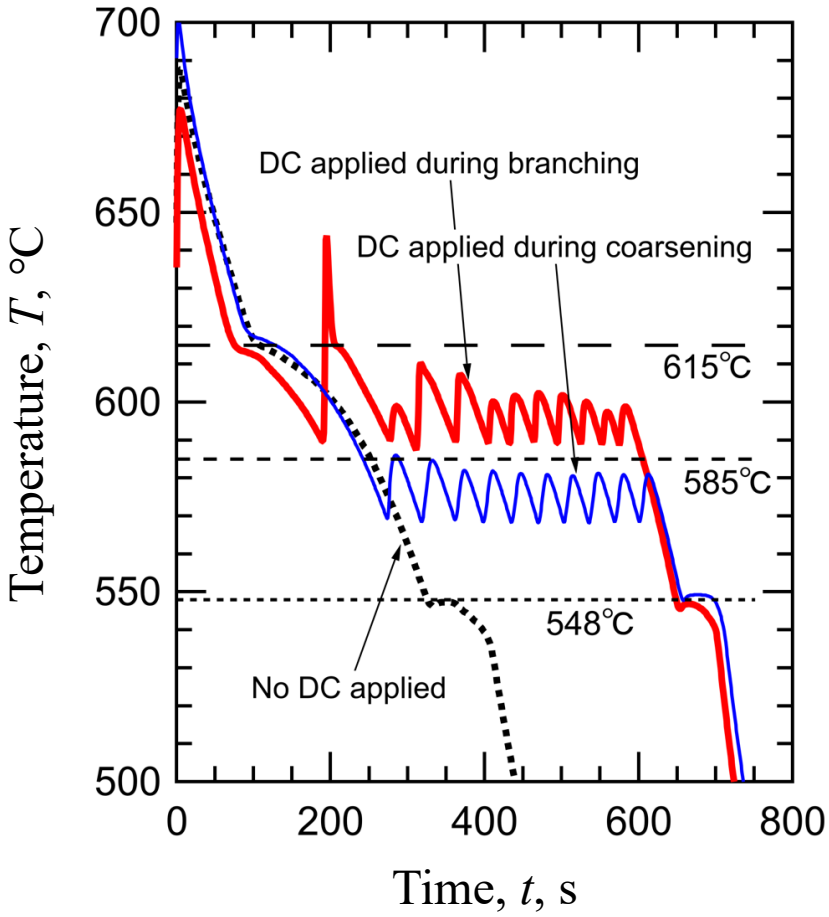

Fig. 4.2. Temperature-time cooling curve for Al-15mass%Cu alloy.

As stated in Table 4.1, the obtained samples were ground with emery paper, then mirror-polished with diamond suspension (1 μm, 0.125 μm), and finally polished with a vibration polishing machine for 8 hours using colloidal silica (0.03 μm). After that, the samples were observed using an optical microscope. Electron backscatter diffraction (EBSD) analysis was performed using JSM-6460A installed in Scanning Electron Microscope (SEM) manufactured by JEOL Ltd. The acceleration voltage was set to 20 kV, and the crystal orientation analysis was performed. In addition, continuous analysis was performed to obtain information in a broader area. The circumference of the dendrite and the secondary dendrite arm spacing (SDAS) was also observed and measured.

Table 4.1 Chemical composition and conditions of application of DC of the sample

No.	Element (mass%)		Application of DC	
	Al	Cu	Times	Temperature (℃)
1	bal.	15.0	-	-
2	bal.	15.0	5	590-600
3	bal.	15.0	10	590-600
4	bal.	15.0	5	570-580
5	bal.	15.0	10	570-580

4.3 Results and Discussions

4.3.1 Effect of DC on SDAS

The thermal analysis curve with no current applied is shown in Fig. 4.2. The liquidus temperature is 615 ℃, and the eutectic temperature is 548 ℃. In addition, the cooling rate (R) was calculated by differentiating the thermal analysis curve.

The branching region is defined as where dendrite branches are thin and long in the solid-liquid coexistence region. Generally, the region where the fraction of solid is 0 to 0.5 is called the branching region. In the Al-15mass%Cu alloy, the branching region is 585 ℃ to 615 ℃. The coarsening region is defined as where dendrite branches grow thick in the solid-liquid coexistence region. The fraction of solid is 0.5 to 1 in the coarsening region. For Al-15mass%Cu alloy, the coarsening region is 548 ℃ to 585 ℃. The DC was applied to samples No.2 and No.3 in the temperature range of 590 ℃ to 600 ℃ during branching. Besides, the DC was applied to samples No.4 and No.5 in the temperature range of 570 ℃ to 580 ℃ during coarsening.

The solidification structure of all samples is shown in Fig. 4.3 and Fig. 4.4. The area shown in black is the dendritic primary α (Al) phase, and the area shown in white in the interdendritic region is the eutectic structure of Al + $CuAl_2$. The solidification microstructure of sample No.1, shown in Fig. 4.3, had a standard structure of Al-15mass%Cu, in which a long elongated primary arm and a vertically developed secondary arm could be observed. The more times the current is applied, the more the arm grows isotropically like an equiaxed one instead of a solidified structure with an elongated primary arm and secondary arms that develop vertically. Specifically, when the current was applied five times, many equiaxed dendrites were observed in the upper part of

sample No.2. When the current was applied ten times, many finer equiaxed dendrites could be observed in the entire sample No.3.

To explore the effect of DC on the solidified structure, it is necessary to focus on the SDAS. Kattamis *et al.* proposed the following equation for the SDAS.[24)]

$$\lambda_2 \propto \left\{\frac{D_L \sigma T}{mC_L(1-k)}\right\}^{1/3} \theta_f^{1/3} \tag{4.1}$$

Where C_L is the solute concentration of the liquid (mass%), D_L is the diffusion coefficient of the solute in the liquid phase (cm^2/s), m is the liquidus gradient (K/mass%), and σ is the solid-liquid interfacial tension (J/cm^2), T is the absolute temperature (K), k is the equilibrium distribution coefficient, θ_f is the local solidification time (s), and λ_2 is the SDAS (μm). It was also proposed that the local solidification time θ_f has a reciprocal relationship with the average cooling rate.

$$\theta_f = \frac{\Delta T_0}{\bar{R}} \tag{4.2}$$

Where ΔT_0 is the solidification temperature range (°C), and $\bar{R}$ is the average cooling rate (K/s). Bower *et al.* proposed the relationship between the local solidification time, θ_f, and the SDAS, λ_2, in the Al-Cu alloy.[25)]

$$\lambda_2 = 7.5 \times \theta_f^{0.39} \tag{4.3}$$

From equations (4.2) and (4.3), the relational expression between the SDAS and the average cooling rate ($\bar{R}$) is in Al-15mass%Cu is expressed by the following equation.

$$\lambda_2 = 33.6 \times \bar{R}^{-0.39} \tag{4.4}$$

Samples were divided into four parts, 0 to 5 mm, 5 to 10 mm, 10 to 15 mm, and 15 to 20 mm from the free surface of the sample, respectively. The measurement of the SDAS of samples is shown in Fig. 4.5. Sample No.1 has a coarse SDAS 5 mm larger than the theoretical value calculated by equations (4.4), except for the position of 0 to 5 mm from

the free surface. In Sample No.2, in the position of 0 to 10 mm from the free surface, the SDAS is smaller than the theoretical value. In Sample No.3, SDAS is much smaller in the position of 0 to 15 mm from the free surface. Therefore, as the times of DC applied during branching increased, the value of the SDAS became smaller over the entire sample. However, when the current was applied in the coarsening region, although the SDAS of samples No.4 and No.5 was smaller than that of sample No.1, it was slightly larger than the theoretical value. Thus, it was concluded that the SDAS became smaller as the DC was applied.

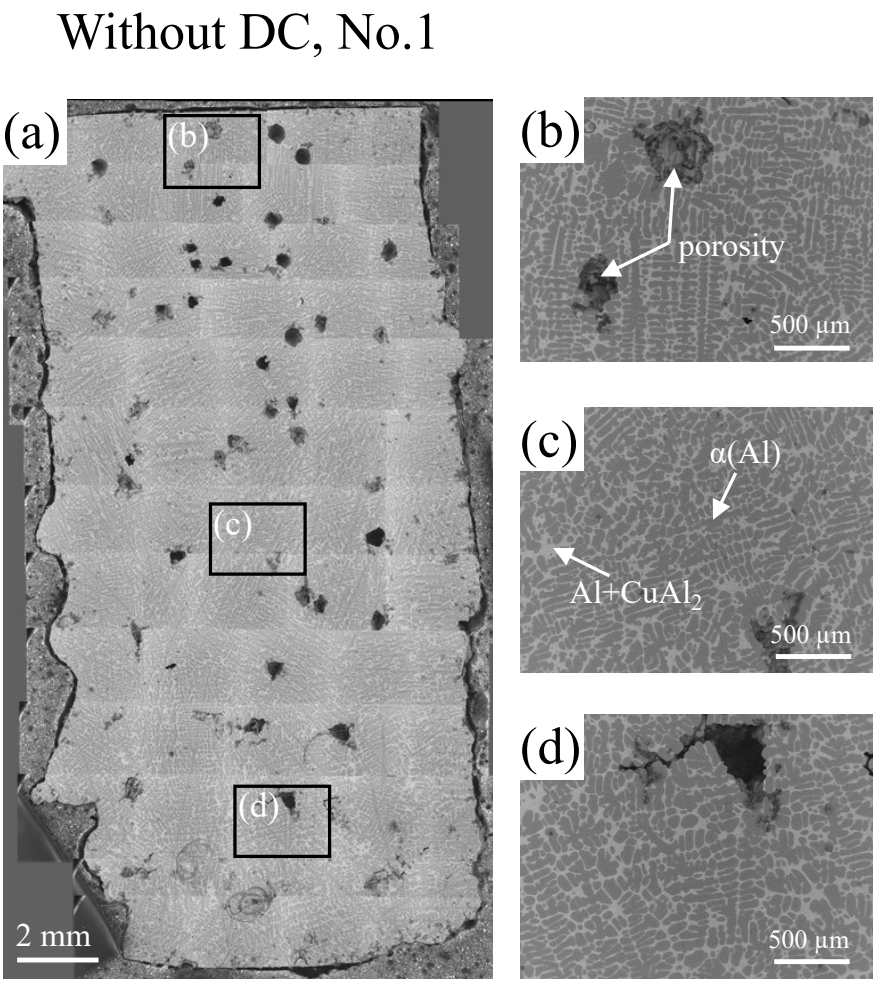

Fig. 4.3. Solidified structure of sample No.1 in (a) longitudinal section parallel to the electrodes, (b) top, (c) center, and (d) bottom.

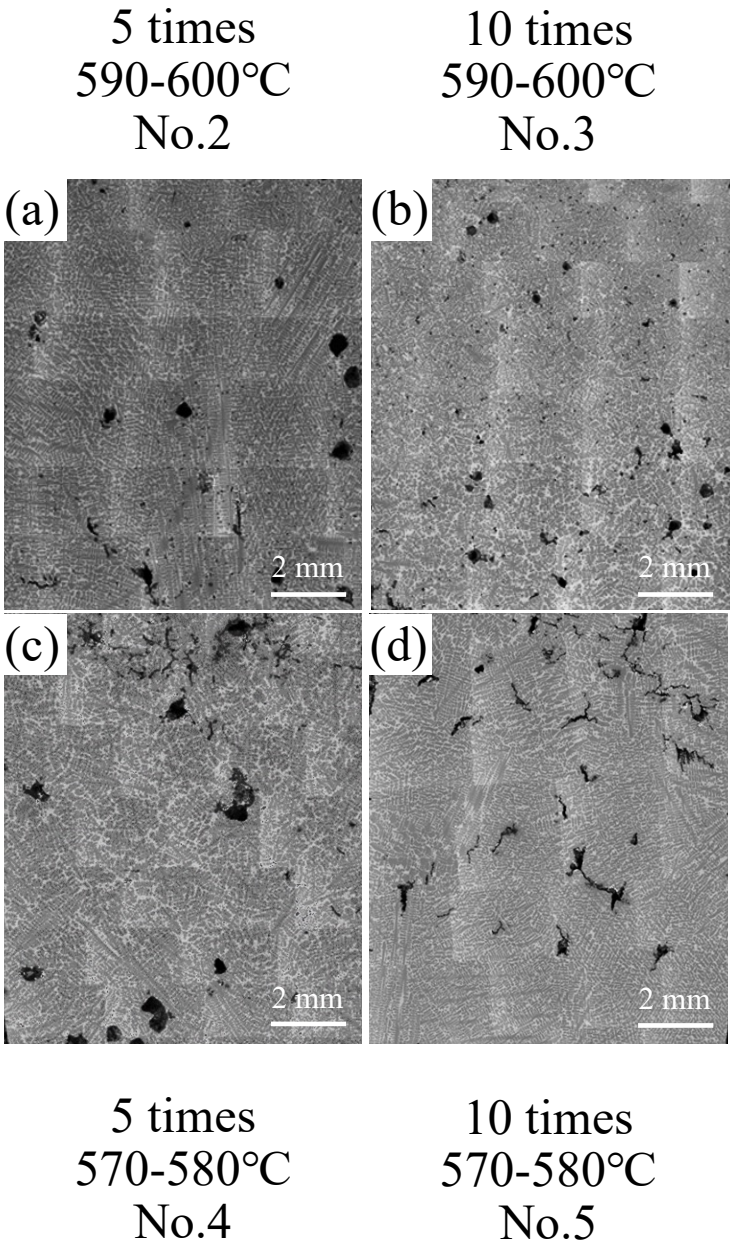

Fig. 4.4. Solidified structure of the sample (a) No.2, (b) No.3, (c) No.4, and (d) No.5 in longitudinal section parallel to the electrodes.

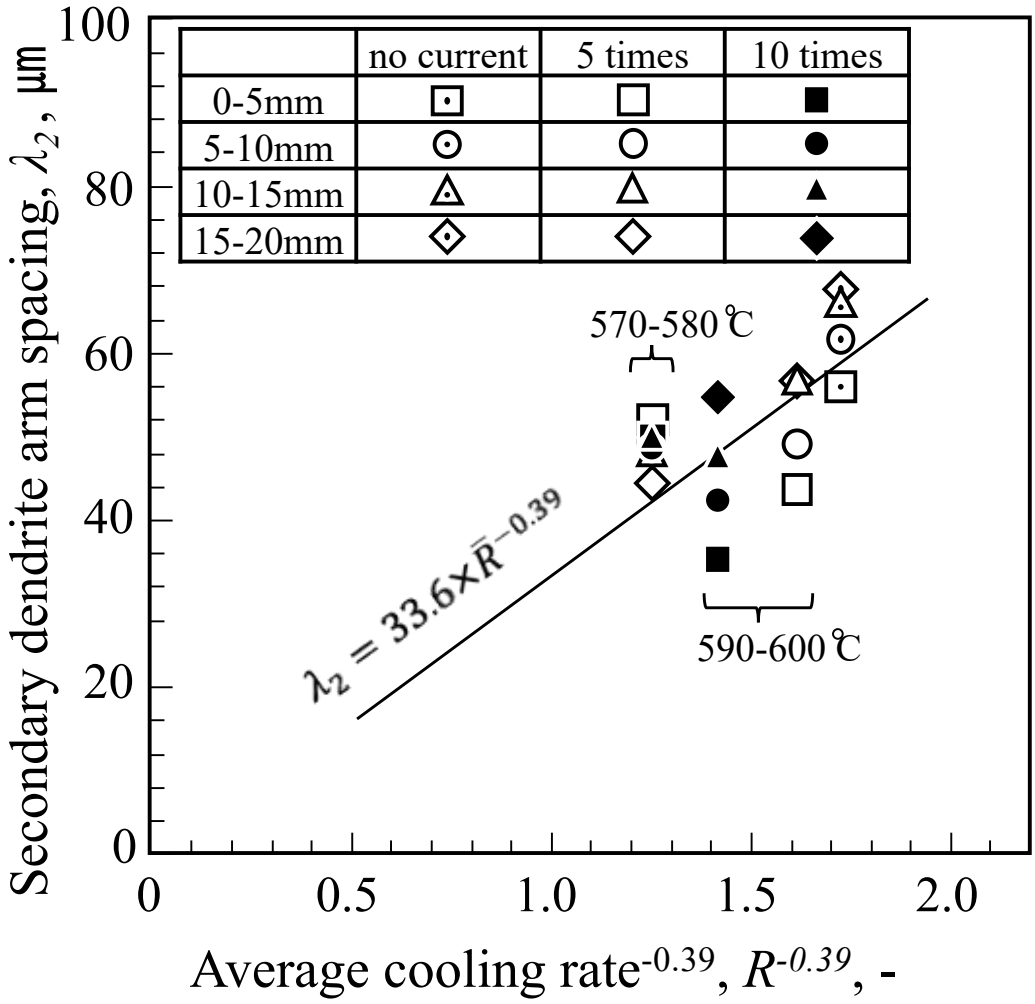

Fig. 4.5. Relationship between average cooling rate$^{-0.39}$ and average secondary dendrite arm spacing.

Since the solute was concentrated at the base of the secondary arm due to the inflow of the liquid phase, there was a difference in solute concentration between the base and the tip of the secondary arm. Also, because the liquid phase in the vicinity of the root was concentrated, the melting point decreased, and the supercooling decreased. Thus the supercooling was larger near the tip, the growth of the root was relatively slower than that of the tip, and there was a difference in the fraction of solid. When the Joule heat was transferred to the secondary arm, the roots with high solute concentration were constricted and remelted, and some parts of the primary dendrites were freed. Finally, equiaxed crystallization occurred with the growth of those new nuclei in the melt. Because the dendrite branches grow thin and long in the branching region, the Joule heat generated by the DC easily remelt the dendrites. On the other hand, the dendrite branches grow thicker in the coarsening region. Thus, it was difficult for the Joule heat generated by the application of DC to remelt the dendrites. Therefore, the effect was much more significant in the range of 590 ℃ to 600 ℃ during branching than that in the range of 570 ℃ to 580 ℃ during coarsening.

4.3.2 Effect of DC on grain size

Inverse pole figures (IPF) of samples are shown in Fig. 4.6, and Fig. 4.7 shows the grain density (n/mm^2) diagrams. According to the IPF of sample No.1, large grains were dispersed throughout the sample. In sample No.2, grains were small in the upper half of the sample, and the crystallographic orientation was anisotropic. In sample No.3, small grains with anisotropic crystallographic orientation were dispersed throughout the sample. Also, grains were relatively small in the upper half of samples No.4 and No.5 compared to that of sample No.1. Fig. 4.8 shows the grain density of various regions of sample No.3, which has the highest grain density. It was observed that the grain density in the vicinity of the centerline was higher than that near the edge. Therefore, the grain density in a 6 mm wide area in the vicinity of the centerline was measured, and the result is shown in Fig. 4.9. The average grain density of the entire sample No.1 was 0.25 per mm^2, and it was 2.90, 8.76, 2.46, and 1.11 per mm^2 for samples No.2, No.3, No.4, and No.5, respectively. According to the results, applying DC during branching does increase the grain density significantly, especially in the upper half of the sample. And the effect of applying ten times was much better than that of five times during branching. Fig. 4.10 shows the average grain size of a 6 mm wide area in the vicinity of the centerline, and Fig. 4.11 shows the average grain radius of samples at different depths. The average grain radius in samples No.1, No.2, No.3, No.4, and No.5 was 1.4 mm, 0.5 mm, 0.2 mm, 0.4 mm, and 0.7 mm, respectively. It was confirmed that the solidification structure was miniaturized and the equiaxed crystal zone was increased by applying the DC in both the branching and coarsening regions. It was worth noting that grains had been refined effectively with the application of ten times of DC during branching.

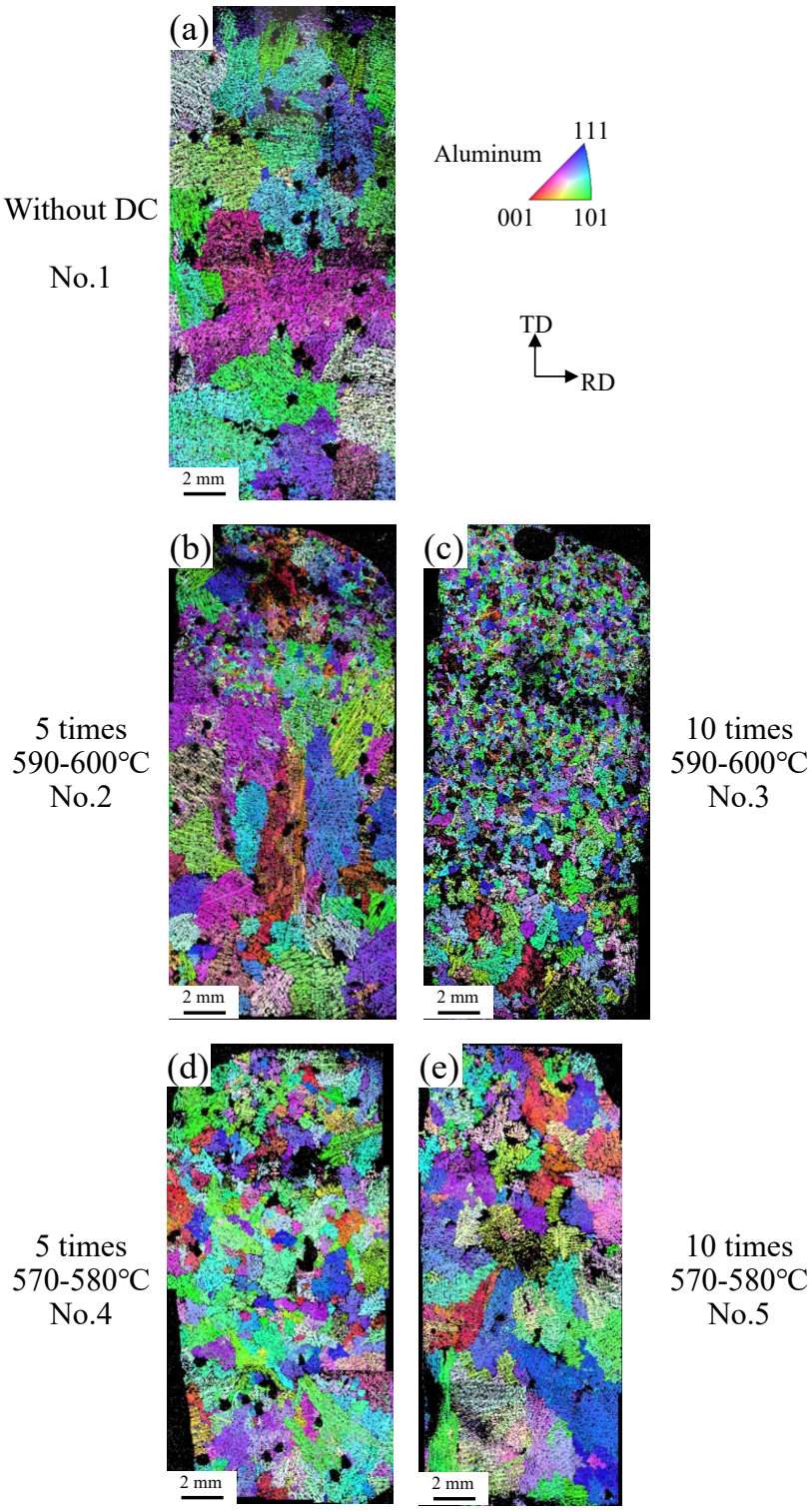

Fig. 4.6. Inverse pole figure of the sample (a) No.1, (b) No.2, (c) No.3, (d) No.4, and (e) No.5

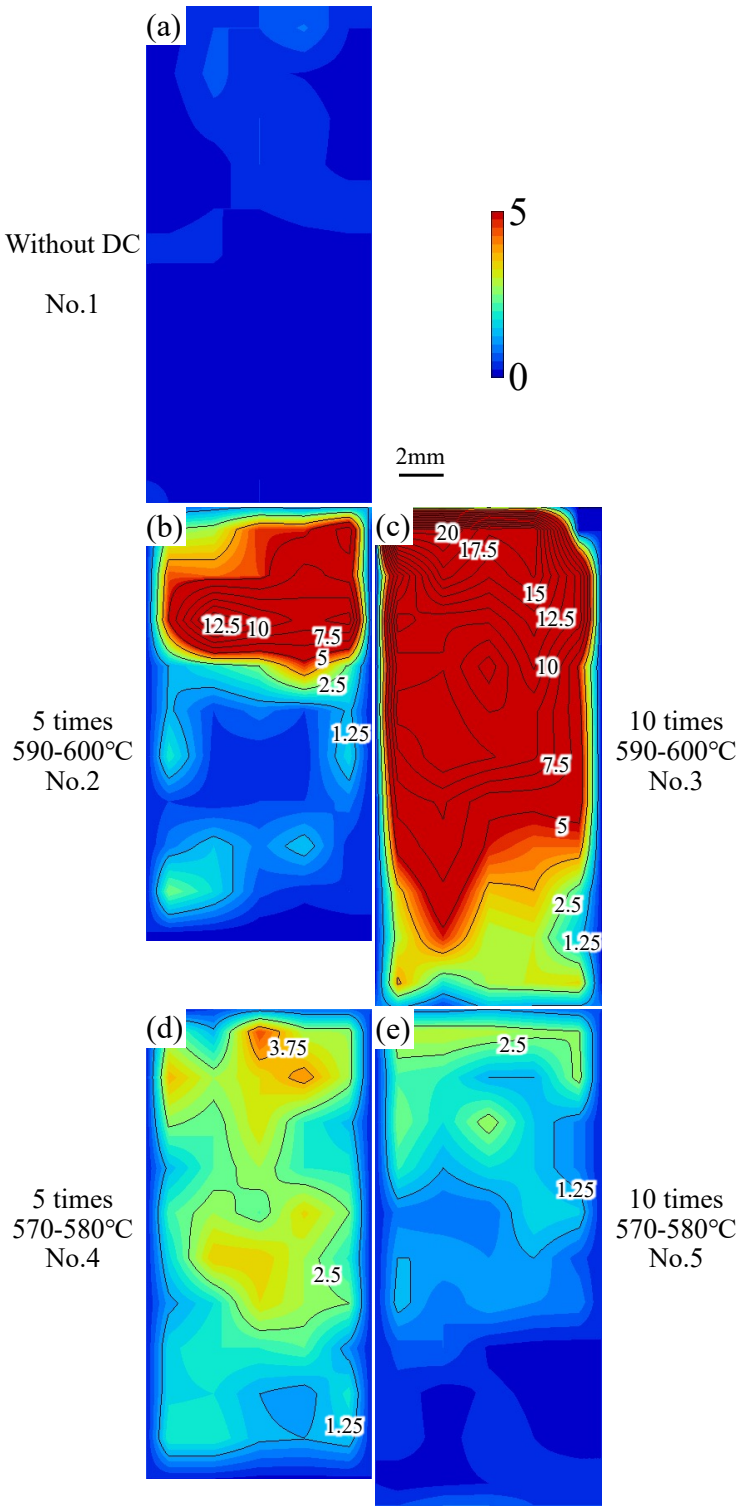

Fig. 4.7. Grain density (n/mm^2) diagram of the sample (a) No.1, (b) No.2, (c) No.3, (d) No.4, and (e) No.5.

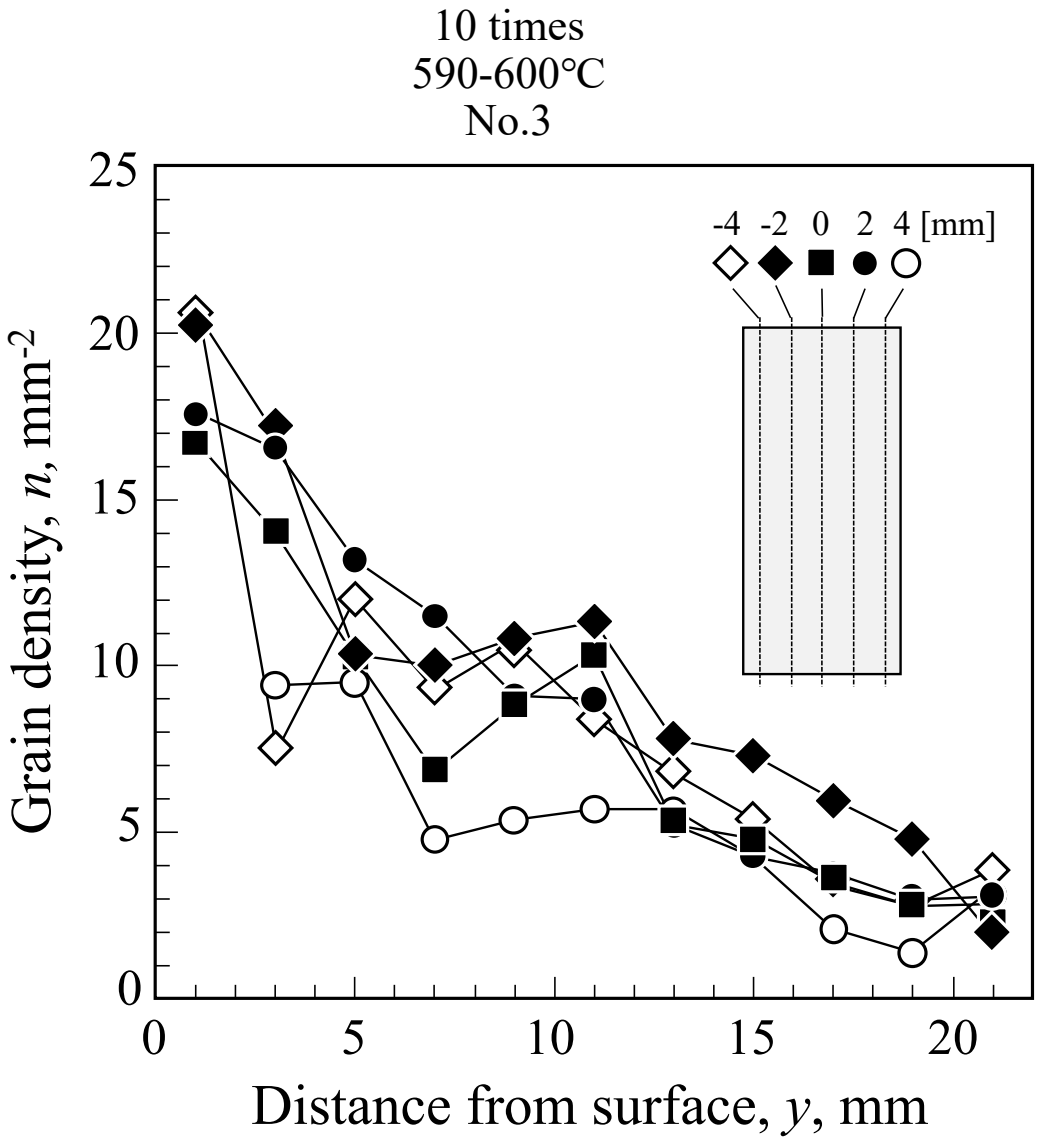

Fig. 4.8. Grain density of sample No.3.

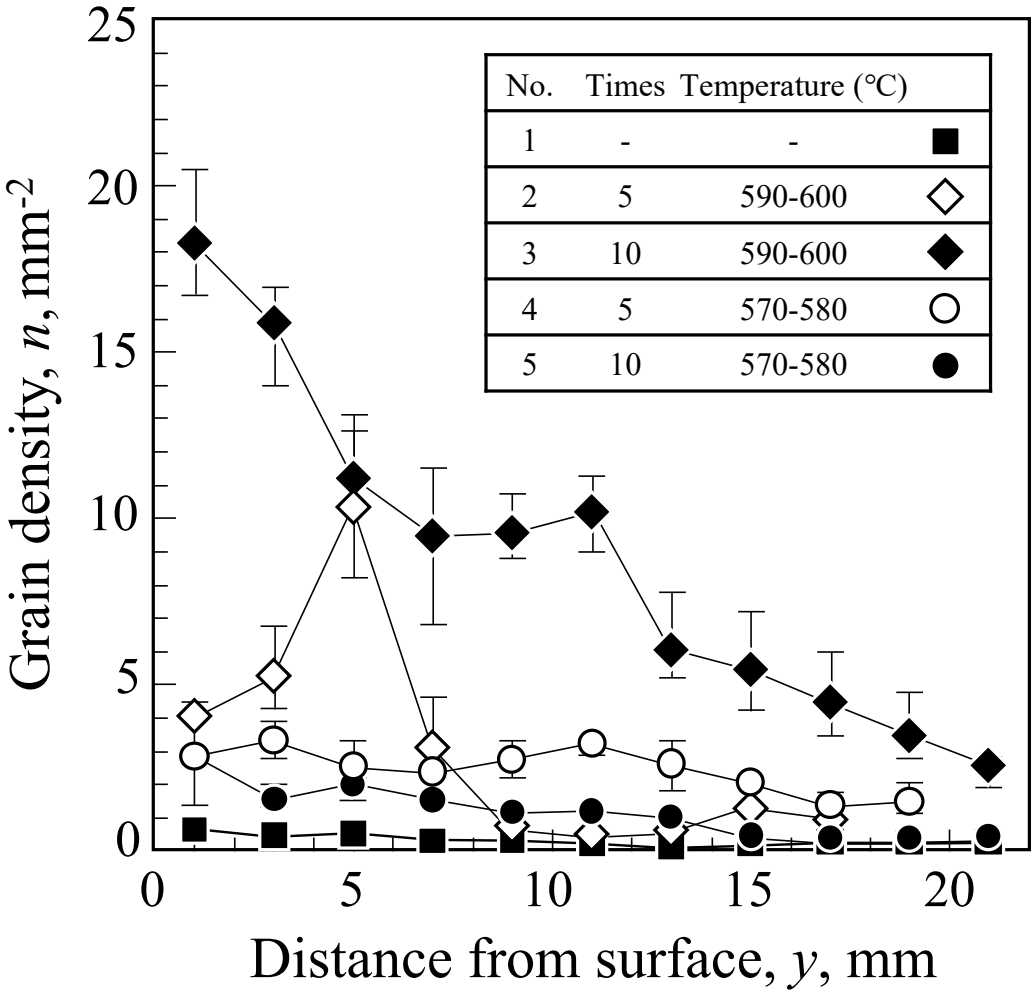

Fig. 4.9. Grain density in a 6 mm wide area in the vicinity of the centerline.

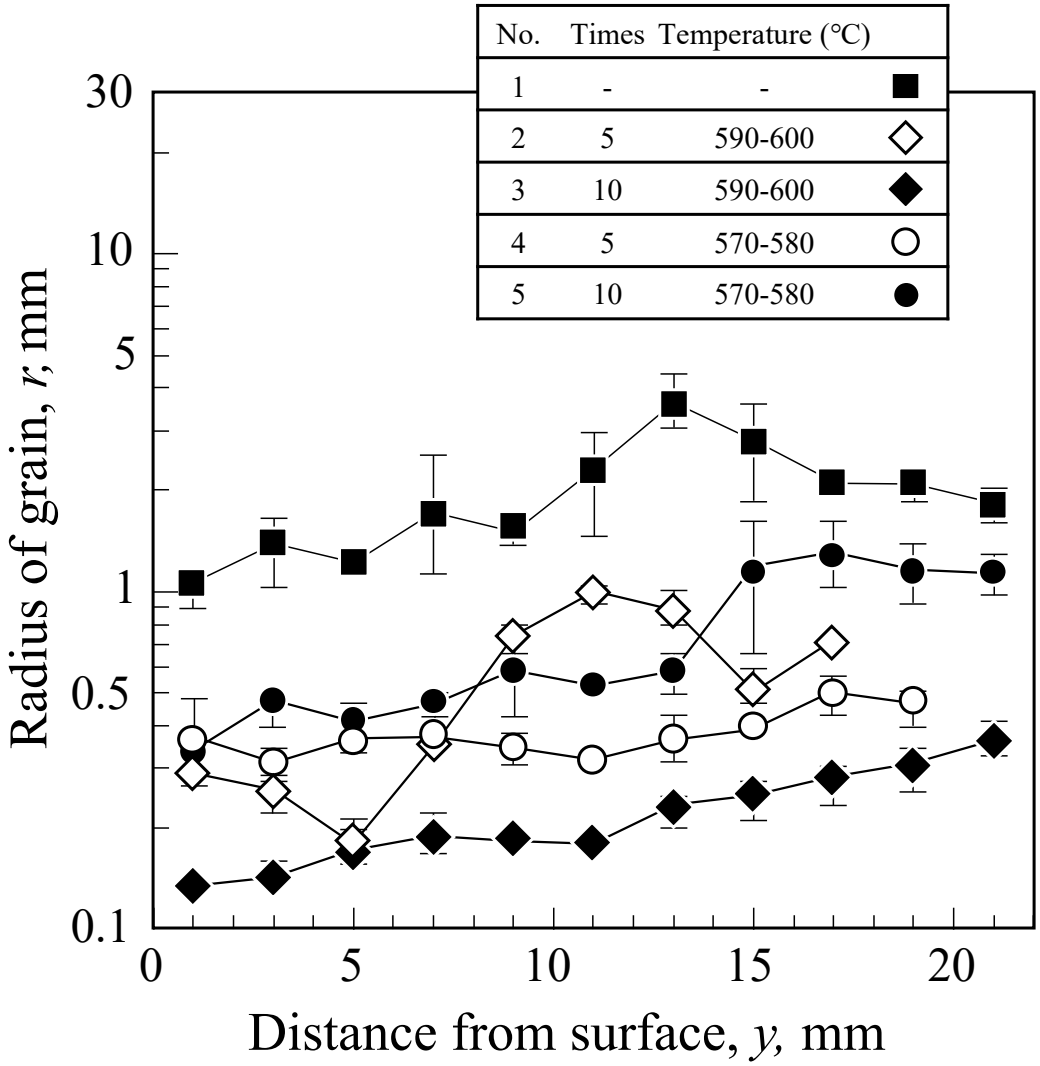

Fig. 4.10. The average grain size of a 6 mm wide area in the vicinity of the centerline.

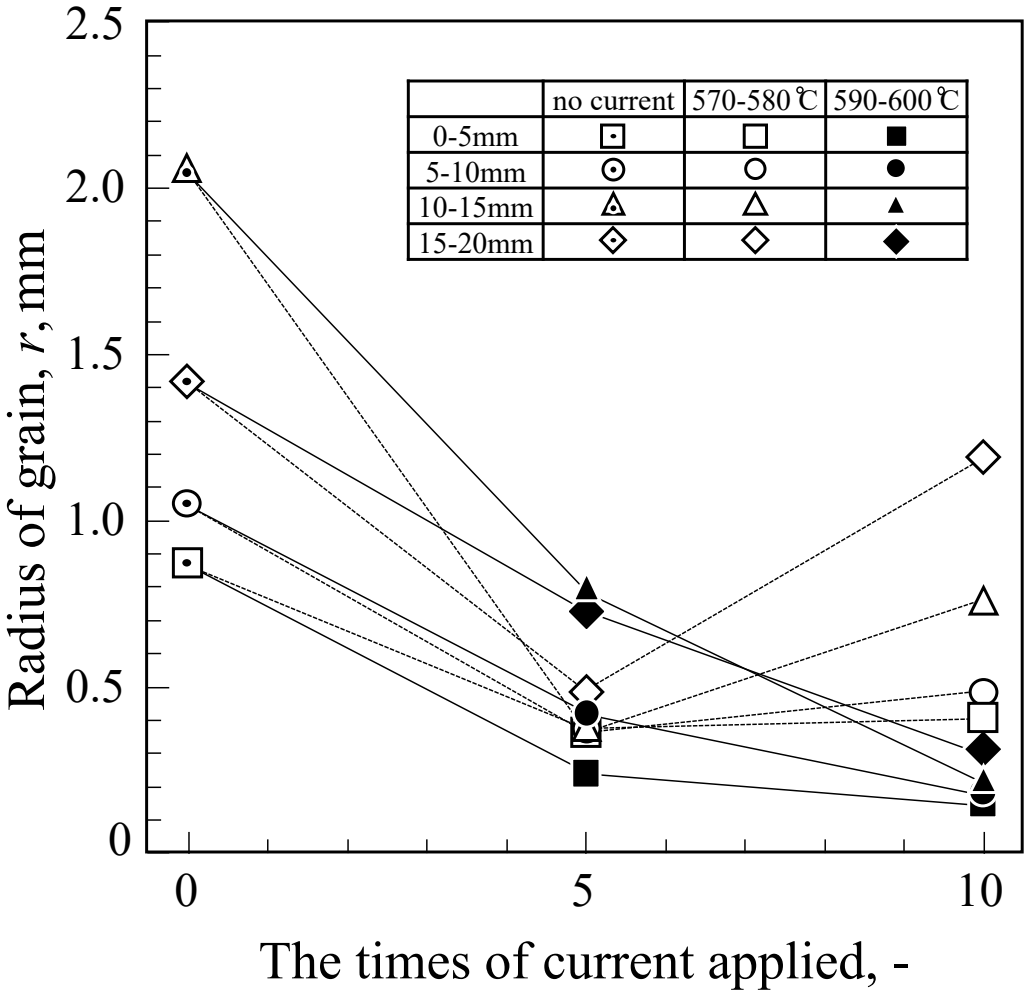

Fig. 4.11. Average grain radius of samples at different depths.

4.3.3 Effect of DC on the complexity of dendrite morphology

During solidification, redistribution of alloying elements causes microsegregation inside the dendrite and interdendritic region. And the convection causes the concentration or the dilution of elements, which is defined as macrosegregation, since solute can be transported by diffusion or convection (or both). In other words, the flow of the liquid phase during solidification would cause macrosegregation. Aritaka *et al.* proposed that the liquid phase flow resistance is important for suppressing macrosegregation.[16] When the size and morphology of equiaxed dendrites are changed independently, equiaxed dendrites can be divided into four types, ① coarse and complex equiaxed dendrites, ② coarse and simple equiaxed dendrites, ③ fine and simple equiaxed dendrites, ④ fine and complex equiaxed dendrites. The relationship of the liquid phase flow resistance between these four types is roughly ④>③=①>②. Therefore, if the equiaxed dendrites are fine and complex in the end period of solidification, it is difficult for the liquid phase to flow between the dendrites, which is effective for suppressing macrosegregation. It was found that the equiaxed dendrites could be refined by applying DC. Therefore, it is necessary to confirm whether the dendrite morphology is also complicated by applying DC. Then, the perimeter of the dendrite per unit area was measured.

As shown in Fig. 4.12, compared to sample No.1, the average perimeter of the dendrite in sample No.2 was 1.2 times longer in the area of 0 to 10 mm, but it was almost the same in the lower half of the two samples. In the case of sample No.3, the average perimeter per unit area became much longer, and the morphology of the equiaxed dendrite became complicated over the entire sample. When the DC was applied in the range of 570 ℃ to 580 ℃ in the coarsening region, the average perimeter per unit area became shorter, which means the equiaxed crystal morphology was simplified. Therefore, it was

considered that applying the DC in the range of 590 ℃ to 600 ℃ during branching is also effective for complicating the equiaxed dendrite morphology. By applying the DC in the coarsening region, the solidified structure became finer, and the number of equiaxed crystals increased, but the dendrite morphology was simplified.

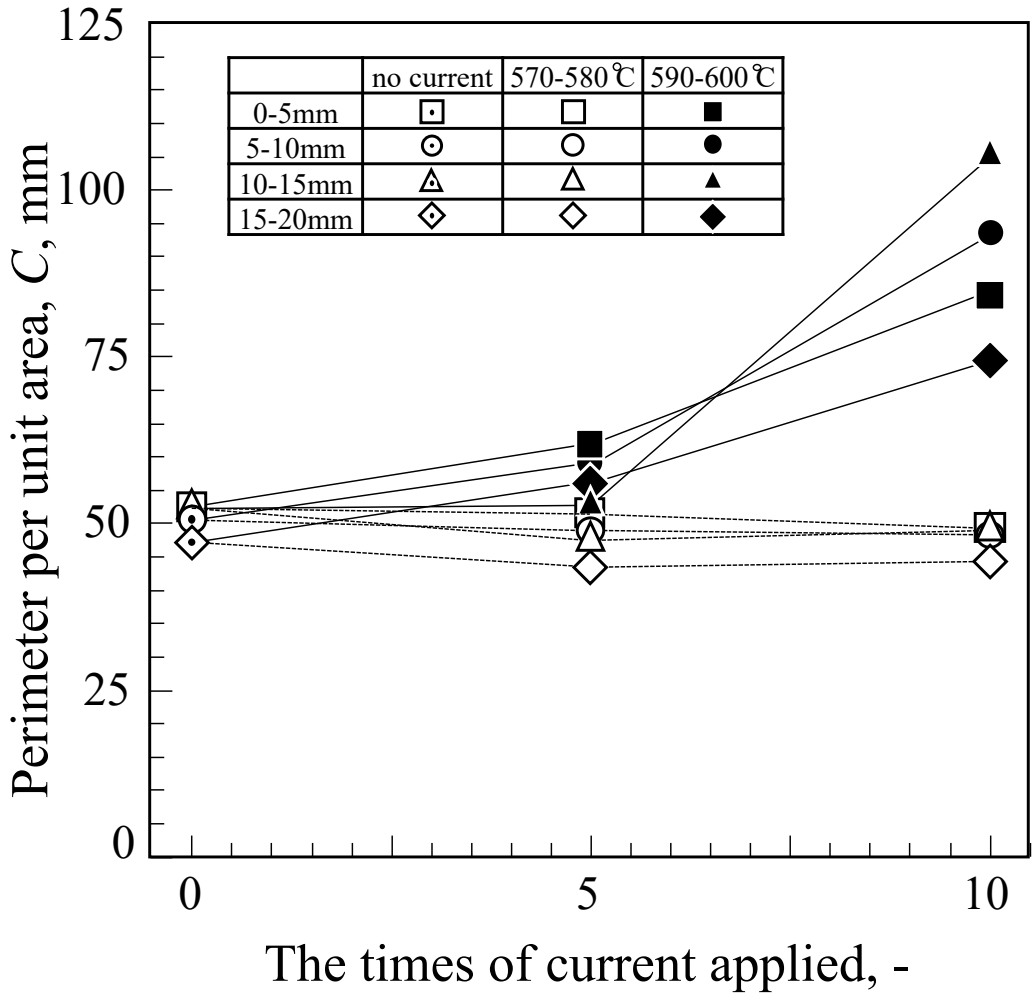

Fig. 4.12. Average grain perimeter of samples at different depths.

4.4 Conclusions

As a model experiment for reducing macrosegregation in continuous casting, the DC was applied in the branching and coarsening regions during solidification using the Al-15mass%Cu alloy. The effect of DC on dendrite melting and equiaxed crystallization were evaluated, and the following conclusions were obtained.

(1) The SDAS decreased due to the application of DC during solidification.

(2) The solidification structure was miniaturized, and the equiaxed crystal zone was increased by applying the DC in both the branching and coarsening regions. Grains had been refined effectively with the application of ten times DC during branching.

(3) By applying the DC, the dendrite morphology was complicated in the branching region, and the dendrite morphology was simplified in the coarsening region.

(4) The miniaturization of solidified structure and the complexity of dendrite morphology required to reduce macrosegregation were obtained by applying the DC in the branching region. Therefore, applying the DC during branching is effective for improving macrosegregation in solidification. This result also provides a new possibility for equiaxed crystallization in steel.

References

1) H. Kajioka, *Mater. Japan*, **34** (1995), 285.

2) H. MORI, N. TANAKA, N. SATO, and M. HIRAI, *Trans. Iron Steel Inst. Japan*, **57** (1971), 263.

3) T. Kawawa, H. Sato, S. Miyahara, T. Koyano, and H. Nemoto, *Tetsu-to-Hagané*, **60** (1974), 486.

4) T. Motegi, and A. Ohno, *J. Japan Inst. Met.*, **46** (1982), 323.

5) K. Sasaki, Y. Sugitani, and S. Ishimura, *Tetsu-to-Hagané*, **66** (1980), 43.

6) M. FUJII, N. FUJII, S. MORIMOTO, and S. OKADA, *J. Japan Inst. Light Met.*, **36** (1986), 353.

7) S. SUZUKI, Y. NISHIDA, I. SHIRAYANAGI, N. IZAWA, and H. MATSUBARA, *J. Japan Inst. Light Met.*, **32** (1982), 395.

8) K. Isobe, *Tetsu-to-Hagané*, **98** (2012), 405.

9) T. Murao, T. Kajitani, H. Yamamura, K. Anzai, K. Oikawa, and T. Sawada, *Tetsu-to-Hagané*, **99** (2013), 94.

10) S. IWASAWA, S. SAIKAWA, T. TOMITA, K. HAYASHI, S. KAMADO, and Y. KOJIMA, *J. Japan Inst. Light Met.*, **8** (2000), 371.

11) Y. Habu, S. Itoyama, T. Emi, K. Sorimachi, and H. Kojima, *Tetsu-to-Hagané*, **67** (1981), 1498.

12) S. KOJIMA, T. IMAI, H. MIZOTA, T. FUJIMURA, and T. MATSUKAWA, *Tetsu-to-Hagané*, **78** (1992), 1794.

13) M. Yamada, S. Ogibayashi, M. Tezuka, and T. Mukai, (1988). *Production of Hydrogen Induced Cracking(HIC) Resistant Steel by CC Soft Reduction*. *In 71st Steelmaking Conference* (pp. 77-85).

14) H. Esaka, T. Shimada, S. Mizoguchi, and H. Kajioka, *J. Japan Inst. Met.*, **54** (1990), 1099.

15) K. WÜNNENBERG, and H. JACOBI, *Tetsu-to-Hagané*, **68** (1982), 1613.

16) E. Aritaka, H. Esaka, and K. Shinozuka, *Tetsu-to-Hagané*, **104** (2018), 293.

17) S. Fukumoto, K. Kimura, and A. Takahashi, *Tetsu-to-Hagané*, **98** (2012), 351.

18) H. ESAKA, and M. TAMURA, *Tetsu-to-Hagané*, **86** (2000), 50.

19) J. Li, J. Ma, Y. Gao, and Q. Zhai, *Mater. Sci. Eng. A*, **490** (2008), 452.

20) T. MOMONO, and K. IKAWA, *J. Japan Inst. Light Met.*, **27** (1977), 560.

21) T. MOMONO, and K. IKAWA, *J. Japan Inst. Light Met.*, **29** (1979), 240.

22) T. MOMONO, and K. IKAWA, *J. Japan Inst. Light Met.*, **26** (1976), 441.

23) M. Nakatani, T. Adachi, Y. Sugitani, S. Kobayashi, M. Yoshihara, and S. Ish imura, *Tetsu-to-Hagané*, **67** (1981), 287.

24) T. Z. Kattamis, J. C. Coughlin, and M. C. Flemings, *Trans. Metall. Soc. AIME*, **239** (1967), 1504.

25) T. F. Bower, H. D. Brody, and M. C. Flemings, *Trans. Metall. Soc. AIME*, **236** (1966), 624.

Chapter 5. Summary

In the industrial steel manufacturing process, macrosegregation occurs in casting, and it is desirable to reduce it as much as possible. However, it is difficult to perform quantitative and highly reproducible analyses. In order to establish and standardize a three-dimensional evaluation method for the solidified structures, and accurately predict the location of segregation for effectively controlling the quality of the casting, in this study, the effectiveness of the local chilled mold for cast steel samples was investigated, and the effect of bridging on macrosegregation and solidification defects was investigated using the improved mold and simulation. In addition, as a verification of a method of reducing central segregation and V-segregation of cast steel, the direct current was applied to Al-15mass%Cu alloy during solidification, and the effectiveness for equiaxed crystallization of dendrite dominated by Joule heat was investigated.

The obtained results are as follows.

A model casting experiment was adopted to understand the formation mechanism of macrosegregation of steel casting that occurred by local bridging during solidification with a laboratory-scale local-chilled mold.

(1) Columnar dendrites and equiaxed dendrites with extremely different morphologies were formed with a high superheating of 100 °C, however, equiaxed dendrites with similar morphology, were formed with a low superheating of 30 °C.

(2) Local chilling successfully formed the columnar dendrite bridging in the sample with high superheating by the laboratory-scale local-chilled mold.

(3) V segregation was formed at the bridging area, and large shrinkage porosities were formed under a high casting temperature, while a lower casting temperature

increased the grain density and formed shrinkage porosities that were smaller in size but larger in number and more dispersed.

(4) In the sample with high superheating of 100 °C, fine and coarse dendrites appeared near the large shrinkage porosity. In the area below the bridging of the casting, point-like or band-like positive macrosegregation occurred in the interdendritic region between columnar dendrites and equiaxed dendrites. And positive macrosegregation occurred in the final solidification region around the shrinkage porosity.

An improved model casting experiment was adopted. The solidification structure morphology was observed, concentration analysis of alloying elements was performed, and the effect of bridging on macrosegregation was investigated.

(1) Solidification proceeded preferentially from the chill plate, and the bridging was formed successfully at a high casting temperature. High casting temperature could cause bridging, but large shrinkage porosities would be formed as well, while lower casting temperature could increase the grain density and form shrinkage porosities that are smaller in size but larger in number and more dispersed, compared with the case cast with no chill plate mold.

(2) Alloying elements were concentrated below the bridging near the mold, which was due to the convection caused by the difference in solidification speed between the chilled part and the others, and the concentrated molten steel from the chilled part flowed into the lower part and solidified.

(3) Around the shrinkage porosity, the concentration of alloying elements was most significant. It was considered that the area around the shrinkage porosity is the final solidified part.

(4) Due to the formation of bridging, macrosegregation was formed, and the difference between positive and negative segregation was increased.

The simulation of the solidification process by local cooling was evaluated. Various changes in the solidification process were calculated.

(1) It succeeded in reproducing the solidification process that forms bridging by local cooling by simulation, confirmed the suction effect due to bridging, and understood that bridging promotes segregation.

(2) In the case of two bridging areas, the maximum negative pressure was about 34 times that of one bridging, and the flow velocity was about 1.6 times. The suction effect could be enhanced, significantly increasing the degree of segregation.

In-situ observations of the solidification of ammonium chloride aqueous solution were carried out to evaluate the progress of solidification and the convection flow in the mold with and without local cooling to better understand the effects of columnar bridging on central segregation.

(1) In the case that H_2O-35mass%NH_4Cl alloy was cast in the mold with the chill plate, and the width of the stainless steel plate was 5 mm, a perfect bridging area was obtained, and the columnar dendrite growth was maintained in the upper and lower areas of the chill plate.

(2) Since the fraction of solid is only about 11% at room temperature, this case could be assumed to be the initial stage of solidification in the actual casting process of steel.

(3) Before the bridging area was blocked, the flow velocity in the center of the bridging area was the largest. After the bridging area was blocked, the flow velocity in the

area above the bridging and below the bridging was increased slightly, which was considered as the result of the formation of the contraction flow.

(4) The convection due to the temperature difference was dominated up to about 5 mm from the side of the mold, but above 5 mm, the convection was dominated by the difference in solute concentration.

As a model experiment for reducing macrosegregation in continuous casting of steel, the DC was applied in the branching and coarsening regions during solidification using the Al-15mass%Cu alloy. The effect of DC on dendrite fusing and equiaxed crystallization were evaluated.

(1) The SDAS decreased due to the application of DC during solidification.

(2) The solidification structure was miniaturized, and the equiaxed crystal zone was increased by applying the DC in both the branching and coarsening regions. Grains had been refined effectively with the application of ten times of DC during branching.

(3) By applying the DC, the dendrite morphology was complicated in the branching region, and the dendrite morphology was simplified in the coarsening region.

(4) The miniaturization of solidified structure and the complexity of dendrite morphology required to reduce macrosegregation were obtained by applying the DC in the branching region. Therefore, applying the DC during branching is effective for improving macrosegregation in solidification. This result also provides a new possibility for equiaxed crystallization in steel.

In this study, the initial, middle, and final stages of the solidification process, accompanied by bridging, were investigated, and the solidification structure and macrosegregation formation mechanism of each part of the medium-carbon cast steel under this solidification mode was obtained. And it is effective for improving macrosegregation in solidification by applying the DC during the branching period of solidification in an Al-Cu alloy. The follow-up research is expected to complete the testing and application of the DC during the branching period of solidification in cast steel.

Acknowledgments

I would like to express my sincere appreciation to my supervisor, Professor Hirofumi Miyahara. All research results were obtained with the continuing guidance, advice, encouragement, and support of Prof. Miyahara.

I would also like to thank Associate Professor Kohei Morishita, I had many discussions with him and received many helpful suggestions and valuable comments.

I would also like to sincerely thank Professor Hiroaki Nakano and Professor Koji Gotoh, who carefully reviewed my dissertation and made precious comments on it.

Discussions with Mr. Yuki Tanaka (technical staff) were also constructive and were greatly appreciated.

I appreciate Mr. Naoya Suemaru and Mr. Yuta Totogawa for their contributions to the experiments of Al-Cu alloys, appreciate Mr. Syuhei Matsusaki for his work on in-situ observations of simulation by water model, appreciate Mr. Hiroki Minami and Mr. Shouichirou Iwakiri for their assistance during the experiment.

I should also thank all the staff and students at Miyahara Laboratory for their kind encouragement and support.

Finally, I am grateful to my parents for their support, love, and encouragement.

MA JUHUAI

May 16, 2023

Fukuoka, Japan